Coupled Metal Hydride Systems for Energy Storage

A thesis accepted by the Faculty of Energy-, Process- and Bio-Engineering of the University of Stuttgart to fulfill the requirements for the degree of Doctor of Engineering Sciences (Dr.-Ing.)

by

Michael Lutz

born in Regensburg

Main Referee:	Prof. Dr. rer. nat. habil. André Thess
Co Referee:	Prof. Dr.-Ing. habil. Thomas Klassen

Date of oral exam: 30.03.2021

Institute for Building Energetics, Thermotechnology and Energy Storage at the University of Stuttgart

2021

Declaration

Ich erkläre, dass ich abgesehen von den ausdrücklich bezeichneten Hilfsmitteln diese Dissertation selbstständig verfasst habe.

Stuttgart, den _____ _____

Michael Lutz

Für meine Eltern

Acknowledgements

I would like to thank the following people, who encouraged and supported me in the past years while working on this thesis.

Prof. André Thess, for his encouragement to pursue new ideas, valuable advices for presenting scientific results and the supervision of this thesis.

Prof. Thomas Klassen, for accepting to co-referee this thesis and for enabling productive collaboration with the Helmholtz-Zentrum Geesthacht.

Dr. Inga Bürger, for the possibility to benefit from her scientific experience, for numerous discussions about this thesis and its results, and for insisting to write “resolutely positive”.

Dr. Marc Linder for creating a pleasant work environment in the group of thermochemical systems and many inspiring discussions.

Christian Brack for advice and help in the lab during the construction of the test bench.

All colleagues in the group of thermochemical systems, for everyday support and discussions during lunch and coffee.

The whole department of Thermal Process Engineering, for support in everyday life and feedback during numerous doctoral seminars.

The Karl-Vossloh-Stiftung, for partially funding this work (S047/10043/2017).

My family, for consistently asking about the progress of this thesis and becoming enthusiastic about hydrogen.

Aslı Aydın, for emotional support and the help to regain motivation after occasionally losing it.

Michael Hauser, for forwarding the job posting at the DLR to me which initially drew my attention on the DLR.

Table of contents

Abstract

In present times, huge efforts are made to transform the present fossil based energy system to a more renewable one. Hydrogen technologies have the potential to contribute to that change. Among them, metal hydrides can be used versatilely, but thermal management with the ambient is necessary which can be challenging – especially for high temperature metal hydrides. Thermal coupling of a metal hydride with another thermochemical system acting as thermal energy storage is an approach to face that challenge. In this thesis, it was investigated how two selected couplings of a metal hydride with another thermochemical system can be used for energy storage. First, the thermal coupling of magnesium hydride MgH_2 with the $Mg(OH)_2$/MgO system was evaluated for hydrogen storage. Second, a system of two metal hydrides being coupled both thermally and on the gaseous side was analyzed for the ability to store electric energy as a thermochemical battery. Both systems can be operated with minimal external heat management, the hydrogen storage reactor in the idealized case even adiabatically. For the adiabatic hydrogen storage reactor, a model was extended and a numerical analysis was conducted to describe the hydrogen release. In addition, an experimental prototype reactor has been designed and tested. For that purpose a test bench was set up to provide both water vapor at up to 10 bar and hydrogen to the reactor. It was found that the thermodynamic properties of the materials fit to each other. The absorption and desorption rates of hydrogen in the MgH_2 have been enhanced by the thermochemical cooling and heating, respectively. The experiments showed that the reaction rate of $Mg(OH)_2$ / MgO system is the limiting step. A water vapor pressure of 10 bar is required to obtain a temperature of 300 °C in the MgO compartment during hydration, which is a higher pressure than the numerical analysis predicted and has never been investigated before. Therefore, material modifications of the $Mg(OH)_2$ / MgO system are required to improve its properties. Nevertheless, the operational principle of the adiabatic storage reactor could be proofed. For the thermochemical battery, an energetic analysis showed that electricity storage and release is feasible with a gas compression- and expansion unit. A storage density of approximately 62.6 Wh L_{mat}^{-1} and an electric efficiency of up to 47% are achievable for some configurations. Depending on the pair of metal hydrides and operating conditions, additional generation of heat or cold is possible.

Zusammenfassung

Heutzutage werden große Anstrengungen unternommen, um das globale Energiesystem zu dekarbonisieren. Wasserstofftechnologien, zu denen auch Metallhydride zählen, haben das Potenzial zu diesem Wandel beizutragen, da sie vielseitig einsetzbar sind. Es ist allerdings Wärmemanagement mit der Umgebung notwendig, was vor allem bei Hochtemperatur-Metallhydriden herausfordernd sein kann. Die Kopplung eines Metallhydrids mit einem thermochemischen Speichermaterial ist ein Ansatz dieses Problem zu lösen. In dieser Arbeit wird untersucht, wie sich zwei ausgewählte gekoppelte Systeme von Metallhydriden mit einem anderen thermochemischen System verhalten und wie sich diese zur Energiespeicherung einsetzen lassen. Bei dem ersten System handelt es sich um einen Wasserstoffspeicher, in dem Magnesiumhydrid und $Mg(OH)_2$ / MgO thermisch gekoppelt sind. Im zweiten untersuchten System wurden zwei Metallhydride sowohl thermisch als auch stofflich gekoppelt und deren Eigenschaften als thermochemische Batterie zur Speicherung elektrischer Energie untersucht. Beide Systeme können mit minimalem Wärmemanagement zur Umgebung betrieben werden; der Wasserstoffspeicher in einer idealisierten Betrachtung sogar adiabat. Die Wasserstofffreisetzung aus dem adiabaten Wasserstoffspeicher wurde zunächst mit einer numerischen Studie untersucht. Darüber hinaus wurde der Prototyp eines Reaktors entworfen und getestet. Es wurde ein Teststand errichtet, um den Reaktor sowohl mit Wasserdampf von bis zu 10 bar als auch mit Wasserstoff zu versorgen und es wurde gezeigt, dass die thermodynamischen Eigenschaften der beiden Materialien zueinander passen. Die Rate, mit der Wasserstoff aufgenommen bzw. abgegeben wurde, ließ sich durch die thermochemische Kühlung bzw. Heizung erhöhen. Es konnte experimentell gezeigt werden, dass die Reaktionsgeschwindigkeit des $Mg(OH)_2$ / MgO Systems den Gesamtprozess limitiert. Entgegen den Erwartungen aus der numerischen Studie, war ein Wasserdampfdruck von 10 bar notwendig, um während der Hydratisierung des MgO eine Temperatur von 300 °C zu erreichen, was zuvor jedoch noch nie experimentell untersucht wurde. Deshalb ist es notwendig das $Mg(OH)_2$ / MgO System zu modifizieren. Das Funktionsprinzip des adiabaten Wasserstoffspeichers konnte dennoch nachgewiesen werden. Für die thermochemische Batterie konnte über eine energetische Analyse gezeigt werden, dass Energiespeicherung bzw. Freisetzung mit einer Kompression bzw. Expansionsmaschine möglich ist. Eine Speicherdichte von etwa 62.6 $Wh\ L_{mat}^{-1}$ und ein Speicherwirkungsgrad von bis zu 47% konnte für manche Konfigurationen erreicht werden. Je nach Materialpaarung und Betriebsbedingungen ist die zusätzliche Bereitstellung von thermischer Energie und Kälte möglich.

Nomenclature

Symbol	Description	Unit
$\Delta_R G_0$	Gibbs free Standard reaction enthalpy	J mol^{-1}
$\Delta_R H_0$	Standard reaction enthalpy	J mol^{-1}
$\Delta_R S_0$	Standard reaction entropy	J mol^{-1} K^{-1}
ν_i	Stoichiometric number of component i	-
μ_i	Chemical potential of component i	J mol^{-1}
$\mu_{0,i}$	Reference chemical potential of component i	J mol^{-1}
E_a	Activation energy	J mol^{-1}
K_{eq}	Equilibrium constant	-
k_0	Pre-exponential factor	s^{-1}
$\dot{m}$	Mass flux	kg s^{-1}
p_i	Pressure of component i	bar
p_0	Reference pressure	bar
p_{eq}	Equilibrium pressure	bar
$\dot{Q}$	Heat flux	W
R	General gas constant	J mol^{-1} K^{-1}
T	Temperature	K
t	Time	s
X	Reacted fraction	-

Acronyms	Description
CAS	Compressed Air Storage
ENG	Expanded Natural Graphite
LOHC	Liquid Organic Hydrogen Carriers
PCM	Phase Change Material
SOFC	Solid Oxide Fuel Cell

1 Introduction

“Water will be the coal of the future.” [Translated to English from [1]]

With this ingenious and perspicacious sentence, science fiction author Jules Verne predicted already in the year 1874 what today drives scientists and engineers all around the world – the development of technologies to decarbonize our global energy system. This thesis analyses how selected coupled metal hydride systems can contribute to this in terms of energy storage. In particular, a system configuration for hydrogen storage and another configuration for the storage of electrical energy are investigated.

1.1 Motivation

Utilizing the components of water – oxygen and hydrogen – is a promising alternative to today’s energy carriers since water is available almost everywhere, while fossil energy carries are not that evenly distributed. For example most of the global coal deposits are in Europe, Eurasia, Asia-Pacific and North America [2]. Avoiding fossil sources, there are many ways to produce hydrogen such as biological processes in algae, electrolysis-, thermolysis- or photosplitting of water [3]. Hydrogen combustion is carbon free and does not emit carbon dioxide. Its energy

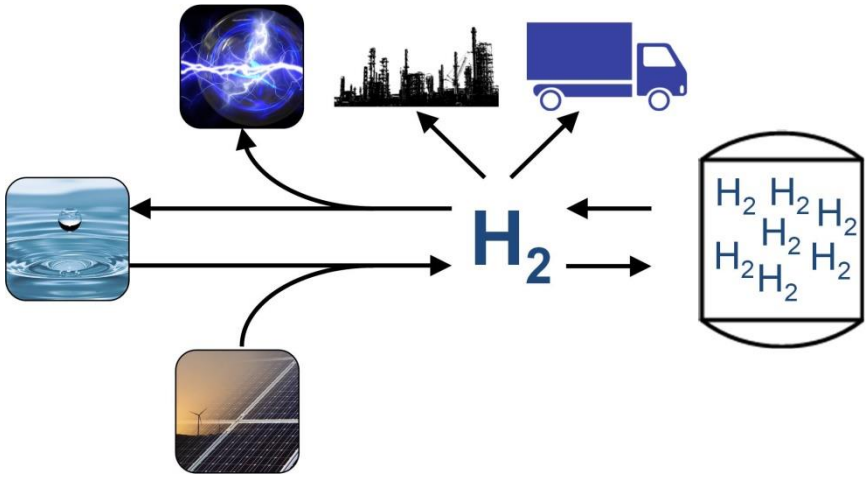

Figure 1 - Possible hydrogen cycle

density with respect to mass of 141.9 MJ kg^{-1} exceeds common fuels based on compounds with C-H bonds [4]. As Figure 1 shows, hydrogen can be used versatilely. Depending on the availability and demand of electrical energy, hydrogen can be generated or consumed for electricity. Storing the hydrogen instead of electricity, it serves as an energy storage device.

Another option is to use it as a precursor for the chemical industry [5]. In addition, hydrogen can serve as fuel to power vehicles [6]. Summing it up, hydrogen is a promising alternative to state of the art fossil fuels.

At standard conditions, hydrogen is a gas with a density of 0.08988 g L^{-1} [7]. Therefore, hydrogen storage devices would require large volumes at these conditions. Subsequently, it is beneficial for hydrogen storage to increase the density [8]. For that purpose, different approaches have been developed. First, hydrogen can be liquefied which requires cooling below its critical temperature of 33.2 K [9]. However, these vessels have to be insulated to the environment to prevent excessive evaporation during the storage time. Still, heat input from the environment cannot be avoided, hydrogen evaporates and after a certain pressure is reached, hydrogen has to be vented from the tank [10]. Second, hydrogen can be stored in its gaseous state via the compression to pressures up to 700 bar or higher. Thereby, the hydrogen density increases up to 39.3 kg m^{-3} [11]. However, the construction of these vessels requires significant effort and some authors identify safety problems [7]. In addition, both liquefaction and pressurizing to 700 bar require 21% and 15% of the hydrogen's lower heating value, respectively [12]. Therefore, the efficiency of the storage system is reduced. Third, hydrogen may be stored with physisorption on the surface of other compounds, such as carbon nanotubes, zeolites or metal organic frameworks [13] [3].

A fourth option is to store hydrogen not in its elementary form, but to convert it chemically to another compound which can be stored or transported with less effort. Several compounds such as ammonia (NH_3) [14], liquid organic carriers (LOHC) [15] or metal hydrides are being discussed for that purpose. Especially metal hydrides are promising candidates for hydrogen storage, since they combine low storage pressures with potentially high storage densities. Metal hydrides are materials that are able to interact with hydrogen. They absorb hydrogen via a chemical gas-solid reaction with the release of thermal energy. Consuming thermal energy the reaction is reversed, releasing the hydrogen again. They exhibit comparatively low storage pressures with comparatively high storage densities. Depending on the metal hydride, the hydrogen capacity is up to 7.6 wt.% for magnesium hydride or even 11.54 wt.% for $LiBH_4$-MgH_2, a reactive hydride composite [16]. Of them, magnesium hydride is of special interest, since it doesn't require rare earths or other compounds being difficult to obtain. Magnesium is the third most common ion in sea water [17] which makes it abundantly available. In addition, it is

non-toxic and it is relatively safe to operate compared to other light element hydrides which may rapidly and exothermally react with air [18]. In addition, magnesium hydride is operable at pressures of 30 bar or less, which also is a safety advantage compared to 700 bar pressure tanks. The hydrogen density in magnesium hydride of 0.11 g cm^{-3} is 50% higher compared to liquid hydrogen [18] [4].

The challenge of using chemical hydrogen storage and of magnesium hydride in particular is the reaction enthalpy of the storage reaction and the temperature level at which the reaction takes place. During hydrogen storage in magnesium, following equation (1), $\Delta_R H = 74.7$ kJ mol^{-1} [19] have to be dissipated.

$$Mg + H_2 \rightleftharpoons MgH_2 + \Delta_R H \quad (1)$$

During the reverse hydrogen release, the same amount of thermal energy has to be supplied. In addition, the temperature of the materials has to be as high as 350 °C [19]. Therefore, thermal management is of utmost importance for any application involving magnesium hydride as hydrogen storage material.

Since the heat of reaction which is released during the hydrogen storage process is required for hydrogen release, it would be beneficial to store it. Among different technologies to store thermal energy, thermochemical heat storage [20] is a promising alternative. This storage principle is similar to the hydrogen storage process itself. During hydrogen storage in MgH_2 an exothermal chemical reaction takes place which releases thermal energy. The thermochemical heat storage material uses that thermal energy to endothermally split up via another chemical reaction. For the reverse reaction the thermochemical heat storage material is recombined and thermal energy is released. That thermal energy drives the hydrogen release from the metal hydride. This behavior can be generalized for any thermal coupling of a metal hydride with another thermochemical material.

For operation, the magnesium hydride and the thermochemical heat storage material have to be in thermal contact. Therefore, they form a thermally coupled pair of thermochemical reactions. Since they only exchange thermal energy with each other, heat exchange with the environment is not necessary and the hydrogen storage system can be adiabatic in the ideal case. Therefore, the

drawback of thermal management using MgH_2 as hydrogen storage material can be avoided while maintaining the advantages of high storage capacity and low pressure.

1.2 State of knowledge

Due to the promising properties of magnesium hydride, it is under investigation for hydrogen storage for approximately 50 years. A lot of progress has been made for the synthesis and improving the thermodynamic and kinetic properties of the material [18]. Due to affinity of magnesium to oxygen and water an oxide layer and a $Mg(OH)_2$ layer may be formed on the magnesium surface, respectively [21]. Therefore, the hydrogen diffusion may be limited which decelerates the synthesis process. Synthetic techniques, such as ball-milling, can cause cracks in these surface layers making unreacted magnesium accessible for hydrogen. A major challenge for the application of magnesium hydride is its thermodynamic stability. Therefore, a lot of effort has been put into destabilizing the MgH_2 [18]. One approach is to destabilize the compound by adding other metals, such as nickel [22]. Other promising candidates are Mg-Cu-Ni-Y [23] or Mg-Sn-Zn compounds [24]. Kalinichenka *et al.* [25] synthesized $Mg_{90}Ni_{10}$ via melt spinning which is a technique to solidify the liquid alloy rapidly. They found that the material is able to dehydrogenate even at 200 °C, which is significantly lower compared to pure MgH_2 [19]. In order to enhance the thermal conductivity of the material, mixing with expanded natural graphite (ENG) is a promising option [26] [27]. Compression of the metal hydride – ENG mixture to pellets at up to 600 MPa is an option to further increase the thermal conductivity [28]. A detailed overview of different approaches to improve the thermodynamics and kinetics of MgH_2, such as nanoscaling, catalyst addition, alloying or synthetic approaches can be found in the publications by Wang and Wang [19] and Yartis *et al.* [18].

Due to its thermal properties, magnesium hydride is also under investigation for thermal energy storage applications such as concentrated solar power plants [29] [30]. However, the scope in this work is its utilization as hydrogen storage material, for which the challenge of thermal management remains [31]. Addressing that, Delhomme *et al.* [32] [33] investigated the coupling of a magnesium hydride tank with a solid oxide fuel cell (SOFC). Thereby, the hydrogen being desorbed from the MgH_2 is fed to the SOFC where electricity is generated. The SOFC stack operates between 750 and 800 °C. Therefore, the waste heat of the SOFC stack can be used to

desorb hydrogen from the magnesium hydride at 300 – 350 °C. At the same time the SOFC stack is cooled since the hydrogen desorption requires approximately 75 kJ mol^{-1}. Giap *et al.* [34] also investigated the interactions between a metal hydride tank and a reverse solid oxide fuel cell.

Besides nesting with another thermal process, it has also been investigated to use a phase-change-material (PCM) to store the heat of reaction during hydrogen absorption. For the metal hydride $LaNi_5$ this was investigated by Darzi *et al.* [35]. For magnesium hydride, the coupling with a PCM was reported by Garrier *et al.* [36] and numerically analyzed by Mellouli *et al.* [37]. During hydrogen absorption, the PCM melts and remains liquid during the storage period. For the reverse reaction, the PCM solidifies and releases the stored thermal energy. The researchers used the PCM $Mg_{69}Zn_{28}Al_3$ for that purpose, which melts/solidifies at a temperature between the desired hydrogen absorption and desorption temperature. Other PCMs that have been under investigation for that purpose are $NaNO_3$ [38] or $LiNO_3$-$3H_2O$ [39]. However, the temperature of the heat storage- and release is identical. In contrast, using a thermochemical heat storage material, that temperature is dependent on the gas pressure. Therefore, the thermochemical alternative exhibits an additional degree of freedom to enhance the processes.

The coupling of magnesium hydride for hydrogen storage with a thermochemical heat storage material has been investigated analytically by Bhouri *et al.* [40]. It can be referred as an adiabatic hydrogen storage system, since no thermal energy has to be exchanged with the environment during operation. They identified magnesium hydroxide $Mg(OH)_2$ as a potentially suited thermochemical heat storage material. It splits up into water vapor and magnesium oxide MgO according to the following reaction equation:

$$Mg(OH)_2 + \Delta_R H \rightleftharpoons MgO + H_2O \tag{2}$$

The reaction enthalpy of reaction (2) is approximately 81 kJ mol^{-1} [41]. As mentioned before, the storage/release temperature of this system can be adjusted with the gas pressure, which is an advantage compared to other thermal energy storage systems (e.g. PCMs). In their paper, the researchers derived an analytical expression for the hydrogen storage time, which is - depending on the assumptions - in the same range as the alternative with the PCM as heat storage material. Additionally, they report that the use of $Mg(OH)_2$ instead of the PCM results in a reduced mass

by factor 4. To support their analytical expression for the hydrogen storage process, Bhouri and Bürger [42] conducted a numerical study of the hydrogen storage process.

The dehydration of magnesium hydroxide to magnesium oxide and its rehydration is known for years. The behavior of the decomposition was already investigated in 1949 [43]. The reaction is especially promising for thermal applications such as thermochemical heat storage [44] [45] [46] or heat pumps [47] [48]. While the rehydration of MgO to $Mg(OH)_2$ has been investigated extensively for water vapor pressures below 1 bar [49] [50] [51], data at higher pressure is rarely reported. Only Zamengo *et al.* [48] reported data about the hydration of MgO at 3.61 bar reaching a temperature of 245 °C in their reactor at most.

Similar to magnesium hydride, the material modifications are investigated to lower the dehydration temperature of magnesium hydroxide. For example Saitou *et al.* [52] investigated sodium citrate for that purpose. Mastronardo *et al.* [53] investigated the influence of carbon nanotube on the performance for heat pump applications. A comprehensive overview over synthetic methods and material modification can be found here [54].

Concluding, the combination of magnesium hydride with magnesium hydroxide forms a system of an endothermal and an exothermal chemical reaction compensating for each other. Due to the nature of gas-solid reactions, a special characteristic of such a system is that the temperature level of the reaction can be adjusted with the gas pressure and vice versa. Besides an initial assessment [40] [42], such a system has not yet been investigated for hydrogen storage.

1.3 Theoretical background

In the previous section, the adiabatic hydrogen storage was briefly introduced which is further investigated in this thesis since it is a promising approach. It is based on the thermal coupling of two thermochemical systems. Therefore, thermochemical gas solid reactions in general and metal hydrides in particular are introduced in this section. In addition, strategies to couple two thermochemical reactions are presented. This leads to the second system investigated in this thesis which extends the thermal coupling of two materials and aims to store electric energy.

1.3.1 Thermochemical gas solid reactions

Thermochemical gas-solid reactions are chemical reactions with the main components being a gas and a solid. Commonly they can be described with the following reaction equation (3).

$$\nu_{\mathrm{A}}\mathrm{A}_{(\mathrm{s})} + \Delta_{\mathrm{R}}H_0 \rightleftharpoons \nu_{\mathrm{B}}\mathrm{B}_{(\mathrm{s})} + \nu_{\mathrm{C}}\mathrm{C}_{(\mathrm{g})} \tag{3}$$

These materials (A) are able to dissociate endothermally into a gas (B) and a solid (C). If the gas (B) is supplied to the solid residue (C) at an appropriate pressure and temperature, exothermal recombination of the reactants takes place. Therefore, during a cycle of endothermal gas release and exothermal gas consumption, these materials operate as gas source with simultaneous heat sink and gas sink with simultaneous heat source, respectively. If thermal energy is supplied to the material, gas has to be withdrawn and vice versa which is illustrated in Figure 2.

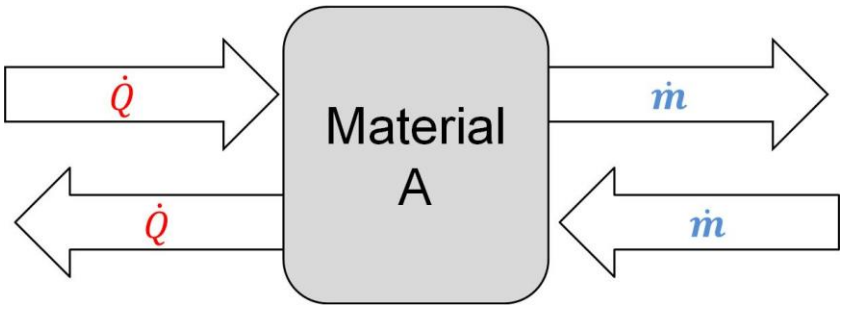

Figure 2 – Single thermochemical material. Either gas ($\dot{m}$) is supplied & heat ($\dot{Q}$) removed or vice versa.

Suppose material A is put in an evacuated and closed container. The container is then heated to a temperature which is assumed to be constant everywhere in the container and high enough for the reaction to take place. Material A will decompose according to equation (3) and a rise in the gas pressure (C) can be measured. After an infinite amount of time and in case not 100% of material

A decomposed, a constant gas pressure will be reached. That pressure is different for every temperature and material. It is commonly referred as equilibrium pressure of the material at a given temperature. At equilibrium conditions, forward- and reverse reaction occur at the same reaction rate. Therefore, it seems the reaction has stopped macroscopically.

A general condition for the chemical equilibrium is [55]:

$$\sum_{\mathrm{i}} \nu_{\mathrm{i}} \mu_{\mathrm{i}} = 0 \tag{4}$$

With μ_{i} being the chemical potential for component i. The chemical potential of an ideal gas i is defined as:

$$\mu_{\mathrm{i}}(p,T) = \mu_{0,\mathrm{i}} + RT\ln\left(\frac{p_{\mathrm{i}}}{p_0}\right) \tag{5}$$

For reaction equation (3), combining equations (4) for the chemical equilibrium and (5) for the chemical potential of the ideal gas and assuming that the chemical potential for the solids is only a function of the temperature and can therefore be incorporated into the equilibrium constant for this case $\sum_{\mathrm{i}} \nu_{\mathrm{i}} \mu_{0,\mathrm{i}} = -RT\ln(K_{\mathrm{eq}})$, yields in:

$$\nu_{\mathrm{C}} \mu_{0,\mathrm{C}} + RT\nu_C \ln\left(\frac{p_C}{p_0}\right) = 0 \tag{6}$$

With the correlation [56]

$$\sum_{\mathrm{i}} \nu_{\mathrm{i}} \mu_{0,\mathrm{i}} = \Delta_{\mathrm{R}} G_0 = \Delta_{\mathrm{R}} H_0 - T\Delta_{\mathrm{R}} S_0 \tag{7}$$

equation (6) simplifies for reaction equation (3) to

$$\nu_{\mathrm{C}} \ln\left(\frac{p_{\mathrm{C}}}{p_0}\right) = \frac{-\Delta_{\mathrm{R}} H_0}{RT} + \frac{\Delta_{\mathrm{R}} S_0}{R} \tag{8}$$

With the knowledge of $\Delta_R H_0$ and $\Delta_R S_0$ for a reaction, the pressure at equilibrium conditions can be calculated depending on the temperature. Alternatively, the thermodynamic parameters $\Delta_R H_0$ and $\Delta_R S_0$ of a reaction can be calculated from a series of experiments measuring the equilibrium pressure at different temperatures. The measured data can be plotted linearly with $\frac{1}{T}$ at the abscissa and $\nu_C \ln\left(\frac{p_C}{p_0}\right)$ at the ordinate with $p_0 = 1\ \text{atm}$. The values for $\Delta_R H_0$ and $\Delta_R S_0$ can be calculated from the slope and the intercept of that line, respectively. From equation (8) it can be seen that there is a correlation between the temperature T and gas pressure p_C. By adjusting the gas pressure, the temperature in the reactive material can be controlled and vice versa which is a key characteristic of thermochemical gas-solid reactions.

The chemical equilibrium indicates the conditions a system will exhibit after an infinite amount of time. It doesn´t allow a statement how fast a reaction proceeds. For that purpose, the reaction rate is introduced. It is dependent on the temperature, the pressure, the reaction progress and can be generally described with *X* being the reaction progress:

$$\frac{\mathrm{d}X}{\mathrm{d}t} = \mathrm{f}(T)\mathrm{h}\left(p, p_{\mathrm{eq}}\right)\mathrm{g}(X) \tag{9}$$

The three functions $\mathrm{f}(T)$, $\mathrm{h}\left(p, p_{\mathrm{eq}}\right)$ and $\mathrm{g}(X)$ can be expressed by a set of kinetic parameters and correlations. For the temperature dependence $\mathrm{f}(T)$, the Arrhenius expression is commonly used

$$\mathrm{f}(T) = k_0 * \mathrm{e}^{\frac{-E_a}{RT}} \tag{10}$$

For the pressure term $\mathrm{h}\left(p, p_{\mathrm{eq}}\right)$ and the mechanism term $\mathrm{g}(X)$ different correlations are available. Frequently used expressions for those can be found in [57] and more specialized on metal hydrides in [58]. With the knowledge of the chemical equilibrium and the reaction kinetics, the thermochemical reaction (equation (3)) can be properly described.

Since the solid decomposes into a gas and a solid, the reactants can be separated fairly easy. The reverse reaction does not take place unless the gas is supplied to the solid at an appropriate pressure and temperature. Therefore, during the period between forward and backward reaction

losses do not occur, which is especially beneficial for the long term storage of thermal energy – an application gas-solid reactions are investigated for [59].

1.3.2 Metal hydrides

Metal hydrides can be classified as thermochemical materials. Following the generalized reaction equation (3), these materials are able to reversibly react with gaseous hydrogen. Therefore, equation (3) can be written for metal hydrides, where M is a metal and MH is the metal hydride [7]:

$$\mathrm{M}_{(s)} + \frac{\mathrm{x}}{2}\mathrm{H}_{2(\mathrm{g})} \rightleftharpoons \mathrm{MH}_{\mathrm{x},(\mathrm{s})} + \Delta_{\mathrm{R}}H_0 \tag{11}$$

The reaction is exothermal for hydrogen absorption and endothermal for hydrogen desorption. A large variety of metal hydrides MH is known. An extensive overview regarding metal hydrides for hydrogen storage is presented by Sakintuna *et al.* [7]. Besides hydrogen storage, it has been investigated how the thermal features of metal hydrides can be used for air conditioning in fuel cell vehicles [60] or for their capabilities to preheat fuel cells in mobile applications [61].

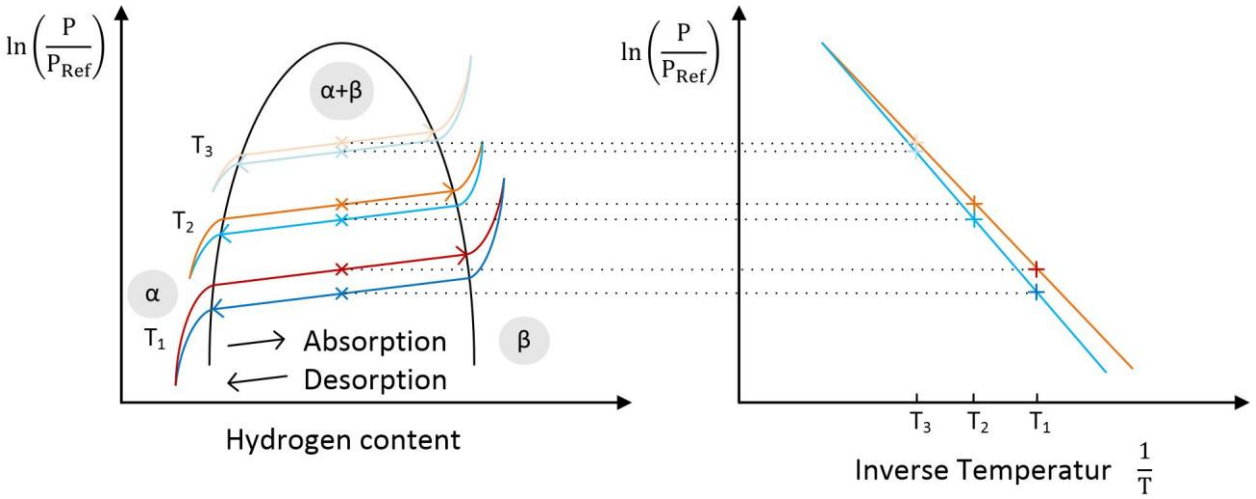

Figure 3 – Pressure-Concentration-Isotherms and van't Hoff – Qualitative illustration.

A common way to obtain equilibrium data for metal hydrides is the measurement of pressure-concentration-isotherms (PCI). Thereby, the metal/metal hydride absorbs/releases hydrogen

while the temperature is kept constant. Repeating the measurement for several temperatures and plotting the hydrogen content in the metal versus the gas pressure yields in a plot that is qualitatively shown in Figure 3. Three regions can be identified. During hydrogen absorption in the so-called α-phase, hydrogen and the metal form an interstitial solid solution. Once the solid solution is saturated, the β-phase starts to form next to the α-phase. That region is called the plateau which is ideally a horizontal line, but measurements often reveal a slope in that region. If the concentration of hydrogen in the metal is further increased, a solid solution in the β-phase is formed until all interstitial sites are occupied with hydrogen [62]. Additionally, it can be experimentally observed that the course of the PCI is different for hydrogen absorption and desorption, which may be called hysteresis. From the plateau region, the van't Hoff line can be derived as it is illustrated in Figure 3. Due to the hysteresis, separate line for absorption and desorption can be obtained.

There are several ways to classify metal hydrides. A common option is to distinguish between the way hydrogen in bound. There are hydrides which locate hydrogen atoms, not molecules [6], in the metal lattice. They can be referred as intermetallic compounds with the general formula $A_mB_nH_x$. Thereby, A and B are metals with strong and less strong affinity for hydrogen, respectively [63]. They are able to form structures such as AB_5, AB_2 or AB with examples being listed in [62]. In another class of metal hydrides, hydrogen is bound covalently to a central atom. These hydrides, such as Mg_2NiH_4, can be referred as conversion materials and exhibit higher gravimetric storage capacity compared to intermetallic hydrides [64]. In this thesis, magnesium hydride is investigated for hydrogen storage. For the experimental investigation an alloy of 90% magnesium and 10% nickel was used, which forms Mg_2NiH_4 grains of approximately 2 μm in size being finely dispersed [25]. It therefore can be classified as a conversion material with pure MgH_2 showing also ionic characteristics [6].

1.3.3 Coupled gas-solid reactions

Single thermochemical reactions have to be either supplied with gas or thermal energy while the other reaction partner has to be withdrawn, as it is illustrated in Figure 2. In contrast, coupled thermochemical reactions behave differently which is illustrated in Figure 4. This applies not only on metal hydrides but, thermochemical materials in general. Either the thermal- or the gaseous side can be coupled while the other side can be handled independently.

- Gaseous coupling: Thermal energy is supplied to material 1, gas is released, transferred to material 2 where it is absorbed and thermal energy is released and vice versa. The two materials have to be reactive with the same gas.
- Thermal coupling: If gas is supplied to Material 1, thermal energy is released, transferred to material 2 where it decomposes and releases a gas and vice versa. Since the gases do not mix, materials reacting with different gases are useable.

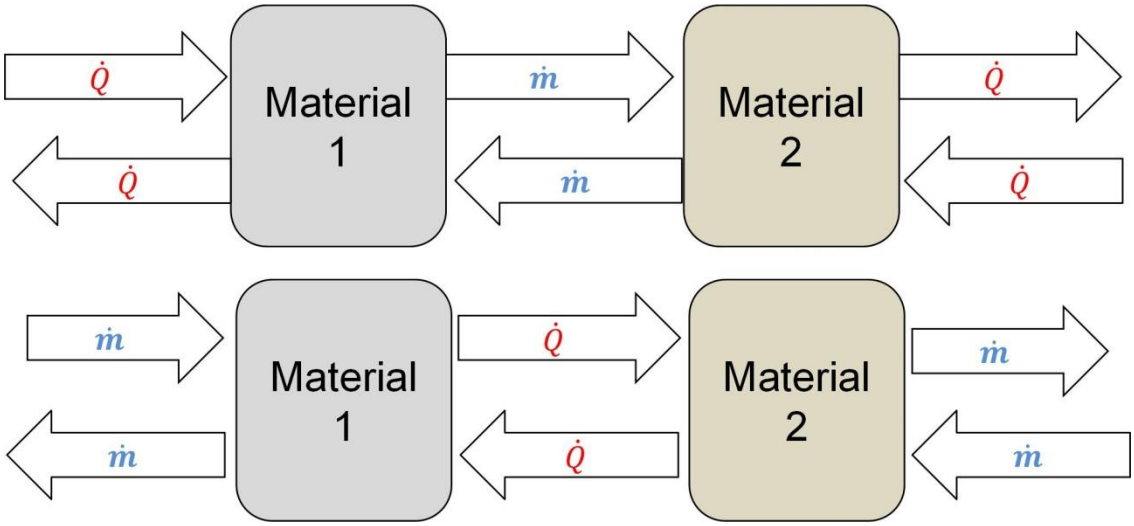

Figure 4 – Two coupled thermochemical materials. Thermal coupling: Gas ($\dot{m}$) has to be supplied and withdrawn. Coupling on the gaseous side: Thermal energy ($\dot{Q}$) has to be supplied and withdrawn.

For any kind of coupling, a pressure and temperature gradient is required for gas flux and heat transfer between the materials, respectively. The two different types of coupling are also shown in Figure 5. For the illustration, vertical and horizontal lines are shown to illustrate the required gradients. In any real system, these lines would be slightly sloped. The gaseous coupling is

qualitatively shown in Figure 5 (A). Suppose that two materials are able to operate between at least three heat reservoirs with different temperatures. The system is able to synproportionate heat from a low and a high temperature level to a medium temperature level. It can also be used to disproportionate heat from the medium level to high- and low temperature heat, as it has been investigated by Kang and Yabe [65]. More details on these processes can be found here [66]. With both synproportionation and disproportionation the two half cycles (shaded areas) may be shifted in time from each other. Since the inputted thermal energy can be released later, the setup also acts as a thermal energy storage device.

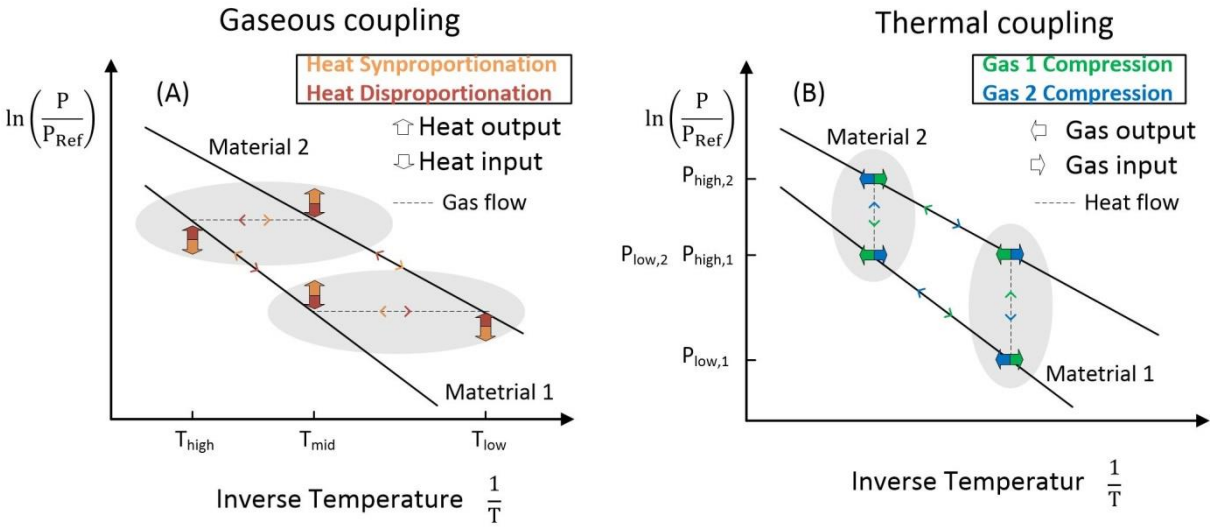

Figure 5 – Thermal and gaseous coupling – Qualitative illustration in van't Hoff plots.

Figure 5 (B) qualitatively shows the option for thermal coupling. Such a system operates between at least three reservoirs with different gas pressures. The setup can be used to compress gas 1 via the expansion of gas 2 and vice versa. Again, the half cycles (shaded areas) can be shifted in time, which makes the system also operable as gas storage. Compared to the gaseous coupled setup, materials reacting with different gases on different pressure levels are feasible, since only thermal energy is exchanged and the gases don´t mix. The thermal coupling of magnesium hydride with magnesium hydroxide will be addressed in the first part of this thesis as the adiabatic hydrogen storage system.

So far, it was demonstrated that a single thermochemical reaction consumes thermal energy and releases a gas or vice versa. As illustrated in Figure 4, two thermally coupled thermochemical systems consume gas and release gas. Two coupled reactions on the gaseous side consume thermal energy and release thermal energy. Therefore, a supply of gas or thermal energy is required from the environment. Instead of interaction with the environment, these flows can be connected as Figure 6 illustrates. Following that thought, a system that is coupled both thermally and on the gaseous side emerges.

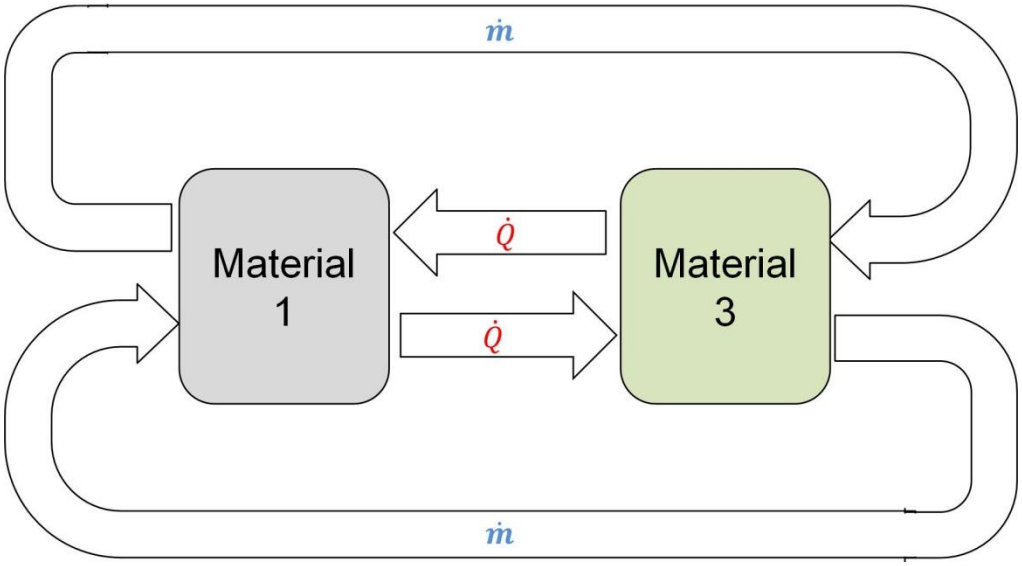

Figure 6 – Both thermal and gaseous coupling.

Such a coupled system is cut off from any external heat- or gas supply. Therefore, another possibility to interact with the environment has to be installed. This can be realized with a compression- and expansion unit as Figure 7 shows. Hydrogen can be desorbed from Material 1, compressed to a higher pressure and stored in Material 3 The thermal energy released by the absorbing gas in material 3 is transferred to material 1, where it drives the desorption. Powering the compressor, electrical energy is stored. As the hydrogen desorbs from material 3, expands in the expansion unit and absorbs in material 1, electrical energy can be regained. Again, the thermal energy released by the absorption reaction in material A drives the desorption in material 3. Hence, a double coupled thermochemical system like this is able to operate as a thermochemical battery.

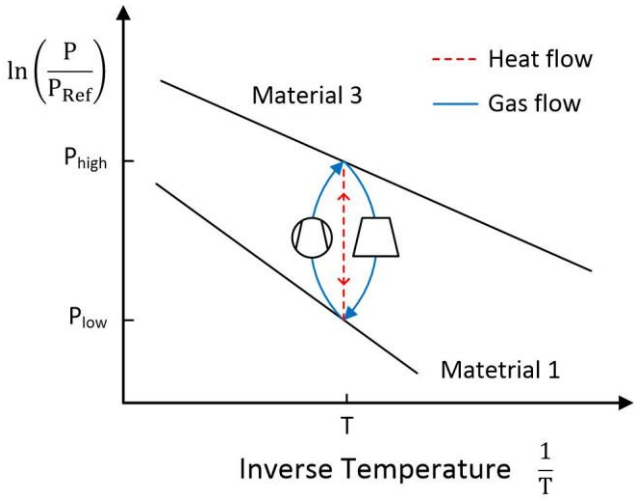

Figure 7 – Thermal and gaseous coupling – Qualitative illustration in van't Hoff plots.

For either kind of coupling that has been introduced, a few requirements for the materials emerge, since materials cannot be coupled arbitrarily. From Figure 5 and Figure 7 it can be seen that the temperature and pressures involved in the processes are strongly dependent on the material characteristics which are illustrated with the van't Hoff lines. The selection of another material results in another van't Hoff line and changes the temperatures and pressure levels of the coupled process. However, with the proper selection of materials, the desired parameters can eventually be achieved. For the materials coupled on the gaseous side, the temperature levels of the heat reservoirs are important. For heat disproportionation, thermal energy has to be transferred to the ambient at T_{low}. Therefore, the minimum temperature T_{low} in the process has to be above the temperature of the ambient. Likewise, for the thermally coupled systems the pressure levels are important. For example, gas has to be released to the environment at P_{low}. Therefore, a mass sink at that pressure level has to be available. For a gas comparatively easy to condense, such as water vapor, a condenser is beneficial for that purpose.

For the doubled coupled process, temperatures and pressures are independent of the environment. Only constrains regarding the reactor vessel have to be regarded, which is of course also the case for the singe-coupled systems.

Besides temperature- and pressure constraints, for all the coupled systems that have been introduced the reaction rate of the materials exhibits another constraint. At the selected reaction points illustrated in Figure 5 and as Figure 7, the reaction rate has to be high enough for the desired applications. While intermetallic metal hydrides, such as $LaNi_5$ are usually considered to

be comparatively fast, unmodified magnesium hydrogenates comparatively slow. Forming an alloy with nickel, which is the material that was used in this thesis, the reaction rate can be enhanced [6]. For the $Mg(OH)_2$ / MgO , which is the partner material of the MgH_2 in this thesis, it is reported that the rehydration rates are lower compared to the very similar $Ca(OH)_2$ / CaO system [46]. Therefore, the influence of the reaction rates on the coupled process is of utmost interest. Nevertheless, the reaction rates can be independently influenced with the gas pressure in the respective system.

Besides constrains involving the materials' intrinsic characteristics, the reaction vessel itself may introduce another constraint. Thermal energy and gas have to be transferred from and to the materials. To exhibit a large surface area and short pathways for the gaseous reactant, thermochemical materials often are in powdery form. Fine powders usually exhibit a poor thermal conductivity, which is why they can be mixed with expanded natural graphite (ENG) and compacted to pellets in order to increase the effective thermal conductivity, as it was done for the $Mg_{90}Ni_{10}$ alloy that was used in this thesis [26] [28]. However, compaction to pellets and ENG incorporation reduce the permeability of the material [67]. For magnesium hydroxide, Kato *et al.* [68] increased the thermal conductivity from randomly arranged pellets of 0.16 $W\,m^{-1}\,K^{-1}$ to 0.55 $W\,m^{-1}\,K^{-1}$ for arranged pellets containing expanded graphite. Therefore, heat transfer limitations can be counteracted on the material side. Other approaches are to design the reaction vessel in a way that the areas available for heat transfer from/to the reactive bed are maximized, for example with the use of capillary tube bundles [69]. In addition, reactor designs with short heat transfer distances are suited to counteract heat transfer limitations [60]. Heat- and mass transfer characteristics of a metal hydride reactor depending on several design parameters can be found in [70].

1.4 Aim of this research

In the previous sections it was described how a metal hydride can be coupled with another thermochemical material. Therefore, this thesis aims to investigate two thermally coupled systems to store hydrogen and electric energy, respectively. The first system is the thermal coupling of magnesium hydride and the $Mg(OH)_2$ / MgO system forming an adiabatic hydrogen storage. To extend the preceding analysis, the hydrogen release from the adiabatic hydrogen storage reactor shall be analyzed numerically. For that purpose, an existing model to describe the hydrogen storage of the reactor shall be extended and adapted to calculate the hydrogen release process. For hydrogen release, a supply of water vapor is necessary. Therefore, it shall be investigated how it can be supplied to the reactor at a pressure of up to 10 bar.

In addition, the coupled adiabatic hydrogen storage reactor shall be experimentally examined for the first time. The feasibility of the system has to be experimentally proven. It shall be investigated how the system's performance can be influenced with the adjustment of reaction temperatures- and pressures. For that purpose, a test bench for hydrogen- and water vapor supply at up to 10 bar as well as a prototype reactor has to be designed and constructed. Thereby, magnesium oxide shall be hydrated at 10 bar water vapor pressure which has never been investigated before.

In an additional step the coupling shall be extended to the gaseous side. Subsequently, a closed system is formed at which the two materials exchange thermal energy and gas solely with each other. A conceptual evaluation of the system for applications in energy storage shall be conducted regarding intrinsic characteristics, energy densities and efficiencies.

2 Journal publications

In the first journal publication, the thermally coupled system of magnesium hydride and magnesium hydroxide is investigated. That system is able to store hydrogen with minimal external heat management. From preceding theoretical studies, it can be concluded that the temperature levels of the two materials fit together and that the hydrogen storage process is feasible. This publication analyzes the hydrogen release from the adiabatic hydrogen storage reactor. Therefore, a model was set up and numerical studies were performed. For hydrogen release, water vapor has to be supplied for the hydration of MgO to $Mg(OH)_2$. Heat transfer to the magnesium hydride takes place and hydrogen is released with an endothermal reaction (2). The publication covers possible system integration for the supply of water vapor at a pressure of up to 10 bar using a high temperature PEM fuel cell.

Paper I

Adiabatic magnesium hydride system for hydrogen storage based on thermochemical heat storage: Numerical analysis of the dehydrogenation

Michael Lutz, Maha Bhouri, Marc Linder, Inga Bürger

Applied Energy

Volume 236, 15 February 2019, Pages 1034-1048

https://doi.org/10.1016/j.apenergy.2018.12.038

Applied Energy 236 (2019) 1034–1048

Contents lists available at ScienceDirect

Applied Energy

journal homepage: www.elsevier.com/locate/apenergy

Adiabatic magnesium hydride system for hydrogen storage based on thermochemical heat storage: Numerical analysis of the dehydrogenation

Michael Lutz[a,*], Maha Bhouri[b], Marc Linder[a], Inga Bürger[a]

[a] Institute of Engineering Thermodynamics, German Aerospace Center (DLR), Pfaffenwaldring 38-40, D-70569 Stuttgart, Germany
[b] Department of Mechanical Engineering, Dalhousie University, Halifax, NS B3H 4R2, Canada

HIGHLIGHTS

- Hydrogen release from a novel storage reactor with high capacities at low pressures.
- Coupled magnesium hydride dehydrogenation and magnesium oxide hydration feasible.
- Water vapor supply to the storage reactor at 10 bar and 350 °C possible.
- Dehydrogenation rate dependent on the vapor supply-pressure.
- Magnesium hydride dehydrogenation reaction fast enough for stationary applications.

GRAPHICAL ABSTRACT

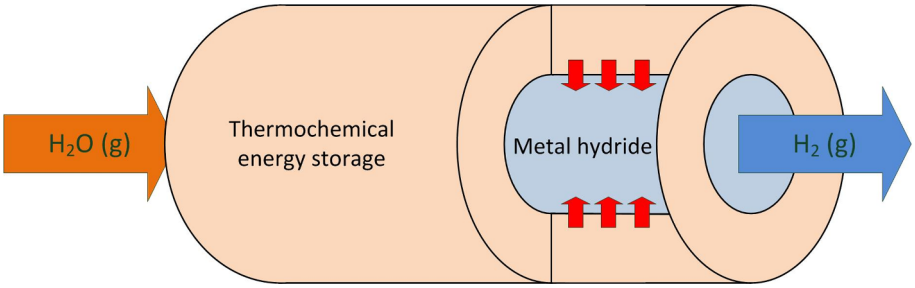

ARTICLE INFO

Keywords:
H_2 storage
Thermochemical heat storage
Magnesium hydride
Magnesium oxide
Dehydrogenation
Numerical study

ABSTRACT

With hydrogen becoming more and more important as storage and carrier for renewable energy, there is an increasing need for flexible and efficient storage technologies. However, existing technologies, such as liquefaction or compression, often require a significant share of the hydrogens lower heating value. High-temperature metal hydrides (HT-MHs), such as magnesium hydride, are a promising alternative. Due to high operation temperatures, their application is challenging. A novel adiabatic hydrogen storage reactor based on the combination of a HT-MH with a thermochemical energy storage system (TCSS), such as $Mg(OH)_2/MgO + H_2O$, can be a solution. In this work, the previously published numerical simulations for hydrogen absorption are extended to the desorption process. A two-dimensional model for the hydrogen release was set up. The performance of the storage reactor is strongly dependent on the thermodynamic equilibrium of the reactions involved and less dependent on the reaction kinetics. Dehydrogenation is possible within 132 min, which is in the vicinity of the hydrogenation time. To enhance the dehydrogenation process, the water vapor pressure can be adjusted aiming for higher temperatures during the MgO hydration. Hydrogen can either be provided at constant pressure or constant mass flow rate.

1. Introduction

The fraction of renewable energy sources in the power grid is increasing continuously. Since their input power is fluctuating, energy storage becomes necessary to buffer times of peak power input. One possibility to use electrical excess energy in the power grid is its conversion to chemical energy using power-to-gas [1] with the electrolysis of water and the storage of the resulting hydrogen as an exemplary technology. For this purpose, Kavadias et al. [2] investigated an energy storage system based on hydrogen. Besides that, there are other

* Corresponding author.
E-mail address: michael.lutz@dlr.de (M. Lutz).

https://doi.org/10.1016/j.apenergy.2018.12.038
Received 12 September 2018; Received in revised form 15 November 2018; Accepted 7 December 2018

Nomenclature

C_p	heat capacity at constant pressure (J kg^{-1} K^{-1})
E_a	activation energy (J mol^{-1})
k_0	pre-exponential factor (s^{-1})
h	heat transfer coefficient (W m^{-2} K^{-1})
M	molar mass (g mol^{-1})
$\dot{m}$	mass source/sink (kg m^{-3} s^{-1})
n	amount of substance (mol)
$\vec{n}$	normal vector (–)
P	pressure (Pa)
P_{el}	electrical power (W)
$\vec{q}$	heat transfer rate via heat-conduction (W)
$\dot{Q}$	volumetric heat source/sink rate (W m^{-3})
R	universal gas constant (J mol^{-1} K^{-1})
t	time (s)
T	temperature (K)
T_M	melting temperature (K)
$\vec{u}$	gas velocity (m s^{-1})
w_{H2}	mass fraction of H_2 in MgH_2 (–)
x_h	hydrogenated fraction of Mg $x_h = n_{MgH2}/(n_{MgH2} + n_{Mg})$ (–)
y_h	hydrated fraction of $Mg(OH)_2$ (–)
ΔH_r	reaction enthalpy (J mol^{-1})
ΔS_r	reaction entropy (J mol^{-1} K^{-1})
ε	bed porosity (–)
θ	kinetic factor (–)
Φ	mixing ratio (–)
κ	permeability (m^2)
λ	thermal conductivity (W m^{-1} K^{-1})
μ	dynamic viscosity (kg s^{-1} m^{-1})
ρ	density (kg m^{-3})

Subscripts

eq	equilibrium
g	gaseous phase
HD	hydrogen domain; MgH_2/Mg compartment
eff	effective
s	solid phase
SD	steam domain; MgO/$Mg(OH)_2$ compartment

Acronyms

Bdry	boundary
HT-PEM	high temperature proton exchange membrane fuel cell
MH	metal hydride
PCM	phase change material
PEM	proton exchange membrane
Ref	reference
TC	thermocouple
TCM	thermochemical material
TCSS	thermochemical energy storage system

approaches of energy storage for this purpose. Zhang et al. [3] compared photovoltaic hydrogen – and battery energy storage systems. They found that, depending on the presumptions of the scenario, hydrogen storage may perform better than battery storage. The stored hydrogen can be used as a precursor for the chemical industry or as energy carrier itself. Due to its low density at ambient conditions of 0.08988 g L^{-1} [4], hydrogen storage is challenging. One possibility to increase the volumetric storage density, hydrogen may be stored in liquid- or in gaseous state compressed up to 700 bar. But hydrogen liquefaction and compression to 700 bar can require up to 40% and 15% of the hydrogen lower heating value, respectively [5]. Therefore, the efficiency of the storage system is reduced significantly.

Besides that, hydrogen can be stored utilizing metal hydrides. Thereby, hydrogen is stored within a chemical compound. Depending on the metal hydride, storage densities vary. High storage densities can be achieved using magnesium hydride, MgH_2, with up to 7.6 wt% [6], or using a $LiBH_4$–MgH_2 composite system with up to 11 wt% [7]. A significant advantage is that the system pressure is more than one order of magnitude lower than in a 700 bar compressed hydrogen tank. The drawback of these metal hydrides systems is that they require an operation temperature of more than 588 K [8] for sufficiently fast hydrogen storage and release. Intensive research has been conducted to reduce the operating temperature and to improve the reaction kinetics. Wang and Wang [6] summarized several strategies regarding MgH_2 including alloying, nanoscaling and catalyst addition. They reported that the drawback of these methods is a reduced overall storage capacity.

Another approach to utilize high-temperature metal hydrides is their thermal integration into an external system. Delhomme et al. [9] used the hydrogen originating from a MgH_2 storage reactor to power a solid oxide fuel cell (SOFC). Since a SOFC operates at more than 750 °C, its waste heat is suited to be used for further MgH_2 dehydrogenation. But thermal integration into an existing system limits the applicability of a metal hydride significantly, as the boundary conditions of the integration partner have to be considered. Those could be the power or the temperature level of the heat required/released, or the heat transfer between the external system and the metal hydride.

This is why a new approach to utilize high-temperature metal hydrides is investigated. We incorporate a water based thermochemical energy storage system (TCSS) within the hydrogen storage unit in a way that the metal hydride storage reactor can be operated independently from external heat management or other processes. The heat of hydrogen absorption is stored within the TCSS. During energy storage, the thermochemical material (TCM) decomposes and releases water vapor. The TCSS provides the previously stored thermal energy if the hydrogen shall be released from the storage reactor. Therefore, water vapor has to be supplied to the decomposed thermochemical material to reverse the energy storage reaction, but no external heat management is required. In the ideal case, the system is adiabatic to the environment and the water vapor can be provided by system integration with e.g. a fuel cell.

Compared to other strategies for thermal energy storage within a metal hydride storage reactor, such as a phase change material (PCM) [10,11], the proposed system shows a higher volumetric storage density, is significantly more lightweight, and has an additional degree of freedom to enhance the hydrogen storage and release processes [12,13].

In previous works, the feasibility and limitations of the new storage reactor were analyzed analytically [12]. In an additional study, its hydrogen absorption behavior has been investigated numerically [13]. It was demonstrated that the storage reactor can be filled with hydrogen within 150 min, which is sufficient for stationary applications. This paper provides a numerical analysis of the hydrogen release from the storage reactor aiming for a hydrogen desorption time in the vicinity of the hydrogen absorption time. Additionally, the water supply to the thermochemical storage media and the influence of the water vapor pressure on the overall hydrogen release are discussed.

2. Materials and operating principle

The aim of the novel hydrogen storage system is to utilize the high storage capacity of a high-temperature metal hydride for hydrogen storage without any external heat management and at a low operating pressure. Therefore, the heat of the absorption reaction of the selected metal hydride (MH) has to be stored within the same reactor using a

suitable thermochemical material (TCM).

In the first analysis [12], magnesium hydride MgH_2 was selected as a high-temperature metal hydride with high gravimetric hydrogen storage density. It is formed according to the following equation with a standard reaction enthalpy of $\Delta H_{r,MH} = 75$ kJ mol^{-1} [13]:

$$Mg + H_2 \rightleftharpoons MgH_2 + \Delta H_{r,MH} \quad (1)$$

Since the heat of the absorption reaction of magnesium hydride should be stored within the system, a suitable heat storage material has to be selected and the two storage media have to be thermally connected. The operating temperature range of the heat storage material has to match the temperature levels at which hydrogen is absorbed and released, respectively. Thermochemical heat storage systems, utilizing gas-solid reactions, are beneficial for this purpose since the reaction products can be separated easily because only the solid and water vapor are involved. In the initial study it was found that the temperatures of the dehydration of magnesium hydroxide $Mg(OH)_2$ and hydration of magnesium oxide, MgO fit well to the temperature levels of the magnesium hydride absorption and desorption reactions. The standard reaction enthalpy of this reaction is $\Delta H_{r,TCS} = 81$ kJ mol^{-1} [12]

$$Mg(OH)_2 + \Delta H_{r,TCS} \rightleftharpoons MgO + H_2O \quad (2)$$

Once there is a hydrogen demand, reactions (1) and (2) are reversed. Water vapor is added to magnesium oxide MgO, and the previously stored energy is released via the hydration of MgO. This energy is used to enable the dehydrogenation of MgH_2. In order to enable heat transfer between the two materials, they have to be thermally connected and the temperature level of the energy releasing reaction has to exceed the temperature of the energy consuming reaction. Hence, for hydrogen release from the storage reactor, the hydration of MgO has to proceed at a higher temperature than the dehydrogenation of MgH_2.

The idea to store the heat of reaction of a high-temperature metal hydride in general is not new. Indeed, the combination of a high-temperature metal hydride and a phase change material (PCM) for energy storage was first investigated by Garrier et al. [10]. The authors demonstrated that the heat of reaction of hydrogen absorption can be stored within the PCM. Hence, operation of the tank without external energy sources was possible [11].

Nevertheless, the use of a thermochemical material (TCM) instead of a PCM as heat storage media has two advantages. First, the energy density of a TCSS per mass is higher than the one of a PCM system [14]. And second, the temperature level at which the energy is stored or released is not fixed to the melting temperature of the PCM. Instead, the temperature can be chosen within certain boundaries, which can result in faster H_2 charging/discharging rates as discussed in [13].

The second point is illustrated in Fig. 1, where the temperature and pressure correlations are shown qualitatively. The performance of a system storing the heat of reaction during hydrogen absorption is strongly dependent on the heat transfer between the metal hydride and the energy storage media [11–13]. Hence, the question arises how to enhance heat transfer between the materials. For a rapid heat transfer, a high temperature gradient between the two storage media is beneficial. For hydrogen storage, the temperature at which the metal is hydrogenated has to be higher than the temperature of the energy storage media – and vice versa for the hydrogen release. The temperature of the metal hydride is dependent on the hydrogen pressure. By varying the pressure, the equilibrium temperature, which is the maximum temperature that can be reached, can be adjusted. But the operating pressure cannot be chosen arbitrarily since there may be restriction from the application: It is limited to the hydrogen supply pressure for the absorption and to the requirements of the system using the hydrogen after its release, such as a fuel cell (compare Fig. 1(A), left).

The temperature of storing and releasing energy of a PCM is limited to its melting – and solidification temperature, respectively. Therefore, this temperature level cannot be changed from the hydrogen storage (heat storage) to hydrogen release (heat release). This is illustrated in Fig. 1(A) right). Subsequently, the operating conditions of the metal hydride compartment have to be chosen in a way that the temperature gradient can be established.

To establish a higher temperature gradient, it would be beneficial if the temperature level of the heat storage material can be varied as well. A PCM does not exhibit this feature, but a thermochemical material

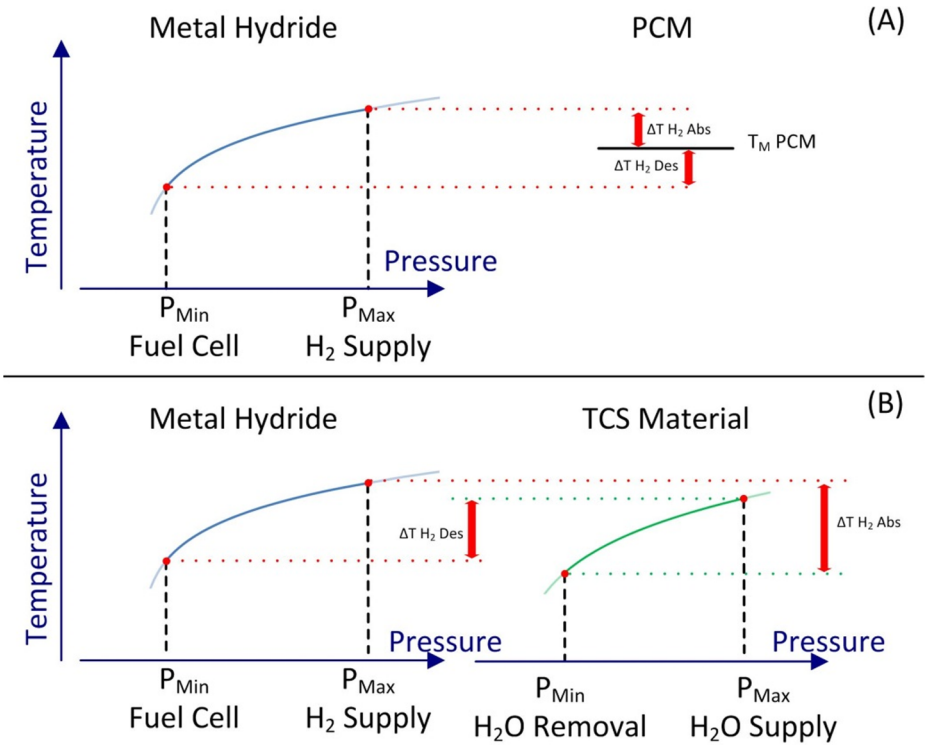

Fig. 1. Heat storage/release during H_2 absorption/desorption. Comparison of PCM and TCM as thermal energy storage media.

does. For our chosen system, the temperature level at which heat is stored is dependent on the water vapor pressure. This is demonstrated in Fig. 1(B) with the two pressure dependent curves of the MH and the TCM. Therefore, the water vapor pressure is an additional degree of freedom to increase the temperature gradient, as the temperature levels of both the metal hydride and the TCM can be varied.

3. Model description

3.1. Setup and assumptions

This new storage reactor has the potential to utilize MgH_2 for hydrogen storage at a low pressure and without external heat management. As a first attempt to investigate the H_2 release process in this new storage rector, a numerical study was conducted, which enables to predict the dynamic behavior of the two storage media. Analogous to the model in [13], a two-dimensional model was set up and solved with the COMSOL Multiphysics® software, version 5.3. The storage reactor is modeled as a double-walled cylinder, separating the metal hydride and the TCM. The geometry and dimensions are shown in Fig. 2. The choice of the storage system dimensions were discussed in Ref. [12], originating from a comparison with the storage concept involving a PCM as thermal energy storage media to be combined with the MgH_2 material. The values are reported in Fig. 2.

The model considers the following physical effects:

- Thermodynamics and reaction kinetics of the MgH_2 dehydrogenation and MgO hydration,
- Heat transfer within the reactive beds and between them,
- Mass transport within the porous beds,
- Density of the reactive solids as a function of chemical reaction progress,
- Temperature dependence of heat capacities at constant pressure of the solids involved,
- Temperature dependence of hydrogen and water vapor properties (density, heat capacity at constant pressure, dynamic viscosity).

Furthermore, the model includes the following simplifications and assumptions:

- The bed porosities are uniform and do not change with the reaction progress (ε = const),
- Local thermal equilibrium is assumed. Hence, the solid phase and gas phase have the same temperature, locally,
- The porosity and tortuosity of the particles are disregarded,
- Bed aging is neglected,
- The storage reactor is adiabatic to the environment, which is a main feature of the storage reactor,

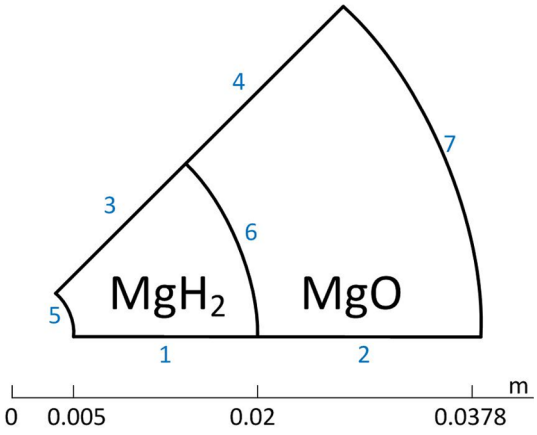

Fig. 2. 2D-Model geometry and boundaries (1–7).

- The equation of state for both the hydrogen and water vapor are given by the ideal gas law,
- The heat transfer resistance across the thin steel-wall between the beds (boundary 6 in Fig. 2) is neglected. This assumption is justified since the thermal conductivity of the steel-wall is higher than the thermal conductivity of the adjacent porous media. Therefore, the heat transfer coefficient between the porous media and the steel wall is set to $h = 10,000\ \mathrm{W\ m^{-2}\ K^{-1}}$ [15]. Subsequently, the temperatures of the porous beds at both sides of the wall are identical,
- Expansion and contraction of the reactive beds are disregarded,
- Heat transfer via radiation is neglected. Nilles [16] concluded after an extensive literature review, that radiation has only a minor influence on the heat transfer in a porous bed up to a temperature of 600 K.

3.2. Reaction kinetics and thermodynamics

The equilibrium pressure in the magnesium hydride bed is calculated with the well-known Van't Hoff equation with the values $\Delta H_{r,HD}$ and $\Delta S_{r,HD}$ referring to the MgH_2 dehydrogenation reaction

$$\frac{P_{eq,H2}}{P_{ref}} = \exp\left(\frac{-\Delta H_{r,HD}}{R\cdot T_{HD}} - \frac{-\Delta S_{r,HD}}{R}\right) \tag{3}$$

with the reference pressure being $P_{ref} = 1$ bar. The reaction kinetics of the MgH_2 dehydrogenation was investigated by Chaise et al. [17]. They found that the dehydrogenation kinetics can be described with the following equation

$$\frac{dx_h}{dt} = 2k_{0,HD}\cdot\frac{x_h}{(-\ln(x_h))^{0.5}}\cdot\ln\left(\frac{P_{eq,H2}}{P_{H2}}\right)\cdot\exp\left(\frac{-E_{a,HD}}{R\cdot T_{HD}}\right) \tag{4}$$

For the equilibrium pressure of the magnesium oxide hydration reaction, data reported by Kato et al. [18] is used

$$P_{eq,H2O} = \exp\left(\frac{-9377}{T} + 15.067\right) \tag{5}$$

This is a numerical value equation at which the value of T has to be inserted in K and the return-value $P_{eq,H2O}$ has the unit MPa.

For the magnesium oxide hydration kinetics, little data is available in the literature – especially at elevated water vapor pressures greater than 1 bar. For a sufficiently high reaction temperature in the MgO bed, the hydration reaction has to proceed at $P_{H2O} > 1$ bar. To the best of our knowledge, there is no kinetic data available for this pressure range. Therefore, the kinetic term to be used in the simulations was estimated for this study. In general, the reaction rate of a gas-solid reaction is influenced by the temperature f(T), the gas pressure h(P, $P_{eq}(T)$) and the conversion g(y_h) [19]

$$\frac{dy_h}{dt} = f(T_{SD})\cdot h(P, P_{eq}(T_{SD}))\cdot g(y_h) \tag{6}$$

with the subscript SD referring to the $MgO/Mg(OH)_2$ compartment. The temperature dependence can be described with the Arrhenius equation [19]:

$$f(T_{SD}) = k_{0,SD}\cdot\exp\left(\frac{-E_{a,SD}}{R\hat{A}\cdot T_{SD}}\right) \tag{7}$$

Kato et al. [18] investigated the MgO hydration kinetics in the temperature range from 373 K to 423 K and within water vapor pressures of 12.3–47.4 kPa. They proposed a model with a negative activation energy which means that the reaction rate reduces with elevating temperatures. While their model is suitable to describe the hydration kinetics in their specified temperature- and pressure ranges, extrapolation to higher temperatures and pressures is not possible. Due to the negative temperature dependency their model predicts little to no reaction occurring at higher temperatures and elevated water vapor

pressures. That is why we use the values reported by Bratton and Brindely [20] for the activation energy, $E_{a,SD}$ and the pre-exponential factor, $k_{0,SD}$. They investigated the vapor phase hydration of magnesium oxide within 351–371 K and water vapor pressures between 36 and 76 kPa. Their model uses the Arrhenius approach to describe the temperature dependence of the reaction rate. The activation energy and the pre-exponential factor are obtained from a linear plot of the logarithmic reaction rate versus the reciprocal temperature. The activation energy is calculated with the slope of this plot and the pre-exponential factor with its y-axis intercept. Since the relationship is linear an extrapolation to higher temperatures is simple. Even though the values of the activation energy and the pre-exponential factor should theoretically be not affected by the extrapolation, the authors are aware that the extrapolation adds some uncertainties to the model. However, since kinetic data is scarce for lower pressure and for higher pressure not available at all, the approach seems reasonable for the objective of this work but should be experimentally addressed in the future.

For the pressure term, the following equation is used

$$h(P, P_{eq}(T_{SD})) = \ln\left(\frac{P_{H2O}}{P_{eq,H2O}(T_{SD})}\right) \tag{8}$$

The pressure term reduces the reaction rate, since it is smaller than unity if the water vapor pressure, P_{H2O} does not exceed 2.7 times the equilibrium pressure, $P_{eq,H2O}(T_{SD})$. This is the case for most of the simulations. For the influence of the conversion, we choose

$$g(y_h) = 1 - y_h \tag{9}$$

which corresponds to a first order chemical reaction. Common approaches for the influence of the conversion on the reaction rate of gas-solid reactions are the Avrami–Erofeev model or the contracting sphere model. Depending on the conversion, these models often yield in $g(y_h) > 1$ [19]. We choose the first order approach here, because for every y_h, $g(y_h)$ is smaller than unity. Hence, it reduces the reaction rate during the course of reaction and is therefore a conservative assumption.

Even though the extrapolation of the temperature dependence adds uncertainties to the model, the estimation of the overall reaction rate equation was done in a conservative way. Hence, hydration reaction rate is generally underestimated which yields in a poorer performance of the storage reactor.

3.3. Heat- and mass transport

The metal hydride bed and the TCM are modeled powders being compressed into pellets. The energy equation used to describe the heat transport in the MgH_2 compartment (HD) and the MgO compartment (SD) is

$$(\rho C_p)_{eff}\frac{\partial T}{\partial t} + (\rho C_p)\vec{u}\nabla T + \nabla\vec{q} = \dot{Q} \tag{10}$$

with

$$\vec{q} = -\lambda_{eff}\nabla T \tag{11}$$

and

$$(\rho C_p)_{eff} = \varepsilon\rho_g C_{p,g} + (1-\varepsilon)\rho_s C_{p,s} \tag{12}$$

The energy source/sink term $\dot{Q}$ is calculated depending on the reaction kinetics. For the Mg/MgH_2 reaction, it is given by:

$$\dot{Q}_{HD} = \rho_{bed,HD,ini}\cdot(1 - wt_{ENG})\cdot w_{H2}\cdot\frac{\Delta H_{r,HD}}{M_{H2}}\cdot\frac{dx_h}{dt} \tag{13}$$

and for the MgO/$Mg(OH)_2$ reaction, its expression is

$$\dot{Q}_{SD} = \rho_{bed,EM8,SD,ini}\cdot\frac{\phi}{1+\phi}\cdot\frac{\Delta H_{r,SD}}{M_{Mg(OH)2}}\cdot\frac{dy_h}{dt} \tag{14}$$

The mass balance of the gaseous phase within the porous media is given by

$$\frac{\partial}{\partial t}(\varepsilon\rho_g) + \nabla(\rho_g\vec{u}) = \dot{m} \tag{15}$$

at which the gas velocity is calculated with the Darcy Law

$$\vec{u} = -\frac{\kappa}{\mu}\nabla P \tag{16}$$

and the mass source/sink term $\dot{m}$ for the two storage media is

$$\dot{m}_{HD} = \rho_{bed,HD,ini}\cdot(1 - wt_{ENG})\cdot w_{H2}\cdot\frac{dx_h}{dt} \tag{17}$$

$$\dot{m}_{SD} = -\rho_{bed,EM8,SD,ini}\cdot\frac{\phi}{1+\phi}\cdot\frac{dy_h}{dt} \tag{18}$$

Note that for the calculation of the released heat $\dot{Q}_{SD}$ and consumed mass $\dot{m}_{SD}$ in the MgO compartment, the apparent density values of the $Mg(OH)_2$ pellets $\rho_{bed,EM8,SD,ini}$ were used. This was done in order to have the same amount of heat and mass involved as in the absorption study [13] allowing for a direct comparison of the results.

3.4. Material properties

3.4.1. Gases

The gaseous phases present in the studied system are hydrogen for the MgH_2 domain and water vapor for the MgO domain. The density of these gases is a function of the pressure and temperature $\rho_g = f(T, P)$, according to the ideal gas law. The dynamic viscosity and heat capacity at constant pressure are both function of the temperature, $\mu_g = f(T)$ and $C_{p,g} = f(T)$, respectively. Their corresponding expressions can be found in [21].

3.4.2. Solids

The solid phases change in composition during the course of the reaction. Therefore, their properties change as well. The heat capacity at constant pressure for the MgH_2 bed is calculated as

$$C_{p,s,HD} = C_{p,MgH2}\cdot x_h + C_{p,Mg}\cdot(1 - x_h) \tag{19}$$

The efficiency of a thermochemical system in terms of heat storage capacity can be improved by material modifications, or through novel production methods [22,23]. To model the transport phenomena taking place in the MgO bed, we use the material data for modified MgO reported by Kato et al. [24]. In order to increase the thermal conductivity of a magnesium hydroxide bed, they modified the pure material with expanded graphite. Data is reported for a mass mixing ratio of $Mg(OH)_2$ and expanded graphite of 8:1; hence, the mixing ratio is $\phi = 8$. We use the data for the modified material being compressed into pellets which are arranged in piles.

$$C_{p,s,SD} = (C_{p,MgO}\cdot(1 - y_d) + C_{p,Mg(OH)2}\cdot y_d)\frac{\phi}{1+\phi} + C_{p,Graphite}\cdot\frac{1}{1+\phi} \tag{20}$$

The density change of the solids with the course of the reactions is calculated as

$$\frac{\partial\rho_{s,HD}}{\partial t} = (\rho_{s,MgH2} - \rho_{s,Mg})\frac{\partial x_h}{\partial t} \tag{21}$$

$$\frac{\partial\rho_{s,SD}}{\partial t} = (\rho_{s,EM8,Mg(OH)2} - \rho_{s,EM8,MgO})\frac{\partial y_h}{\partial t} \tag{22}$$

All parameters used in the simulations are listed in Table 1. Some of the parameters were calculated with data reported in the literature. For the MgO bed porosity, the EM8 data of the hydrated material reported by Kato et al. [24] was used. Since a constant bed porosity was assumed, we used the value of $\varepsilon_{SD} = (\rho_{s,EM8,Mg(OH)2} - \rho_{bed,EM8,SD,ini})/\rho_{s,EM8,Mg(OH)2} = 0.32$. As the density of bulk MgO is greater that the bulk density of $Mg(OH)_2$, we

Table 1
Parameters used in the simulations.

Parameter	Symbol	Value	Unit	Reference
MgH_2/Mg bed				
Activation energy MgH_2 dehydrogenation	$E_{a,HD}$	41	kJ mol^{-1}	[17]
Pre-exponential factor MgH_2 dehydrogenation	$k_{0,HD}$	10	s^{-1}	[17]
Reaction enthalpy of MgH_2 dehydrogenation	$\Delta H_{r,HD}$	75	kJ mol^{-1}	[17]
Reaction entropy of MgH_2 dehydrogenation	$\Delta S_{r,HD}$	135.6	J mol^{-1} K^{-1}	[17]
Heat capacity at constant pressure MgH_2	$C_{p,MgH2}$	f(T_{HD})	J kg^{-1} K^{-1}	[25]
Heat capacity at constant pressure Mg	$C_{p,Mg}$	f(T_{HD})	J kg^{-1} K^{-1}	[26]
Heat capacity at constant pressure H_2	$C_{p,H2}$	f(T_{HD})	J kg^{-1} K^{-1}	[21]
Permeability hydrogen – porous medium HD	κ_{HD}	$5 \cdot 10^{-14}$	m^2	Estimated
Dynamic viscosity hydrogen	μ_{H2}	f(T_{HD})	kg s^{-1} m^{-1}	[21]
Density hydrogen	ρ_{H2}	f(T_{HD}, P_{HD})	kg m^{-3}	[21]
Solid density MgH_2	$\rho_{s,MgH2}$	1649	kg m^{-3}	Calculated
Solid density Mg	$\rho_{s,Mg}$	1973	kg m^{-3}	Calculated
Molar mass hydrogen	M_{H2}	2	g mol^{-1}	[12]
Apparent bed density MgH_2 at t = 0 s	$\rho_{bed,HD,ini}$	1138	kg m^{-3}	[27]
Bed porosity	ε_{HD}	0.31	–	[17]
Mass fraction of H_2 in MgH_2	w_{H2}	0.06	–	[17]
Effective thermal conductivity MgH_2/Mg bed	$\lambda_{eff,SD}$	4.2	W m^{-1} K^{-1}	[17]
ENG content MgH_2 discs	wt_{ENG}	5	wt.%	[17]
MgO/$Mg(OH)_2$ bed				
Activation energy MgO hydration	$E_{a,SD}$	74.475	kJ mol^{-1}	[20]
Pre-exponential factor MgO hydration	$k_{0,SD}$	$3 \cdot 10^5$	s^{-1}	[20]
Reaction enthalpy of MgO hydration	$\Delta H_{r,SD}$	81	kJ mol^{-1}	[18]
Heat capacity at constant pressure MgO	$C_{p,MgO}$	f(T_{SD})	J kg^{-1} K^{-1}	[28]
Heat capacity at constant pressure $Mg(OH)_2$	$C_{p,Mg(OH)2}$	f(T_{SD})	J kg^{-1} K^{-1}	[29]
Heat capacity at constant pressure Graphite	$C_{p,Graphite}$	f(T_{SD})	J kg^{-1} K^{-1}	[30]
Heat capacity at constant pressure Steam	$C_{p,Steam}$	f(T_{SD})	J kg^{-1} K^{-1}	[21]
Permeability steam – porous medium SD	κ_{SD}	$5.75 \cdot 10^{-14}$	m^2	Estimated
Dynamic viscosity steam	μ_{Steam}	f(T_{SD})	kg s^{-1} m^{-1}	[21]
Density steam	ρ_{Steam}	f(T_{SD}, P_{SD})	kg m^{-3}	[21]
Density EM8 particles $Mg(OH)_2$	$\rho_{s,EM8,Mg(OH)2}$	1056	kg m^{-3}	[24]
Density dehydrated EM8 particles	$\rho_{s,EM8,MgO}$	1529	kg m^{-3}	Calculated
Apparent bed density at t = 0 s	$\rho_{bed,EM8,SD,ini}$	714	kg m^{-3}	[24]
Initial amount of MgO	$n_{MgO,ini}$	10,942	mol m^{-3}	Calculated
Bed porosity	ε_{SD}	0.32	–	Calculated
Molar mass H_2O	M_{H2O}	18	g mol^{-1}	Calculated
Molar mass $Mg(OH)_2$	$M_{Mg(OH)2}$	58.3	g mol^{-1}	Calculated
Effective thermal conductivity MgO/$Mg(OH)_2$ bed	$\lambda_{eff,SD}$	0.55	W m^{-1} K^{-1}	[24]
Mixing ratio of graphite in $Mg(OH)_2$ pellets	ϕ	8	–	[24]

used this fraction to calculate the bulk density of the dehydrated EM8 $\rho_{s,EM8,MgO}$. For the calculation of the initial amount of MgO, data reported by Kato et al. [24] was used.

3.5. Initial- and boundary conditions

This analysis aims at investigating the hydrogen release from the storage reactor. The boundary conditions are related to the process where hydrogen is required. In the present study, we assume that hydrogen will be used to feed a PEM fuel cell. Unless specified otherwise, the following initial- and boundary conditions are used in the simulations for the reference case. The numbering of the boundaries (Bdry) follows the denomination in Fig. 2.

The pressure at which the hydrogen is released is set to $P_{HD,Bdry5} = 1$ bar. The water vapor is supplied to the MgO bed at $P_{SD,Bdry7} = 5$ bar. As it will be proven later, the waste heat of a HT-PEM fuel cell is sufficient to evaporate enough water for the hydration reaction of MgO. Thereby, the water vapor pressure can reach up to 10bar.

Since the storage reactor is adiabatic to the environment, the boundary condition of thermal insulation is applied at boundaries 1–5 and 7, hence the heat flux across these boundaries is $-\vec{n} \cdot \vec{q} = 0$. The resistance to heat transfer across the middle wall (boundary 6) is disregarded. Accordingly, the heat transfer coefficient on both sides of the wall is set to $h = 10,000$ W m^{-2} K^{-1}

Before hydrogen can be withdrawn from the storage reactor, it has to be charged. We assume that loading is completed and the system has enough time to reach thermal equilibrium state. Hence, the initial temperature is the same everywhere within the system. It is set to $T_{0,HD} = T_{0,SD} = 553.15$ K, since this is the threshold temperature, at which the MgH_2 dehydrogenation reaction is just sufficiently fast at a H_2 pressure of 1 bar. The initial pressure is set to $P_{0,HD} = 1.1$ bar, which is slightly above the thermal equilibrium pressure at 553.15K. One can assume that a valve is opened initially. Therefore, the pressure $P_{HD,Bdry5}$ is reduced to its desired value of 1 bar within the first minute of the simulations. To avoid an initial sudden jump in the pressure of the MgO compartment, its initial pressure is set to $P_{0,SD} = 5$ bar. The hydrogen storage media is “full of hydrogen”, hence, $x_{h,0} = 0.998$. In contrast, the MgO bed is “empty of water”, thus, $y_{h,0} = 0.001$.

3.6. Mesh refinement study

In order to minimize the numerical uncertainties, a mesh refinement study was conducted. Therefore, four different meshes were compared to their influence on characteristic simulation results. The comparison is shown in Table 2.

The deviation of these characteristic values from mesh 3 to mesh 4

Table 2
Mesh refinement study.

	Mesh 1	Mesh 2	Mesh 3	Mesh 4
Number of quadrilateral elements	56	195	8352	17,250
Max T_{HD} middle MgH_2 Bed in K	561.8	566.29	565.62	562.39
Deviation from coarser mesh	–	0.79%	−0.12%	−0.57%
Average T_{SD} at t = 500 min MgO bed	552.72	553.25	553.13	553.1
Deviation from coarser mesh	–	0.10%	−0.02%	−0.01%
Max P_{HD} middle MgH_2 bed in Pa	$1.34 \cdot 10^5$	$1.28 \cdot 10^5$	$1.25 \cdot 10^5$	$1.25 \cdot 10^5$
Deviation from coarser mesh	–	−4.38%	−2.31%	−0.03%

does not exceed 0.60%. Hence, mesh 3 is chosen for the simulations. It consists of 8352 quadrilateral elements with an average element quality greater than 0.99.

4. Validation

The model set up in this work consists of two parts – the MgH_2/Mg system and the MgO/$Mg(OH)_2$ system which are regarded as sub-models. Both sub-models should be validated separately. The magnesium hydride dehydrogenation model was validated against the experimental and numerical data reported by Chaise et al. [17,31]. The authors performed a dehydrogenation experiment within a cylindrical tank, monitoring the course of the temperature at several points within the tank. Their experimentally determined pressure within the tank was used as an input parameter for our model. Our simulation results for the temperature and the desorbed volume of H_2 was compared to their experimental results. The results are shown in Fig. 3. The predicted temperatures at three selected locations of the MgH_2 bed, represented by solid lines in Fig. 3(a), deviate no more than 0.5% from the experimental values. The minimum temperatures of our model match well with the experimental values which are displayed with markers. For completeness, the author's numerical results are also displayed with dashed lines. In case of the desorbed volume of H_2, Fig. 3(b) shows that our model predicts slightly faster hydrogen desorption rate compared to the author's experimental result. Nevertheless, overall, it can be stated that the model for the magnesium hydride dehydrogenation provides a reliable description of the evolutions of temperature and H_2 desorbed rate, and thus can be considered as validated.

Regarding the MgO/$Mg(OH)_2$ system, there is no experimental data reported in the literature for the selected temperature – and pressure range of this study. That is why the magnesium oxide hydration reaction kinetic was estimated as mentioned in Section 3.2. The estimated rate was compared with an experiment performed by Zamengo et al. [32], where the authors hydrated MgO in a packed bed reactor at a water vapor pressure of 361 kPa. During steady hydration, they found an average reaction rate of approximately $1.40 \cdot 10^{-4}$ s^{-1} within their system. In our reference case at a water vapor pressure of 500 kPa, the simulated reaction rate during steady hydration rate is approximately $0.80 \cdot 10^{-4}$ s^{-1}. Thus, our model predicts lower reaction rates that may take place in the real process. A detailed validation is not shown here, but as we will proof in the results section, this approach is justified since the hydration kinetics are not limiting the performance of the present storage reactor.

5. Results and discussion

For the hydrogen release from the storage reactor, water vapor has to be supplied to the MgO bed. First, we address the fundamental question, from where the water vapor can be supplied. Then, the results regarding the reference case are evaluated, which corresponds to the requirement of the dehydrogenation of MgH_2 at the initial – and boundary conditions reported above. Afterwards, the performance of the storage reactor at different boundary conditions is demonstrated. Also, it is shown how selected parameters of the materials are affecting the performance.

5.1. Water vapor supply for energy release

In order to release the required energy for the MgH_2 dehydrogenation, water vapor has to be supplied to the MgO bed. The energy is released via the hydration of MgO to $Mg(OH)_2$ according to Eq. (2); but where does the water vapor come from? There are two options for the water vapor to be provided. First, the exhaust gas of the fuel cell, which includes water vapor, can be used. Second, the waste heat from

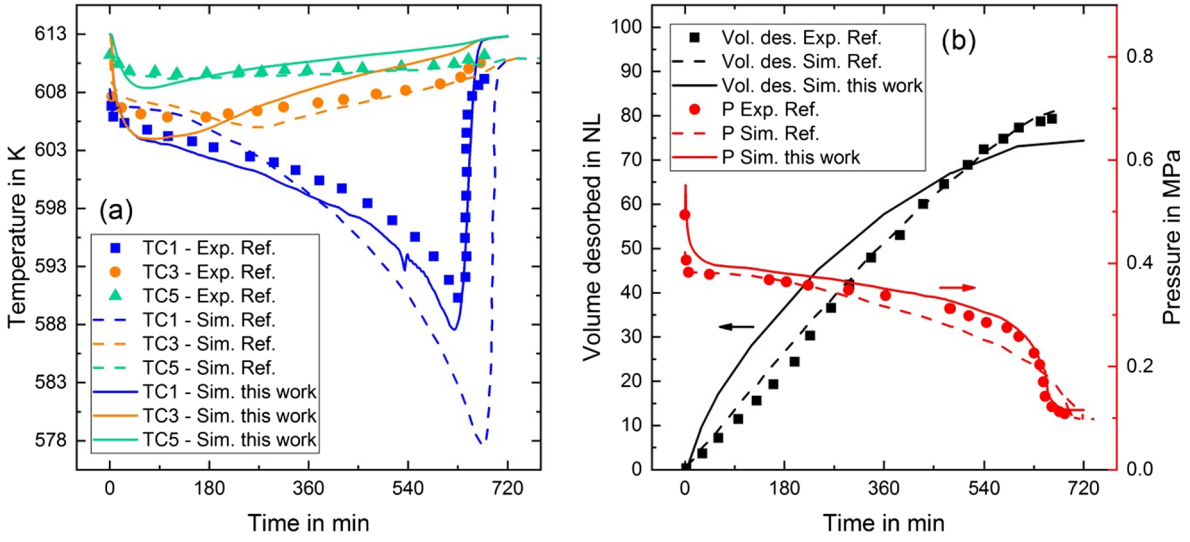

Fig. 3. Simulation results of temperatures and desorbed volume of H2 compared to literature data [29].

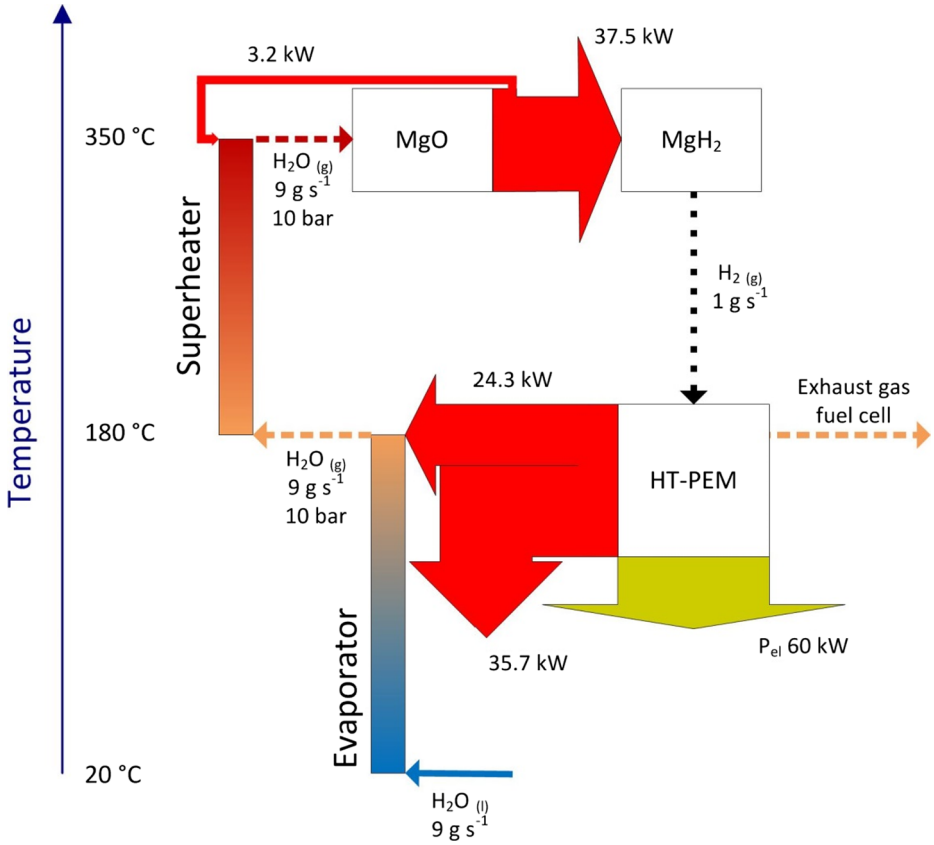

Fig. 4. Water vapor supply for operation. Dashed & dotted arrows: Mass flows; proportional, solid arrows: Energy flux.

the fuel cell can be used to evaporate water from an external tank. The exhaust gas of the fuel cell may be contaminated with unreacted hydrogen, which would pile up in the MgO compartment impeding the water vapor. Thus, an additional piece of equipment would be necessary for gas separation or conversion of unreacted hydrogen. That is why we demonstrate the second case here. An illustration of the water vapor supply is shown in Fig. 4. Gaseous mass flows are represented by dashed and dotted lines, liquid mass flow rates by solid lines, and heat fluxes by proportional arrows.

Suppose the desired mass flow rate of hydrogen to be converted in the fuel cell is $1\,g\,s^{-1}$ and its electric efficiency is 50% which yields in an electric power of 60 kW. To provide the energy to release this amount of hydrogen, $8.3\,g\,s^{-1}$ water vapor is needed based on the reaction enthalpies. In fact, some more is required and the total amount is $9.0\,g\,s^{-1}$ which is due to the temperature level at which the water vapor has to be supplied. To provide the water vapor, liquid water has to be preheated, evaporated and superheated. The question being addressed here is, to what extend the fuel celĺs waste heat is sufficient for preheating and evaporation.

First, liquid water is fed to an evaporator from an external tank at 20 °C. Then, the waste heat of the high temperature PEM fuel cell at 180 °C is used to heat up this water from 20 °C to 180 °C and to evaporate it at 180 °C corresponding to a water vapor pressure of approximately 10 bar. For this heat-up and evaporation, roughly 40% of the fuel cells waste heat is required. So the amount of energy provided from the fuel cell is more than sufficient. Furthermore, the water vapor has to be heated to the temperature of the reacting bed. Thus, if we assume that the temperature level at which the energy is released in the MgO compartment is 350 °C, which is the hydration equilibrium temperature at a water vapor pressure of 10 bar, the water vapor has to be superheated to 350 °C. This superheating may happen inside the MgO bed itself, but for illustrational purposes, the superheating step is displayed separately. As the temperature level of the fuel cells waste heat is only 180 °C, it cannot superheat the water vapor to 350 °C. Therefore, a part of the thermal energy provided by the MgO hydration reaction has to be used leading to the slightly increased water vapor demand than calculated arithmetically. However, this is only a small fraction of the released energy, as for superheating the water vapor from 180 °C to 350 °C, roughly 8% of the heat of reaction is required. If the water vapor is supplied to the MgO bed at a pressure lower than the assumed 10 bar, such as 5 bar, the temperature to which the water vapor has to be superheated is also lower, due to the lower equilibrium temperature. Concluding, it can be stated that it is possible to provide sufficient water vapor to the reactive bed using water from an external tank and the waste heat of a fuel cell at 180 °C, which is in turn supplied with the hydrogen released from the reactive bed.

Note that for the simulations, we assume that the water vapor is provided at the desired temperature and does not need to be superheated with energy emerging from the MgO hydration reaction.

5.2. Analysis of the reference case

5.2.1. Temperatures and reaction progress

The hydrogen pressure level required by the fuel cell is assumed to be 1 bar. Subsequently, desorption for the reference case takes place at a H_2 pressure of 1 bar. As proven before, water vapor can be supplied to the storage reactor at a pressure up to 10 bar. Nevertheless, for the reference case a water vapor pressure of 5 bar was chosen.

Initially, the storage reactor is “full of hydrogen” and “empty of water” and the temperature in the whole storage reactor is 553 K. Due to the adiabatic nature of this process, no heat is transferred to the surrounding. Subsequently, the involved heat is attributed to the chemical reactions or to the heat up of the materials which is referred to as “sensible” energy or heat.

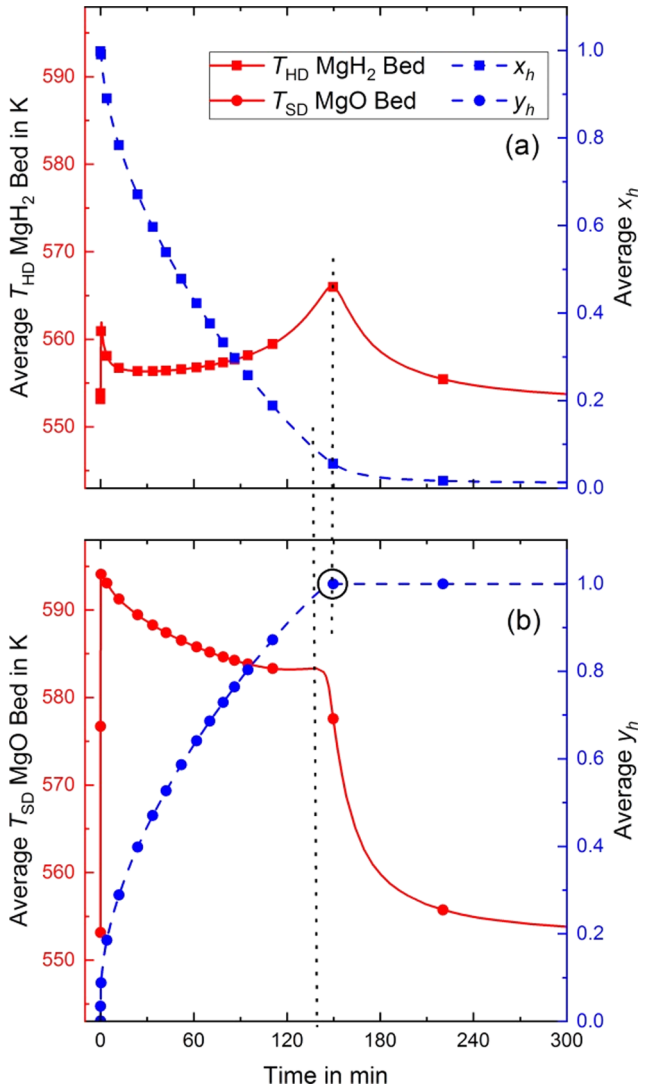

Fig. 5. Course of average bed temperatures and average reacted fractions x_h and y_h; Reference case.

The behavior of the storage system during hydrogen release is shown in Fig. 5 for the reference case. It can be seen that the average temperature of the MgO bed rises sharply within the first few minutes (see Fig. 5(b)). The hydration reaction reaches the thermodynamic equilibrium, corresponding to an equilibrium temperature of approximately 595 K at a pressure of 5 bar. As a result, the average temperature rises in the MgH_2 bed, as shown in Fig. 5(a). Due to the temperature gradient to the MgO compartment, a lot of heat is transferred to the MgO bed leading to a rapid hydrogen release. Subsequently the pressure and its according equilibrium temperature increase. As time proceeds, the average temperature in the MgH_2 bed exceeds the equilibrium temperature of approximately 553 K at the H_2 pressure of 1 bar, because the fraction of the material that has already been completely dehydrogenated increases its temperature.

While approaching the equilibrium temperature, the MgO hydration reaction releases a large amount of heat at the beginning which is stored sensibly in the reactive bed, as illustrated in Fig. 5(b). Transferring this sensible stored energy to the MgH_2 bed takes some time. This is the reason why the temperature in the MgO bed falls slightly after its initial peak. Once the exothermic MgO hydration reaction is completed (y_h=1), the temperature in both beds decreases, because the previously sensibly stored energy is transferred to the MgH_2 bed and no more heat is released. The dehydrogenation reaction now consumes the sensible energy at a low reaction rate until the initial temperature of 553 K is reached throughout the bed again. This is expected as the reactor is adiabatic to its surrounding and the energy ratio of the exothermic reaction and the endothermic reaction has been balanced.

The previously studied numerical analysis for the hydrogen absorption predicted an absorption time of 150 min [13] using the same geometry. The time until 90% of the MgH_2 is dehydrogenated in this work is 132 min, which is sufficient for stationary applications. Hence, the required times for Mg hydrogenation and MgH_2 dehydrogenation for this reference case is within the same range.

The spatial distributions of the temperature and reacted fractions are shown in Fig. 6. For the temperature of the heat storage media the rapid initial heat up of the whole MgO bed within the first 60 s is obvious (see Fig. 6(A)). The whole compartment reacts to the chemical equilibrium, and a reacted fraction of $y_h \approx 0.1$ is reached, as seen in Fig. 6(B) at t = 60 s. However, after the initial start-up, the MgO hydration reaction proceeds at the wall separating the two reactive beds. This is because heat is transferred through the wall, which means that the particles adjacent to the wall are no longer in thermochemical equilibrium. Hence, the reaction proceeds until the equilibrium is reached again. The same happens to the particles in the MgH_2 bed, but vice versa. Hence, two reactive fronts originate at the steel wall separating the materials moving into opposite directions. Such a front is typical for a system being limited by heat transfer. The same behavior can be observed during the hydrogen loading process both for our storage reactor [13] and for other tank geometries [33], where the authors used a helical coil heat exchanger for heat-management within the MgH_2 storage unit. The reactive front is narrow for the MgO compartment (y_h) and wide for the MgH_2 compartment (x_h). This is due to the difference in the effective thermal conductivities of the reactive beds of 0.55 $W m^{-1} K^{-1}$ and 4.2 $W m^{-1} K^{-1}$ for the MgO and MgH_2 bed, respectively.

5.2.2. Thermal power released and consumed by the reactive beds

The course of the absolute power released and consumed by the reactive beds is shown in Fig. 7. It can be seen that the power released by the MgO hydration reaction has an initial peak. This is due to the initial conditions far from the thermochemical equilibrium. Hence, the driving force of the chemical reaction is rather high. The initial reaction proceeds rapidly everywhere in the bed and consequently, a large part of heat is released, heating up the reactive bed. After the first minute, the released power equals the absolute value of the consumed power. The curves show a superposed behavior until the MgO hydration reaction is completed at approximately 150 min. The dehydrogenation reaction continues to consume the initially sensibly stored heat.

5.2.3. Detailed process evaluation in several points

For a detailed evaluation of the process, six points were selected to evaluate their local temperature course and reaction rate progress. The points are located at the gas manifolds (P1 and P6), in the middle of both beds (P2 and P5), and close to the heat exchanging wall (P3 and P4). The results are displayed in Fig. 8.

First of all, it is obvious that the reaction starts at the heat exchanging wall and it takes some time to observe significant H_2 release and MgO hydration at the points far from the wall (compare Fig. 8(a) and (b)). From the temperature graphs, it can be noticed that even initially, Point P4 at the wall does not reach the equilibrium temperature of 594 K. This indicates that the energy released there is immediately transferred to the MgH_2 bed where it is consumed by the dehydrogenation reaction. The reason for this behavior is that the thermal conductivity of the heat generating bulk is clearly lower than the one from the heat consuming bulk. Thus, the whole MgH_2 pellet can be seen as heat sink with almost homogenous temperature distribution. This is different for the MgO pellet bulk with lower thermal conductivity, which generates larger temperature gradients for the same heat flux. The same effect can also be seen in point P3. After a fast rise

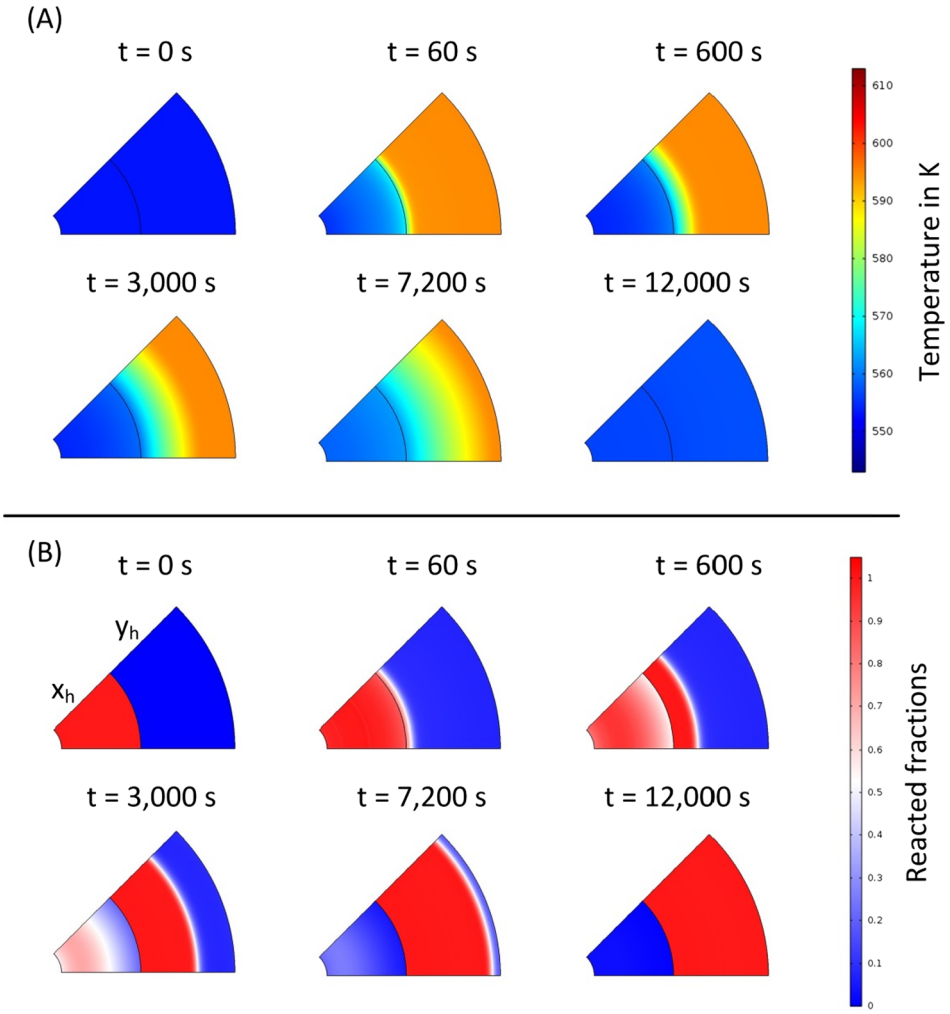

Fig. 6. Spatial distribution of the temperature and reacted fractions; Reference case.

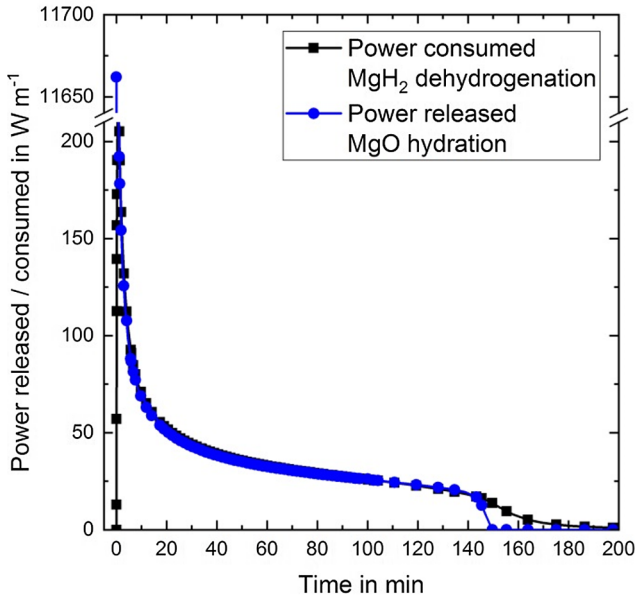

Fig. 7. Power released by the MgO hydration reaction, and consumed by MgH2 dehydrogenation reaction (Absolute values); Reference case. Note the cut in the y-axis.

in temperature, the heat flux delivered from the MgO bulk is not sufficient to compensate the heat distribution within the pellet and the endothermic reaction completely. Consequently, the temperature drops. At the end of the dehydrogenation process, the temperature approaches the initial temperature again, as the sensibly stored energy is used to complete the dehydrogenation reaction.

Furthermore, a comparison between the reaction progress at P1 (close to the exit manifold) and P2 (middle of the pellet) is interesting. While the conversion in P1 is faster at the beginning and slows down as the reaction proceeds, after around 75 min, P1 and P2 are almost identical. This behavior shows the influence of the gas transfer through the pellet which is on the one hand negligible for P1 and on the other hand the small pressure drop from P1 to P3 is overcompensated in P3 due to the higher temperature and corresponding equilibrium pressure.

Looking at the temperature and reacted fraction evolutions at point P6 in Fig. 8(b) and (d), it can be seen that the material at the H_2O manifold reaches quickly the chemical equilibrium at the beginning of the hydration reaction. During this linear section, it is obvious that the compartment is limited by heat transfer, as more heat can be released than disposed: the small amount of heat that is conducted towards the MgH_2 bed cools the bed down infinitesimally below the equilibrium temperature. Then, the hydration reaction proceeds infinitesimally to release energy until the equilibrium temperature is reached again. After about 125 min, the reaction is accelerated rapidly when the temperature starts to decrease in P6 – when the reaction front reaches P6.

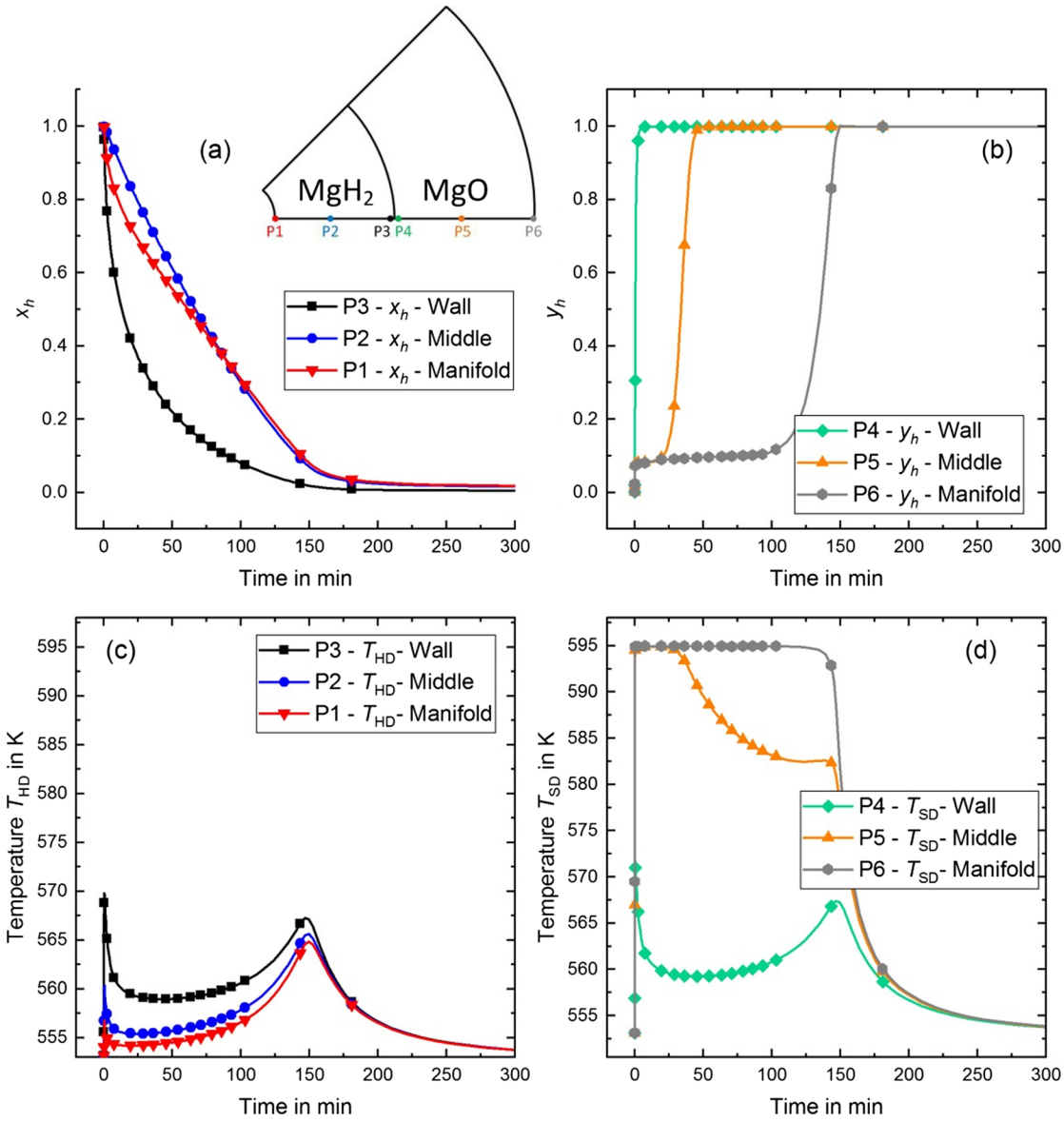

Fig. 8. Detailed evaluation of the reaction progress at three different points (P1–P6) in each compartment; Reference case.

5.3. Sensitivity analysis

5.3.1. Influence of the thermal conductivity

Previous studies on storage systems combining the MgH_2 material with a PCM [8], or with magnesium hydroxide [12,13], have shown that heat transfer is the limiting step in achieving high storage system performance. To confirm these findings and have an impression on the threshold values, we varied the thermal conductivity of both reactive beds independently, and evaluated its influence on the reaction progress. The results are shown in Fig. 9. While the thermal conductivity was varied within the MgH_2 bed (see Fig. 9(a)), the MgO bed properties were the same as in the reference case and vice versa. Values of up to 20 W m^{-1} K^{-1} were chosen, since it has been proven to increase the thermal conductivity of Mg-Ni alloys with expanded natural graphite and compaction to more than 20 W m^{-1} K^{-1} [34]. It is obvious that the reaction progress is faster if the thermal conductivity is increased. However, increasing the effective thermal conductivity from 4.2 W m^{-1} K^{-1} in the MgH_2 bed to 15 W m^{-1} K^{-1} yields no improvement of the reaction progress without considering the MgO bed. This reveals that there is a threshold after which the storage reactor is not limited by heat transfer any more. The effective thermal conductivity of $\lambda_{eff,MgH2bed}$ = 4.2 W m^{-1} K^{-1} seems to be close this threshold value. In contrast, doubling the thermal conductivity from $\lambda_{eff,MgObed}$ = 0.55 W m^{-1} K^{-1} to $\lambda_{eff,MgObed}$ = 1.1 W m^{-1} K^{-1} for the MgO bed results in almost 50% faster hydration without considering the MgH_2 bed. Hence, during practical operation for the considered geometry, there are limitations by heat transfer for the MgO bed. Future work should concentrate on enhancement of thermal conductivity of MgO. However, without affecting the permeability for water vapor (compare H_2 charging case at low water vapor pressures [13]).

5.3.2. Influence of the MgO hydration kinetics

The term for the reaction rate of the MgO hydration was estimated due to the lack of literature coverage of the MgO hydration reaction at elevated water vapor pressures. In order to justify this approach, we conducted a parametric study to evaluate the influence of the reaction rate on the storage reactor performance. Therefore, we varied the reaction rate by multiplying the estimated term with a factor θ. This influence was compared to the influence of the thermal conductivity $\lambda_{eff,SD}$ of the porous MgO bed. The criterion to evaluate the performance is the time required to dehydrogenate 90% of the MgH_2. The properties of the MgH_2 media were not varied.

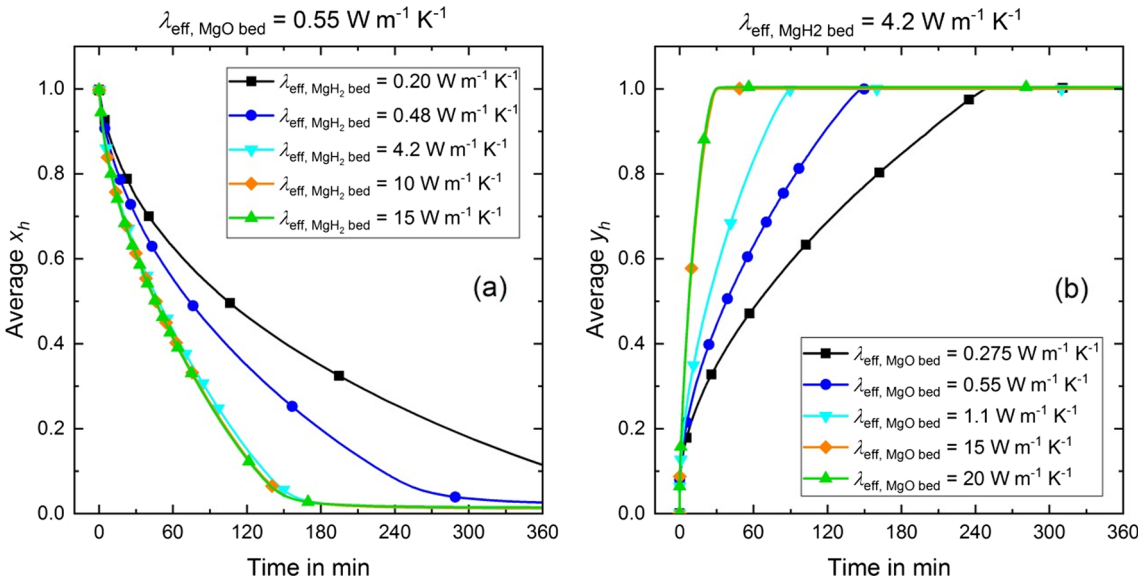

Fig. 9. Influence of the thermal conductivity on the dehydrogenation time; Blue line with circular markers: Reference case.

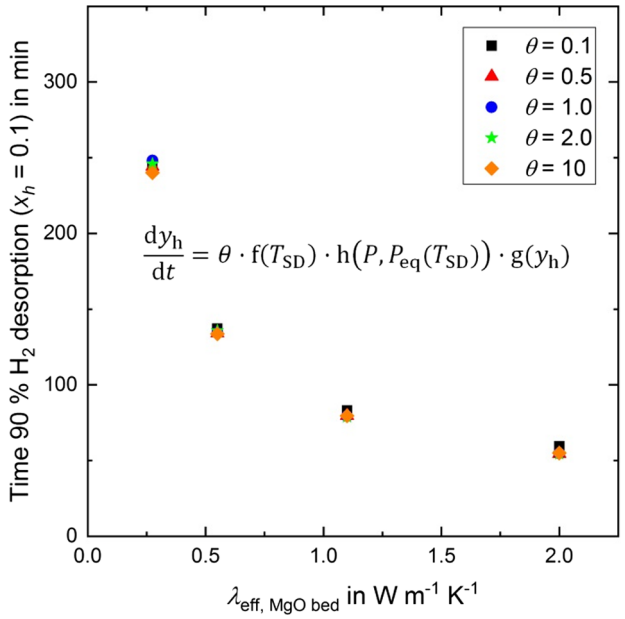

Fig. 10. Influence of the MgO hydration rate and the thermal conductivity of the MgO bed on the dehydrogenation time.

The results are shown in Fig. 10. It can be seen that varying the MgO hydration rate between two orders of magnitude has little influence on the storage reactor performance – especially at an effective thermal conductivity of $\lambda_{eff,SD} = 0.55$ W m^{-1} K^{-1}, which is the value reported in the literature for the selected material [24]. Furthermore, it can be seen that the curve approximates a threshold with increasing $\lambda_{eff,SD}$. This is in accord with the results presented previously. Concluding here, our simulation results indicate that the prediction of the system performance is not sensitive to the estimated reaction kinetics of the MgO hydration at elevated water vapor pressures, at least for our geometry. Changing the storage reactor design may result in a better heat transfer from the MgO bed to the MgH_2 bed, and in case the dehydrogenation and hydration processes are not limited by heat- or mass transfer, a detailed evaluation of the MgO hydration kinetics would be necessary.

5.3.3. Influence of MgO hydration water vapor pressure

The temperature level at which the heat of the hydration reaction is released can be controlled through the variation of the water vapor pressure. This presents a strong advantage in comparison to the PCM usage. To evaluate the influence of the water vapor pressure on the dehydrogenation and hydration reactions, several simulations were conducted. The initial pressure and the boundary condition at boundary 7 in Fig. 2 were varied between 3bar and 10bar. The results are shown in Fig. 11.

It can be seen that the average temperature in the MgO rises sharply in the beginning until the chemical equilibrium is reached (compare Fig. 11(d)). A higher water vapor pressure results in a higher equilibrium temperature. This leads to an increased temperature gradient between the two reactive beds, and hence, to an enhanced heat transfer. Subsequently, the reactions in both reactive beds proceed faster. This is evident from Fig. 11(a) and (b).

In Fig. 11 it is evident that the MgH_2 dehydrogenation time is strongly dependent on the temperature that can be reached during the MgO hydration. For instance, when the maximum temperature in the MgO Bed is 577 K, it takes approximately 240 min to dehydrogenate 90% of the MgH_2 bed (see Fig. 11(a)). In contrast, this time is reduced to roughly 85 min when the maximum temperature in the MgO bed is 623 K. The temperature that can be reached as a maximum is the equilibrium temperature of the MgO hydration, which is dependent on the water vapor pressure. Hence, the knowledge of the thermochemical equilibrium temperature is crucial for the evaluation of the storage reactor performance.

As mentioned before, for the $Mg(OH)_2/MgO + H_2O$ system, the existing data on the hydration reaction is scarce. Not only kinetic data at the required pressure range for our studied system are missing, but also data on the thermodynamics, especially on the hysteresis behavior of this material. Thus, a comparison with similar gas-solid systems can help to give an estimate for the present system and allow conclusions on the feasibility of the overall process, for instance at which hydration pressure the system should be operated, and if this corresponds to a feasible operation condition.

The similar reaction system $Ca(OH)_2/CaO + H_2O$ exhibits a slight hysteresis. Schmidt et al. [35] summarized the onset temperatures found by different authors for this reaction system which are not the same for hydration and dehydration reactions. For this system, hysteresis becomes smaller with increasing gas pressure [36]. In case the $Mg(OH)_2/MgO + H_2O$ system exhibits a similar behavior, a high water vapor pressure would be required to reach the desired hydration temperature. Hence, the storage reactor performance may be affected by hysteresis. But even in case a water vapor pressure of 10bar is required

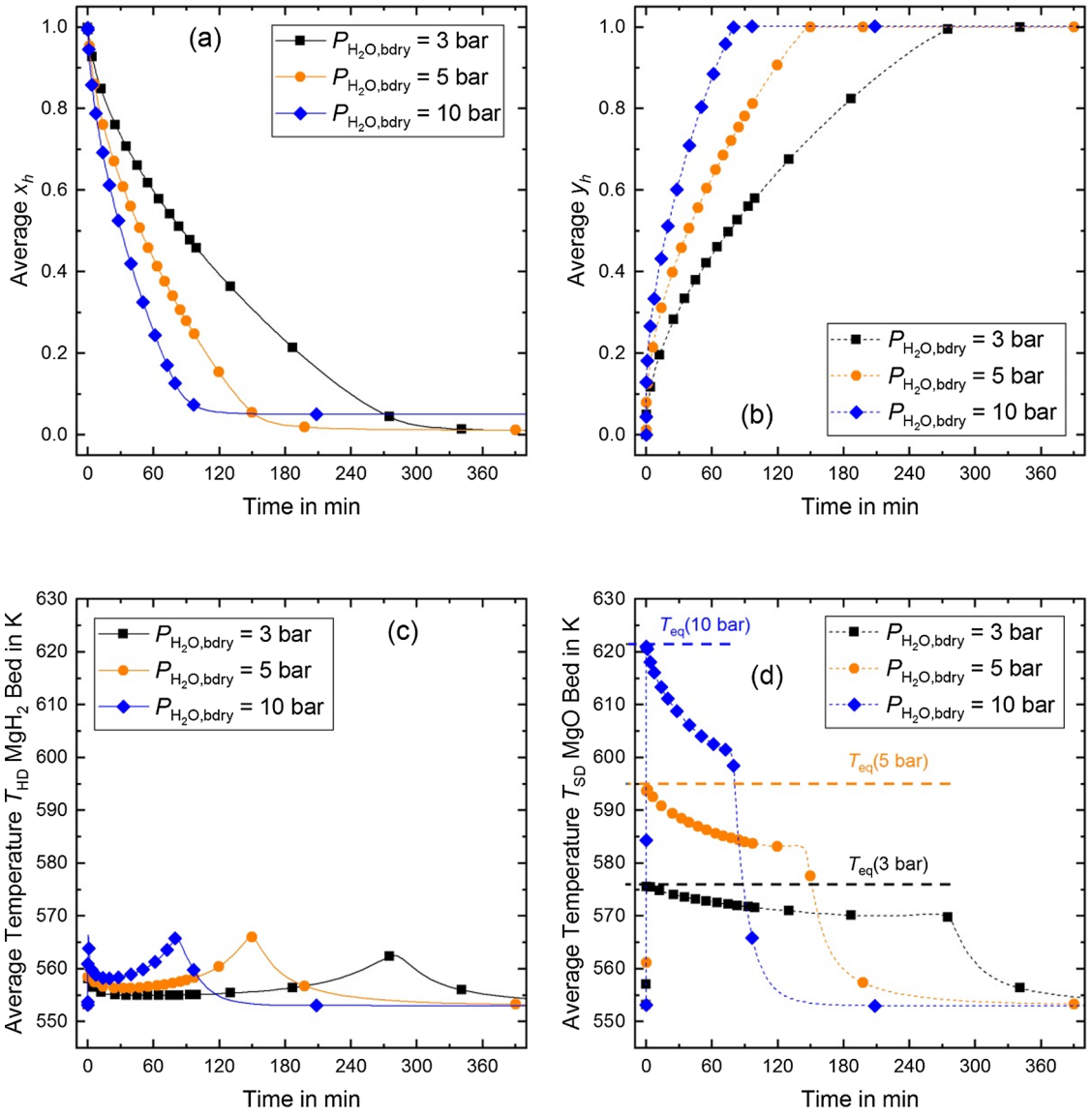

Fig. 11. Storage reactor performance at three different MgO hydration water vapor pressures.

to obtain a hydration equilibrium temperature of 577 K, the system is still operable. In our simulation, the hydration equilibrium pressure is $P_{eq}(577\ K) = 3$ bar, as it can be seen in Fig. 11(d). This would correspond to a hysteresis of approximately 46 K at 10bar. Kiyabu et al. [37] did a computational screening of several reactions for thermal energy storage looking for promising reactions. One criterion for exclusion of a reaction was a hysteresis greater than 50 K. They did not exclude the $Mg(OH)_2/MgO + H_2O$ system. Since Kiyabu et al. did not investigate higher pressure and temperature levels, experimental investigation is currently missing. However, the hysteresis of the reaction mainly affects the required temperature level for evaporation. As discussed above, the estimation for the system is again conservative as 3 bar pressure is required but 10 bar available (Compare Section 5.1).

5.3.4. Operation under a mass flow rate control

A fuel cell demands a constant mass flow rate of hydrogen in order to operate in steady-state. Hence, for practical operation, the hydrogen mass flow rate is a matter of interest and the question arises whether the storage reactor is able to provide hydrogen at a specified mass flow rate. Therefore, a simulation with a mass flow rate of $1.5 \cdot 10^{-4}$ kg m^{-2} s^{-1} at which the storage reactor is emptied within approximately 4 h was conducted and the obtained results were compared to the one of reference case, where a pressure boundary condition of 1 bar was applied (The area refers to boundary 5 in Fig. 2). The simulation results indicate that the mass flow rate can be maintained for the desired time. As shown in Fig. 12(a), an initial rise in pressure attests that more hydrogen is released from the bed than is actually removed by the boundary condition. Right after the peak, this ratio changes and the pressure begins to decrease slowly. The mass flow rate was set to 0 kg m^{-2} s^{-1} when the average reacted fraction in the MgH_2 bed reaches $x_h = 0.05$. By that time, 95% of hydrogen is released and the storage reactor can be considered as empty. However, the remaining unreacted MgH_2 (5% of the material) keeps reacting. This is why the pressure rises to the equilibrium pressure of 1.6 bar at 570 K. The new boundary condition also affects the course of the converted fractions. While they are curved in the reference case (Fig. 12(b) and (d)), they follow a linear trend with the mass flow boundary condition (Fig. 12(a) and (c)). This indicates a constant reaction rate in both beds. Additionally, the reaction rate is not influenced by the temperature gradient between the beds. Subsequently, the storage reactor is neither limited by heat transfer nor by the reaction kinetics, but by the H_2 mass flow rate boundary condition. Heat transfer between the reactive beds is sufficient to provide the desired hydrogen mass flow rate for 4 h. A further increase of the desired mass flow rate will lead to limitations

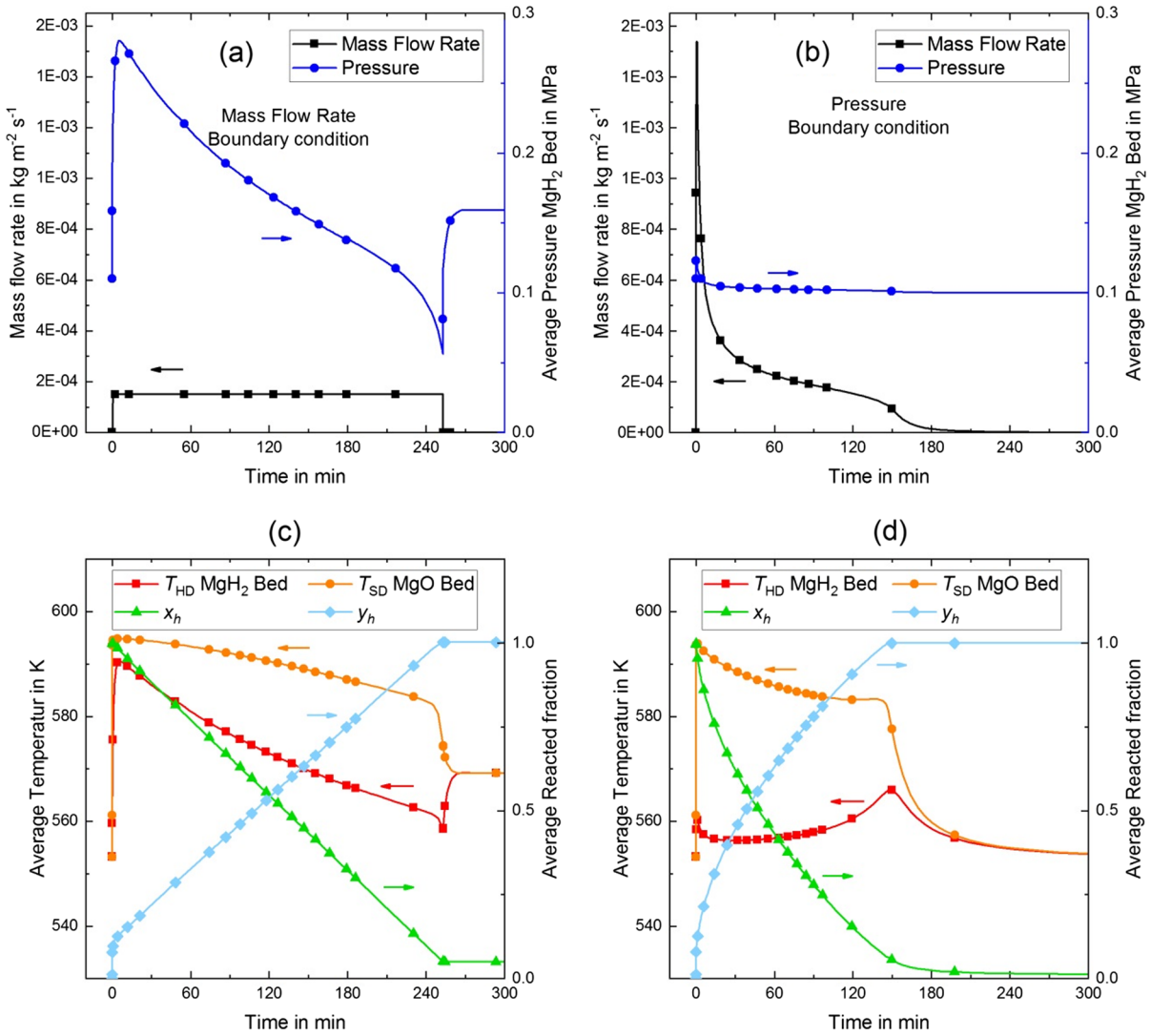

Fig. 12. Comparison of mass flow rate boundary condition and pressure boundary condition at the hydrogen outlet (Boundary 5 in Fig. 2).

regarding either heat transfer or reaction kinetics.

Summarizing here, hydrogen can be released from the metal hydride not only with a constant mass flow or at a constant pressure level, but also sufficiently fast which makes the storage reactor suitable for different operation modes.

6. Conclusion

In this work we demonstrated the feasibility of releasing hydrogen from an adiabatic magnesium hydride storage reactor that offers high storage capacities at low gas pressures. A thermochemical energy storage material (TCM) stores the heat of reaction released during the hydrogenation of magnesium and releases it for the dehydrogenation. The $Mg(OH)_2/MgO + H_2O$ reaction is well suited for this purpose, since it operates within the same temperature range as magnesium hydride. While the feasibility of the hydrogen uptake process was investigated in previous studies, this work focused on the dehydrogenation of the MgH_2. Therefore, we set-up and solved a numerical model of the storage reactor using the COMSOL Multiphysics® software. The model takes into account the thermodynamics, reaction kinetics, heat- and mass transfer as well as material properties depending on the temperature, pressure and reaction progress. The main findings can be summarized as:

- First, the energy for the MgH_2 dehydrogenation is provided by the hydration of MgO. Hence, the storage reactor has to be supplied with water vapor for hydrogen release. We demonstrated analytically, that the waste heat of a high temperature fuel cell and a small fraction of the heat released by the hydration reaction is sufficient to provide water vapor at 350 °C and even at 10 bar starting with liquid water at 20 °C.
- Second, we found that the time required for the MgH_2 dehydrogenation is strongly dependent on the thermal conductivity of the porous beds. For our selected geometry, the storage reactor is limited by heat transfer within the powder bulk while the reaction kinetics plays a minor role. Additionally, the performance is dependent on the equilibrium temperature of the MgO hydration. Dehydrogenation is possible within 132 min, which is the same time frame as for the hydration. Subsequently, the storage reactor is suited for stationary applications.
- Third, the temperature level at which the thermal energy is released from the TCM can be adjusted with the water vapor pressure rendering the proposed system more flexible than a system using PCM. Supplying water vapor at higher pressures to the MgO bed, results in higher equilibrium temperatures within the heat storage media. Subsequently, the temperature gradient between the porous beds is increased leading to an enhanced heat transfer and a faster MgH_2 dehydrogenation.

Summarizing, the present study demonstrates a storage concept utilizing a high temperature metal hydride based on its thermal coupling with a thermochemical heat storage material. Compared to similar technologies, the system can be more lightweight and exhibits a higher volumetric storage capacity at a pressure below 30 bar. Since the storage reactor can be operated adiabatically, no external heat management is required. The results showed that the presented mathematical model is appropriate to describe the hydrogen release from the storage reactor, thus it can be used for future design studies and as basis for an experimental validation.

References

[1] Lewandowska-Bernat A, Desideri U. Opportunities of power-to-gas technology in different energy systems architectures. Appl Energy 2018;228:57–67.
[2] Kavadias K, Apostolou D, Kaldellis J. Modelling and optimisation of a hydrogen-based energy storage system in an autonomous electrical network. Appl Energy 2018;227:574–86.
[3] Zhang Y, Campana PE, Lundblad A, Yan J. Comparative study of hydrogen storage and battery storage in grid connected photovoltaic system: Storage sizing and rule-based operation. Appl Energy 2017;201:397–411.
[4] Sakintuna B, Lamari-Darkrim F, Hirscher M. Metal hydride materials for solid hydrogen storage: a review. Int J Hydrogen Energy 2007;32(9):1121–40.
[5] Jensen JO, Vestbø AP, Li Q, Bjerrum N. The energy efficiency of onboard hydrogen storage. J Alloy Compd 2007;446–447:723–8.
[6] Wang Y, Wang Y. Recent advances in additive-enhanced magnesium hydride for hydrogen storage. Prog Nat Sci: Mater Int 2017;27(1):41–9.
[7] Busch N, Jepsen J, Pistidda C, Puszkiel JA, Karimi F, Milanese C, et al. Influence of milling parameters on the sorption properties of the LiH-MgB2 system doped with TiCl3. J Alloy Compd 2015;645:S299–303.
[8] Vajo JJ, Skeith SL, Mertens F. Reversible storage of hydrogen in destabilized LiBH4. J Phys Chem B 2005;109(9):3719–22.
[9] Delhomme B, Lanzini A, Ortigoza-Villalba GA, Nachev S, De Rango P, Santarelli M, et al. Coupling and thermal integration of a solid oxide fuel cell with a magnesium hydride tank. Int J Hydrogen Energy 2013;38(11):4740–7.
[10] Garrier S, Delhomme B, De Rango P, Marty P, Fruchart D, Miraglia S. A new MgH2 tank concept using a phase-change material to store the heat of reaction. Int J Hydrogen Energy 2013;38(23):9766–71.
[11] Mellouli S, Ben Khedher N, Askri F, Jemni A, Ben Nasrallah S. Numerical analysis of metal hydride tank with phase change material. Appl Therm Eng 2015;90:674–82.
[12] Bhouri M, Bürger I, Linder M. Feasibility analysis of a novel solid-state H2 storage reactor concept based on thermochemical heat storage: MgH2 and Mg (OH) 2 as reference materials. Int J Hydrogen Energy 2016;41(45):20549–61.
[13] Bhouri M, Bürger I. Numerical investigation of H2 absorption in an adiabatic high-temperature metal hydride reactor based on thermochemical heat storage: MgH2 and Mg (OH) 2 as reference materials. Int J Hydrogen Energy 2017;42(26):16632–44.
[14] Alva G, Lin Y, Fang G. An overview of thermal energy storage systems. Energy 2018;144:341–78.
[15] Bürger I. Investigation of a new reactor concept for hydrogen storage in complex hydrides. Verlag Dr. Hut; 2014.
[16] Nilles M. Wärmeübertragung an der Wand durchströmter Schüttungsrohre. Düsseldorf: VDI-Verlag; 1991. p. 44.
[17] Chaise A, De Rango P, Marty P, Fruchart D. Experimental and numerical study of a magnesium hydride tank. Int J Hydrogen Energy 2010;35(12):6311–22.
[18] Kato Y, Yamashita N, Kobayashi K, Yoshizawa Y. Kinetic study of the hydration of magnesium oxide for a chemical heat pump. Appl Therm Eng 1996;16(11):853–62.
[19] Vyazovkin S, Burnham AK, Criado JM, Pérez-Maqueda L, Popescu C, Sbirrazzuoli N. ICTAC Kinetics Committee recommendations for performing kinetic computations on thermal analysis data. Thermochim Acta 2011;520(1–2):1–19.
[20] Bratton RJ, Brindley GW. Kinetics of vapour phase hydration of magnesium oxide. Part 2 – Dependence on temperature and water vapour pressure. Trans Faraday Soc 1965;61:1017–25.
[21] COMSOL Multiphysics, version 5.3, Material Library, COMSOL, Inc. < www.comsol.com > .
[22] Mastronardo E, Bonaccorsi L, Kato Y, Piperopoulos E, Milone C. Efficiency improvement of heat storage materials for MgO/H2O/Mg(OH)2 chemical heat pumps. Appl Energy 2016;162:31–9.
[23] Mastronardo E, Bonaccorsi L, Kato Y, Piperopoulos E, Lanza M, Milone C. Thermochemical performance of carbon nanotubes based hybrid materials for MgO/H2O/Mg(OH)2 chemical heat pumps. Appl Energy 2016;181:232–43.
[24] Kato Y, Zamengo M, Fujioka K. Effect of thermal conductivity enhancement of thermochemical energy storage material on unused heat utilization system. In: Proceedings of the 15th international heat transfer conference (IHTC-15), Kyoto; 2014.
[25] National Institute of Standards and Technology (NIST) – magnesium dihydride. [Online]. Available: < http://webbook.nist.gov/cgi/cbook.cgi?ID=C7693278&Units=SI&Mask=2&Type=JANAFS&Plot=on#JANAFS > [accessed 07 03 2018].
[26] National Institute of Standards and Technology (NIST) – Magnesium. [Online]. Available: < http://webbook.nist.gov/cgi/cbook.cgi?ID=C7439954&Units=SI&Mask=2&Type=JANAFS&Plot=on#JANAFS > [accessed 07 03 2018].
[27] Chaise A, De Rango P, Marty P, Fruchart D, Miraglia S, Olivès R, et al. Enhancement of hydrogen sorption in magnesium hydride using expanded natural graphite. Int J Hydrogen Energy 2009;34(20):8589–96.
[28] National Institute of Standards and Technology (NIST) – magnesium oxide. [Online]. Available: < http://webbook.nist.gov/cgi/inchi?ID=C1309484&Type=JANAFS&Plot=on > [accessed 07 03 2018].
[29] National Institute of Standards and Technology (NIST) – magnesium hydroxide. [Online]. Available: < http://webbook.nist.gov/cgi/cbook.cgi?ID=C1309428&Type=JANAFS&Table=on#JANAFS > [accessed 07 03 2018].
[30] Poco Graphite, Inc. [Online]. Available: < http://poco.com/Portals/0/Literature/Semiconductor/IND-109441-0115.pdf > [accessed 29 03 2018].
[31] Chaise A. Etude expérimentale et numérique de réservoirs d?hydrure de magnésium. Grenoble I: Energie électrique. Université Joseph-Fourier; 2008.
[32] Zamengo M, Ryu J, Kato Y. Composite block of magnesium hydroxide-expanded graphite for chemical heat storage and heat pump. Appl Therm Eng 2014;69(1–2):29–38.
[33] Wu Z, Yang F, Zhang Z, Bao Z. Magnesium based metal hydride reactor incorporating helical coil heat exchanger: simulation study and optimal design. Appl Energy 2014;130:712–22.
[34] Pohlmann C, Kieback B, Röntzsch L. Composite materials of melt-spun Mg90Ni10 and graphite: microstructural changes during cyclic hydrogenation and the impact on gas and heat transport characteristics. Int J Hydrogen Energy 2014;39(16):8331–9.
[35] Schmidt M, Gutierrez A, Linder M. Thermochemical energy storage with CaO/Ca(OH)2-Experimental investigation of the thermal capability at low vapor pressures in a lab scale reactor. Appl Energy 2017;188:672–81.
[36] Schaube F, Koch L, Wörner A, Müller-Steinhagen H. A thermodynamic and kinetic study of the de-and rehydration of Ca(OH)2 at high H2O partial pressures for thermo-chemical heat storage. Thermochim Acta 2012;538:9–20.
[37] Kiyabu S, Lowe JS, Ahmed A, Siegel DJ. Computational screening of hydration reactions for thermal energy storage: new materials and design rules. Chem Mater 2018;30(6):2006–17.

Summary of individual contributions in Paper I:

- Formulation of the publication´s research goal:

  The goal was to set up a numerical model to draw conclusion about the hydrogen release process from the adiabatic tank and to investigate the water vapor supply to the reactor.

- Creation of the Model:

  A two-dimensional model was set up regarding heat transfer, mass transfer and the material´s thermodynamics and reaction equations. Due to lack of literature data, assumptions were made which will be discussed with experimental data throughout this dissertation.

- Partial validation of the model with experimental data from the literature.

  In the model, two thermochemical materials are represented with their thermodynamics and reaction kinetics. Experimental data for the validation at the desired operating conditions was only available for one of the materials. Due to lack of experimental data for the other material, the properties were assessed conservatively and discussed.

- Visualization and presentation of the data.

  Selection of relevant data and determining a comprehensible way of presenting it.

- Analysis and deductive reasoning:

  The influence of various parameters on the hydrogen release process was investigated. The limiting process was identified. The most critical assumption, which is the extrapolation of equilibrium data, was also identified and will be addressed in this dissertation.

- Writing of the manuscript and publishing in *Applied Energy*.

The results of the numerical models for hydrogen storage- and release from the adiabatic hydrogen storage reactor indicate that hydrogen can be withdrawn from the reactor with the supply of water vapor to the MgO bed at up to 10 bar. However, assumptions and simplifications are involved which is why an experimental investigation is necessary. In the second publication, for the first time, a test bench and a prototype reactor are designed in lab-scale to conduct the experimental proof of concept of the adiabatic hydrogen storage concept. The bottleneck of the system is identified and suggestions for optimizations are given.

Paper II

High capacity, low pressure hydrogen storage based on magnesium hydride and thermochemical heat storage: Experimental proof of concept

Michael Lutz, Marc Linder, Inga Bürger

Applied Energy

Volume 271, 1 August 2020, 115226

https://doi.org/10.1016/j.apenergy.2020.115226

Applied Energy 271 (2020) 115226

Contents lists available at ScienceDirect

Applied Energy

journal homepage: www.elsevier.com/locate/apenergy

High capacity, low pressure hydrogen storage based on magnesium hydride and thermochemical heat storage: Experimental proof of concept

Michael Lutz*, Marc Linder, Inga Bürger

Institute of Engineering Thermodynamics, German Aerospace Center (DLR), Pfaffenwaldring 38-40, D-70569 Stuttgart, Germany

HIGHLIGHTS

- Experimental hydrogen storage and release from a novel adiabatic storage reactor.
- Coupling of a metal hydride with a thermochemical heat storage material.
- Magnesium hydride and magnesium hydroxide suitable for hydrogen storage.
- Magnesium oxide hydration at 9.75 bar results in reactor temperature of 300 °C.

GRAPHICAL ABSTRACT

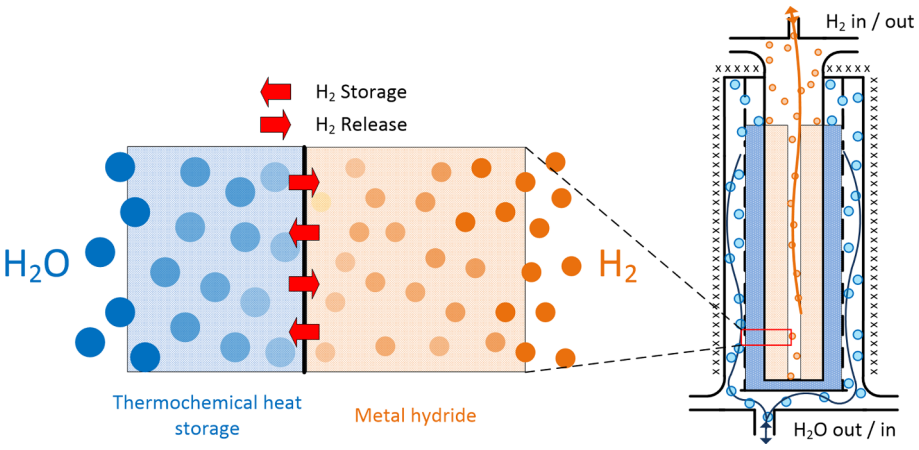

ARTICLE INFO

Keywords:
Hydrogen storage
Thermochemical heat storage
Magnesium hydride
Magnesium hydroxide

ABSTRACT

With hydrogen becoming more and more important as energy carrier, there is a need for high capacity storage technologies preferably operating at low pressures. Chemical storage in metal hydrides is promising for that purpose, but they require thermal management for hydrogen release and storage, respectively. To overcome this challenge, it is beneficial to store the heat needed for hydrogen release during hydrogen storage in the storage system keeping the additional effort to provide that heat low. In this work, the experimental proof of concept of an adiabatic storage reactor is presented. Magnesium hydride and magnesium hydroxide have been used for hydrogen storage and thermochemical heat storage, respectively. A prototype reactor has been developed and experimentally investigated. It was found that the operating temperature of the materials can be adjusted with the gas pressure in a way to establish a temperature gradient from the MgH_2 to the $Mg(OH)_2$ and vice versa. Hydrogen storage and release is enhanced by the thermochemical heating/cooling. A pressure of 9 bar is sufficient to store hydrogen with a capacity of 20.8 g_{H2} L^{-1} based on the two materials only, without the steel vessel or insulation. In the heat storage compartment, 300 °C have been reached at 9.75 bar during heat release which is high enough to drive the MgH_2 dehydrogenation.

* Corresponding author.
E-mail address: michael.lutz@dlr.de (M. Lutz).

https://doi.org/10.1016/j.apenergy.2020.115226
Received 4 February 2020; Received in revised form 14 May 2020; Accepted 17 May 2020

1. Introduction

For a successful transformation of the global energy systems towards renewable energy there is a need for large scale energy storage. Storing energy chemically in the form of hydrogen is beneficial, since hydrogen can be combusted, transported or used as a precursor for other chemical compounds, such as power-to-gas [1]. Hence, there is an increasing need for efficient hydrogen storage. State of the art hydrogen storage technologies, such as liquefaction or pressurized storage, lack efficiency, pose safety threats or have low storage densities. Additionally, political regulations have to be taken into account. In Japan, a country leading in hydrogen technologies, extensive and expensive safety measures have to be installed if hydrogen is stored above 10 bar in housing environments [2,3]. Therefore, it would be beneficial to store hydrogen at a pressure as low as possible. This is challenging due to its low density at ambient pressure and 273 K of 0.08988 g L^{-1} [4].

Thermochemical systems have the advantage that the hydrogen is not stored in its elementary form, but within liquid [5] or solid chemical compounds [6]. With these systems, higher volumetric densities can be achieved than in gaseous storage. Metal hydrides have been studied intensively for that purpose [4]. The challenge of utilizing metal hydrides and other thermochemical systems is their heat of reaction which has to be managed. This is especially challenging with increasing reaction temperatures. One example of a promising thermochemical system is based on the reversible formation of magnesium hydride. However, as its operating temperature is at around 300 °C, the thermal management becomes difficult, especially the low-cost supply of thermal energy at that temperature level. An option to overcome this disadvantage is to store the heat during hydrogen absorption in a way that it is available for the hydrogen release. Heat storage and release have to take place at a temperature level fitting to the reaction temperature of the metal hydride. Using a phase change material operating in that temperature range for that purpose has been investigated before [7,8]. Intrinsically, the temperature levels of heat storage and release are identical for the PCM, which is its melting point. However, it would be beneficial if the temperature level of heat storage is lower than the temperature level of the heat release. Thermochemical heat storage material utilizing a gas-solid reaction exhibit this feature, because the gas pressure can be adjusted. This is why in the present work the combination of magnesium hydride, as a high temperature metal hydride, with magnesium hydroxide as thermochemical heat storage is investigated experimentally for stationary, centralized hydrogen storage, which may have advantages over decentralized systems [9].

The main idea of the so-called adiabatic storage concept is the combination of an exothermal reaction with an endothermal one compensating for each other. Therefore, the reactor can be operated with minimal heat management, since the heat of reaction during hydrogen storage is available for the hydrogen release making it adiabatic to the environment. Compared to heat storage in a PCM, the usage of the thermochemical heat storage material yields in higher storage densities [10] and in an additional degree of freedom, since the reaction temperature can be adjusted with the gas pressure.

Magnesium, which is non-toxic [11] and abundantly available, is the main compound of both reactions. In this study, magnesium hydride is used for hydrogen storage [12].

$$Mg + H_2 \rightleftharpoons MgH_2 + 75\frac{kJ}{mol} \quad (1)$$

The heat of reaction is stored in the $Mg(OH)_2$/MgO system.

$$Mg(OH)_2 + 81\frac{kJ}{mol} \rightleftharpoons MgO + H_2O \quad (2)$$

For hydrogen storage, the heat of absorption is conducted to the $Mg(OH)_2$ bed, where the heat is consumed by its dissociation to MgO and H_2O. For the heat transfer to emerge, the temperature in the MgH_2 bed has to be higher than the temperature in the $Mg(OH)_2$ bed. For hydrogen release, water vapor has to be supplied to the MgO bed. The previously stored thermal energy is released and transferred to the MgH_2 bed. Hence, the temperature gradient has to be reversed. The feasibility of this system has been investigated analytically [13] before. Thereafter, a numerical study for hydrogen storage [14] and hydrogen release [15] was conducted. A more detailed description of the system can be found there. In this work the experimental proof of concept of this new hydrogen storage reactor is presented.

Besides cost [16], the volumetric storage density and the pressure level are important parameters for stationary hydrogen storage systems. The pressure level may translate directly into cost if safety regulations are regarded. Additional incorporation of the thermochemical heat storage material results in a heavier system compared to the metal hydride alone, but for stationary application the weight of the system is not that important. Additionally, the energy being required to compress hydrogen to that pressure for storage, which is 15% of its lower heating value in the 700 bar case [17], has not to be brought up, improving the systems overall efficiency significantly. Furthermore, in contrast to compressed hydrogen storage systems, the adiabatic storage rector impedes the hydrogen release by itself in case of a leak. This is due to the endothermal nature of the hydrogen release.

To reach a sufficiently high temperature level in the MgO compartment for the dehydrogenation of $Mg_{90}N_{i10}$ and drive the hydrogen release reaction, approximately 10 bar of water vapor are required. There are two options to provide this water vapor. Suppose, the hydrogen is used in a high temperature PEM fuel cell operating at 180 °C, the waste heat of such a fuel cell can be used to evaporate water from an external tank at a pressure of 10 bar. Approximately 40% of the HT-PEM's waste heat is sufficient to heat liquid water from 20 °C to 180 °C and to evaporate it at 180 °C. A more detailed analysis of this systems integration can be found in [15]. Another option is to directly use the fuel cell's exhaust gas, which contains water vapor, and feed it to the MgO compartment after compression to 10 bar. Both options would be feasible in case of stationary hydrogen storage.

In this work, a prototype reactor for stationary hydrogen storage was developed and tested. First the experimental setup is presented, followed by the experimental characterization of the system. Afterwards, starting points for optimization and a summary are shown.

2. Experimental setup

The adiabatic storage concept utilizes two thermochemical reactions involving hydrogen and water vapor. Therefore, the experimental test bench consists of three main components – The water vapor infrastructure, the hydrogen infrastructure and the prototype reactor. The whole setup is shown in Fig. 1.

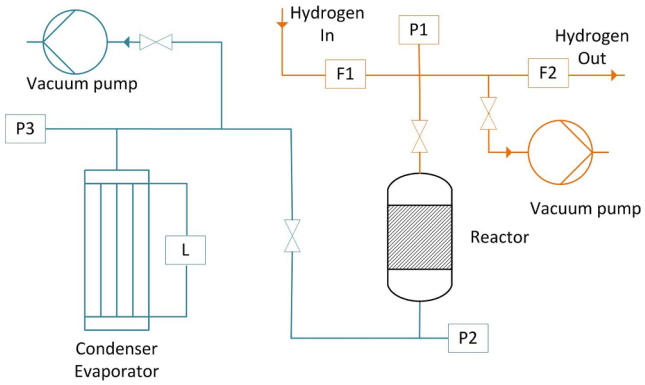

Fig. 1. Test bench schematic; Hydrogen- and water vapor infrastructure orange and blue, respectively; F: Flow meter; P: Pressure sensor; L: Level meter. (For interpretation of the references to colour in this figure legend, the reader is referred to the web version of this article.)

2.1. Water vapor infrastructure

Water vapor is supplied or withdrawn from the reactor with a tube bundle heat exchanger acting as evaporator or condenser, respectively. The heat exchanger is tempered with thermal oil while its water side is closed to the environment. Thaťs why with adjustment of the oil temperature, the water vapor pressure in the heat exchanger and, thus, in the reactor can be controlled. It has been demonstrated that thermochemical reactions can be supplied with water vapor using this system [18]. The present setup allows for water vapor pressures from 50 mbar to 10 bar, which corresponds to oil temperatures from 33 °C to 180 °C. The evaporator/condenser is equipped with a guided wave radar level meter (VEGAFLEX 81, VEGA Grieshaber KG, ± 2 mm) measuring the level of the liquid water in the tube bundle. The change in level corresponds directly to the water uptake/release from the thermochemical reaction. Hence, the reacted fraction of the thermochemical reaction can be calculated from the level change. The pressure in the reactor was measured by the pressure sensor P2 (Cerabar M PMP55, Endress + Hauser Messtechnik GmbH + Co.KG, ± 0.15%) as shown in Fig. 1.

2.2. Hydrogen infrastructure

Hydrogen can be supplied- or withdrawn from the reactor using the volume-flow-controllers F1 (F-232MI, Bronkhorst High-Tech B.V., ± 0,5% Rd plus ± 0,1% FS) and F2 (F-111AI, Bronkhorst High-Tech B.V., ± 0,8% Rd plus ± 0,2% FS). Minimal hydrogen flow rates are 4.3 g h^{-1} and 2.7 g h^{-1} for inflow and outflow, respectively. The operating pressure ranges from 1 bar to 50 bar and is measured with pressure sensor P1 (PA-21Y, KELLER AG, ± 0.4 bar). The controllers can either be operated sustaining a constant volume flow rate or a constant pressure.

2.3. Materials and prototype reactor

For the metal hydride, an alloy of 90% Magnesium and 10% Nickel was used. The $Mg_{90}Ni_{10}$ alloy was melt-spun, mixed with 10 wt% expanded natural graphite and compressed to pellets with 30 mm diameter at 300 MPa. A central hole with 5 mm diameter was drilled through the pellet to allow for hydrogen distribution and insertion of thermocouples. These pellets were manufactured at Fraunhofer Institute for Manufacturing Technology and Advanced Materials IFAM in Dresden, Germany [19]. For the thermochemical heat storage material, magnesium hydroxide $Mg(OH)_2$ was obtained from Sigma-Aldrich (Nr. 63081), which is an unmodified, fine, white powder.

The prototype reactor is displayed in detail in Fig. 2. It consists of a double tube with 234 g $Mg_{90}Ni_{10}$ (red) in the inner tube and 400 g $Mg(OH)_2$ (grey) in the outer tube. With a gravimetric hydrogen capacity of 5.3 wt% for the $Mg_{90}Ni_{10}$ pellets, the amount of metal hydride was chosen in a way that approximately 12 g hydrogen can be stored. To take up the heat of absorption, 400 g $Mg(OH)_2$ are needed assuming that 84% of the $Mg(OH)_2$ react. Several thermocouples (Type K, ± 1.5 °C) are incorporated into the reactor. For clarity, only the thermocouples that are referenced in the results section are shown in Fig. 2. These thermocouples are on the same height, the ones in the $Mg(OH)_2$ section are slightly offset along the circumference. Due to large flanges at both ends of the reactor, the height of the thermocouple's positions was chosen to be at a position the least thermal losses were assumed. Since the $Mg_{90}Ni_{10}$ pellets have a central hole and the $Mg(OH)_2$ powder is kept in place with a sinter metal filter, diffusion pathways for the hydrogen and water vapor are 10 mm and 13 mm, respectively. Therefore, mass transfer limitations can be excluded.

2.4. Experimental procedure and evaluation

For hydrogen storage, the adiabatic storage reactor was completely depleted of hydrogen before the initiation of the hydration experiment. For that purpose the $Mg_{90}Ni_{10}$ was repeatedly exposed to vacuum until the temperatures didńt decline anymore. The $MgO/Mg(OH)_2$ was exposed to the water vapor for several hours until no further change in temperatures has been measured indicating that the hydration is complete. The system's components were tempered to the desired temperatures, which may be different for separate experiments. The initial temperatures are reported at the respective analysis section. It was chosen to be not too high, because a heat-up of the bed due to the exothermal reaction should be observed. It should not be too low as well, since the majority of the exothermally released heat should drive the endothermal reaction and not only heat-up the bed. At the same time, the dehydration of $Mg(OH)_2$ should not take place at the initial temperature. The selected initial temperatures comply with these criteria. The reaction was initiated by increasing the hydrogen pressure to the desired value. Accordingly, for hydrogen release, the adiabatic storage reactor was fully loaded with hydrogen before the experiment. It was ensured with the increase of the hydrogen pressure at least 15 bar above the equilibrium pressure, waiting until the temperatures levelled off and no further pressure decrease in the closed reactor could be observed. Full dehydration of the $Mg(OH)_2$ before the experiment's initiation was ensured with additional heat up using the external heating and application of vacuum until the temperatures levelled off. The hydrogen release reaction was initiated by a sudden increase in water vapor to the desired value and setting the desired hydrogen volume flow rate in the mass flow controller.

The reactor is heated with an external heating wire to the initial temperature. During the course of the experiments this external heating was kept turned on to compensate for thermal losses. For the experimental evaluation it is important that the endothermal thermochemical reaction is not driven by input of thermal energy from the external

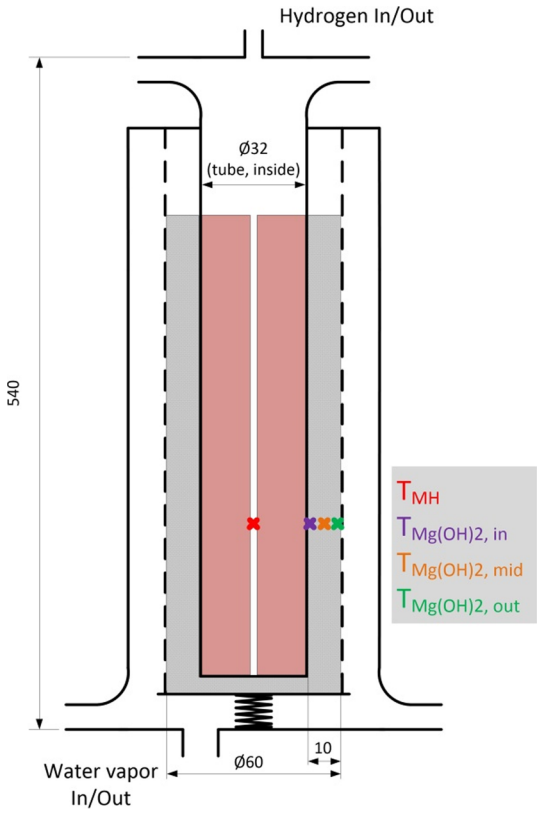

Fig. 2. Reactor schematic including thermocouples; $Mg_{90}Ni_{10}$ (red); $Mg(OH)_2$ (grey); Dashed line: Sinter metal filter; Dimensions in mm; Not to scale; Inner tube's wall thickness: 4 mm. (For interpretation of the references to colour in this figure legend, the reader is referred to the web version of this article.)

heating wire, but from the thermal energy by the exothermal reaction. This is the case if the temperature levels in the reactor are higher during the experiment than before starting it. Unless stated otherwise this was the case in all presented experiments.

The conversion of the thermochemical heat storage reaction is monitored by the change of the liquid level in the evaporator/condenser. The level-meter works with guided wave radar. Therefore, its signal is subject to fluctuations if the liquid surface is uneven which is the case during evaporation and condensation. Rapid jumps in the signal in both directions have been observed during condensation. Since they do not have a physical meaning, they have been disregarded. For evaluation, the signal from the level meter had to be smoothed. That is why in the result section, the conversion calculations are shown for the compensated and smoothed data as well as the raw, non-smoothed data.

The reacted fractions of the materials have been calculated based on the maximum experimental possible conversion. For the $Mg_{90}Ni_{10}$, 100% of reacted fraction corresponds to 12.4 g of hydrogen uptake/release. For the $Mg(OH)_2$, it was experimentally determined that approximately 80% of the filled in $Mg(OH)_2$ reacts. This value was obtained during the first heat-up of the $Mg(OH)_2$ filled into the reactor. Therefore, the material was dehydrated and the water was condensed in the evaporator/condenser until no further condensation was observed. From the amount of condensed water, the reacted fraction was calculated. This is why 99 g water uptake/release represents 100%.

3. Hydrogen storage

Previous analytical calculations indicated that with the present materials, hydrogen storage in the adiabatic storage reactor is possible at 10 bar hydrogen pressure or below [13]. In this section the hydrogen storage properties of the reactor prototype are evaluated. During hydrogen storage, the metal hydride reacts with hydrogen which takes place in the inner tube and is the exothermal reaction. The endothermal reaction happening in the outer tube is the dissociation of $Mg(OH)_2$. For successful hydrogen storage, the temperature in the metal hydride has to be higher than the temperature in the thermochemical heat storage material for a temperature gradient to be established.

To evaluate the influence of the thermochemical heat storage material on the reactor's performance during hydrogen absorption, a reference experiment was conducted at which only the magnesium hydride was active. The heat storage material did not participate since it was present as MgO which is inert at these conditions. This experiment is shown with open markers in Fig. 3. Both experiments were started with a pressure increase to 9 bar hydrogen. It can be seen that the temperature in the magnesium hydride (red) rises sharply to the theoretical equilibrium temperature. Heat transfer into the inert MgO bed takes place and subsequently, temperatures rise as well and a temperature gradient can be observed since the thermocouples are placed in different bed-depths (see Fig. 2). For the combined experiment, the thermochemical heat storage material $Mg(OH)_2$ dissociates endothermally into MgO and water vapor. While the temperature course for the magnesium hydride is the same for the first 15 min, the temperatures in the magnesium hydroxide are lower than during the reference experiment. This behavior proofs that the $Mg(OH)_2$ starts to dissociate, creating a heat sink.

Furthermore, after 15 min, the operating mode was changed from pressure control to flow rate control. At approximately 15 min the flow rate into the reactor was set to 4.3 g h^{-1}. The temperature (and pressure, not displayed) starts to rise. Hence, the hydrogen absorption rate of the reactor from that moment on is below 4.3 g h^{-1}. In the combined experiment this is the case after approximately 50 min. Subsequently, more hydrogen can be stored in less time.

Overall, it is evident that the temperature of the metal hydride sticks to the equilibrium temperature for the displayed time frame, indicating that here the limiting reaction is the dehydration of $Mg(OH)_2$. The hydrogenation reaction could proceed faster in case the heat of reaction would be removed more quickly by the thermochemical heat sink.

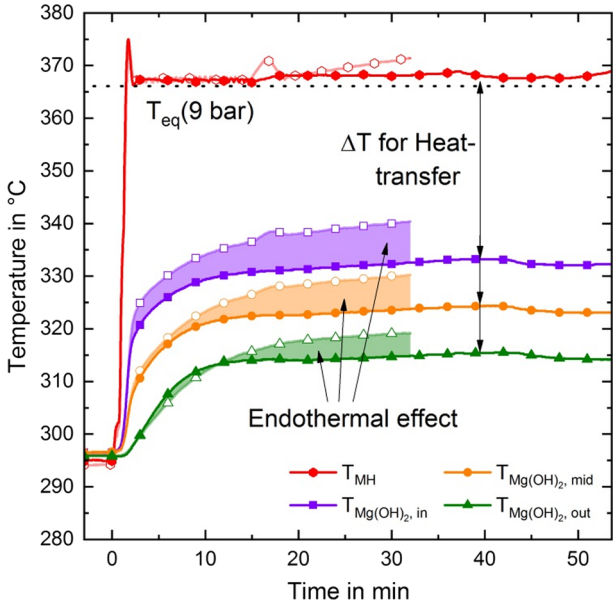

Fig. 3. Reactor temperatures during hydrogen storage at 9 bar hydrogen pressure and 60 mbar water vapor partial pressure; Open markers: Reference experiment; Full markers: Combined experiment; Thermocouple positions in Fig. 2.

3.1. Influence of temperature level on the hydrogen storage process

The reaction temperature is a crucial factor in every chemical reaction. According to the Arrhenius law higher temperatures yield in faster reaction rates. In order to evaluate the influence of the reactor temperature on the hydrogen storage process, the initial temperature was increased by 50 K. To draw conclusion on the reaction kinetics, the temperature difference, and thus, heat-transfer between the reactive beds was aimed to be identical in both cases. Hence, hydrogen absorption pressure was also increased to 25.7 bar. The temperature difference during operation was estimated to be 45 K, as it can be seen in Fig. 4(A). In both cases, the magnesium hydride (red) reacts quickly to the respective equilibrium conditions. During hydrogen absorption the pressure was kept constant throughout the absorption. In both cases, the magnesium hydride temperature starts to decrease at around 62 min. Since the pressure did not change, the materials' reaction rate decreases – probably due to getting close to the full capacity. Viewing the temperature course in the magnesium hydroxide (orange), it is evident, that at the lower temperature, it is rather flat after an initial heat-up. At the higher temperature, the initial heat-up is less pronounced. Instead, the material slowly heats up to a maximum. Only at the maximum the temperature difference matches the temperature difference with the comparison-process. Before that, it is even higher which indicates an increased reaction rate in the endothermal $Mg(OH)_2$ dehydration in the experiment at the higher temperature level. This can be confirmed by viewing the course of the reacted fraction in Fig. 4(B). At the same time, the reaction rate in the exothermal H_2 absorption is significantly enhanced, indicating that the reactive heat sink in the $Mg(OH)_2$ is more active.

In contrast to the initial temperature of 295 °C, in this experiment the $Mg(OH)_2$ is able to dehydrate at 345 °C, which is why the initial pressure in the compartment was higher at the higher temperature. At the beginning of the process, the valve to the tempered condenser was opened, and the desired set pressure was reached quickly while only a small fraction of the materials reacted. Therefore, the first few minutes of the hydrated fraction are not shown in Fig. 4(B). The $Mg(OH)_2$

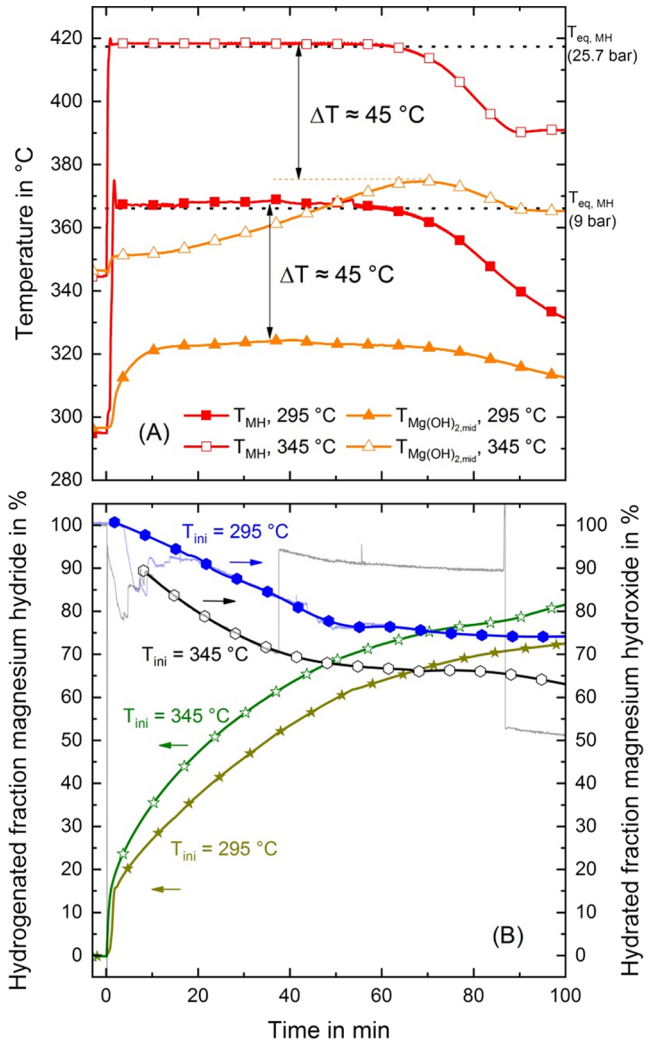

Fig. 4. Influence of the temperature level; 60 mbar water vapor partial pressure; Open markers: Initial temperature 345 °C; Full markers: Initial temperature 295 °C; Light blue and grey lines: Original, unsmoothed data. (For interpretation of the references to colour in this figure legend, the reader is referred to the web version of this article.)

dehydration rate slows down with time. This is in agreement with the temperature course, since the temperature (orange, open markers) is rising slowly which means that less heat is consumed. At its maximum the same temperature difference of 45 K is reached as in the comparison process, indicating that the same reaction rate is reached in the two cases.

In Fig. 4(B) it can be seen that the conversions of the hydrogen storage – and heat storage reaction do not correspond to each other. In the 295 °C case, 73% of the MgH_2 have reacted while only 26% of the $Mg(OH)_2$ has been dehydrated after 100 min. In the 345 °C case it is similar with 81% and 36%, respectively. The amount of materials has been chosen in a way that corresponding conversions could be expected. However, the heat of hydrogen absorption is not completely consumed by the endothermal $Mg(OH)_2$ dehydration since thermal losses to the environment are present. With the H_2 pressure increasing to the desired value, the temperature level in the reactor increases by 75 K. Therefore, not only a temperature gradient to the $Mg(OH)_2$ bed, but also to the environment is established and thermal losses cannot be avoided in this small, single tube prototype reactor. In a larger system though, thermal losses will be a minor issue since the majority of the material will be in an inner bulk being more adiabatic, rather than on the outside of the storage reactor.

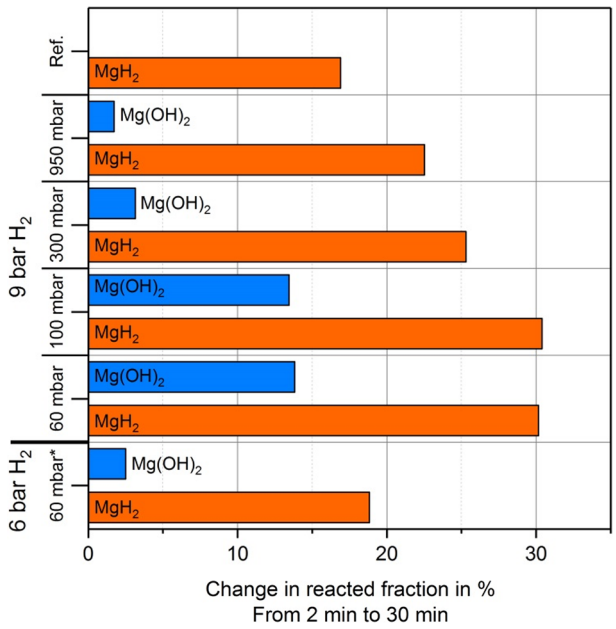

Fig. 5. Influence of water vapor condensation pressure and hydrogen pressure on hydrogen storage process; To avoid influences of the startup procedure, the timeframe for 2 min to 30 min is shown; Ref.: Reference experiment with inert heat storage material.

It can be concluded here, that with a higher temperature level in the reactor, faster hydrogen storage can be achieved. Since the equilibrium conditions are met almost instantly in both cases, the $Mg_{90}Ni_{10}$ hydrogenation in the prototype reactor is not limited by mass transfer or its kinetics but by heat transfer. It would be able to react even faster if the heat of reaction would be withdrawn more effectively. A larger heat sink, like the acceleration of the $Mg(OH)_2$ dehydration, would be beneficial for that purpose. Increasing the temperature level has this effect. Overall it can be concluded that in the present setup the $Mg(OH)_2$ dehydration rate is the limiting factor for the hydrogen absorption process.

3.2. Influence of water vapor pressure and hydrogenation pressure

The adiabatic storage reactor is a complex system with several parameters, such as operating temperatures or gas pressures, being tunable to enhance the hydrogen storage process. In Fig. 5, the influence of the water vapor condensation pressure and hydrogen storage pressure are shown. To eliminate influences of the startup procedure, the reaction progress from 2 min to 30 min is shown for various operation conditions. Two minutes after the start of hydrogen absorption, the pressure has adjusted to the desired value and MgH_2 temperatures are in steady-state. For every case, the change in the reacted fraction is shown with 100% being the maximum achievable reacted fraction. For comparison, the reference experiment discussed in Fig. 3 is included as well. The blue and orange bars in Fig. 5 represent the reacted fraction of the $Mg(OH)_2$ and $Mg_{90}Ni_{10}$, respectively. Ideally, the reacted fractions would be identical since the amount of material was chosen to compensate for each other. Thus, if there were no thermal losses, the heat being released by the exothermal hydrogenation would be consumed by the endothermal dehydration one-to-one and the reacted fractions would be the same. For the reference experiment, which was discussed in detail in Fig. 3, there was no endothermal dehydration, as the material was present as inert MgO.

It is obvious that the water vapor condensation pressure influences the reaction rate. The difference in the reacted fractions between 60 mbar and 100 mbar is marginal, a clear difference to 300 mbar and 950 mbar can be seen, where significantly less $Mg(OH)_2$ has reacted.

This indicates that the increased water vapor pressure slows down the reaction. With the heat source of the MgH_2 being the same, this can be attributed to reduced kinetics of the $Mg(OH)_2$ dehydration. As it is the nature of gas-solid reactions, increased pressure of the gaseous reactant reduces the dissociation reaction rate. In the present experiment, this effect leads to less thermochemical cooling and therefore, less hydrogen storage. Concluding here, for fast hydrogen storage, the water vapor condensation pressure should be kept as low as possible, but a reduction from 100 mbar to 60 mbar does not have a significant effect on the hydrogen uptake. At 100 mbar, which corresponds to a H_2O condensation temperature of 46 °C, heat release to the ambient would still be possible.

Additionally, it can be seen that the hydrogen pressure of 6 bar compared to 9 bar reduces the reaction rate for both materials significantly. Even though the equilibrium temperature is also reached instantly at 6 bar for the $Mg_{90}Ni_{10}$, the overall temperature level is lower since its equilibrium temperature is only 348 °C, compared to 366 °C at 9 bar. That temperature is too low for the $Mg(OH)_2$ dehydration to take place at a sufficiently fast rate. This can be seen at the very low value of reacted fraction in the defined timeframe in Fig. 5.

4. Hydrogen release

For the release of hydrogen from the adiabatic storage reactor, the chemical reactions for hydrogen- and heat storage have to be reversed and a temperature gradient in the opposite direction is necessary. For heat transfer, the temperature, at which the thermal energy is released, has to be higher than the magnesium hydride dehydrogenation temperature. Previous analytical [13] and numerical [15] investigations indicated that a water vapor pressure of 9 bar should be sufficient to drive the process by reaching a temperature level of around 340 °C. However, to the best of our knowledge, the hydration of MgO at that high pressure has not been investigated before. Hence, the temperature that can be achieved in the reactor during MgO hydration is of utmost interest.

Analogue to the hydrogen absorption, a reference experiment was conducted to evaluate the influence of the thermochemical heat storage reaction on the hydrogen release. During the reference experiment, no thermochemical heat was released. All thermal energy required for the dehydrogenation of magnesium hydride had to be taken from the environment, which results in a cooldown of the material. This behavior is shown in Fig. 6. A hydrogen flow rate of 2.7 g h^{-1} was applied and, thus, the magnesium hydride bed (red) cools down. For the reference experiment, the desired flow rate of 2.7 g h^{-1} could be sustained for 19 min. Afterwards, it slowly starts to decline. For clarity, that curve is not shown in Fig. 6. With reduced temperature, the reaction rate is reduced, which is why it levels off after approximately 30 min. The MgO bed cools down as well a little delayed, which is due to the thermal resistance of the set-up. Again, a temperature gradient can be observed in the MgO bed which is due to the position of the thermocouples in different depths, as shown in Fig. 2.

In contrast, for the experiment with both reactions participating, the temperature profile is different. The process was initiated by opening a valve between the evaporator and the reactor. Again, at the same time, the outflow of hydrogen at 2.7 g h^{-1} was started. It can be seen, that the temperature course in the MgO exhibits a sharp peak in the beginning. Then, temperatures decrease until they start to increase to a maximum. The temperature in the magnesium hydride follows that trend. The initial spike in the MgO temperature is probably attributed to adsorption of water vapor on the material surface, but not to the hydration reaction [20]. From the subsequent temperature course it can be deduced that the exothermal hydration accelerates at approximately 15 min. The maximum temperature that could be achieved at a water vapor pressure of 9.75 bar is 298.7 °C. This temperature is lower than expected, but high enough for heat transfer to the MgH_2 bed, because its dehydrogenation is able to happen below that temperature. In contrast to the reference experiment, the desired hydrogen mass flow rate of 2.7 g h^{-1} could be sustained for 83 min before it starts to decline.

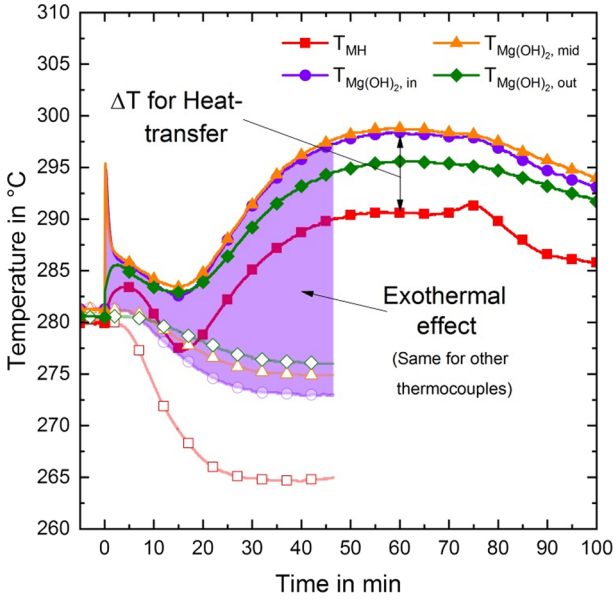

Fig. 6. Reactor temperatures during hydrogen release at 2.7 g h^{-1}; 9.75 bar water vapor pressure (only full markers); Open markers: Reference experiment; Full markers: Combined experiment; Thermocouple positions in Fig. 2.

This maximum temperature achieved during MgO hydration is probably not the chemical equilibrium temperature at that pressure, but an effective equilibrium including thermal losses to the environment. Nevertheless, this temperature is way lower than estimated analytically [13] and numerically [15] before. Extrapolation of equilibrium data obtained at pressures below 1 bar predicts a chemical equilibrium of 348 °C at 9.7 bar [20]. It is well-known that the reaction system of $Mg(OH)_2$ / MgO – just as many other gas–solid reactions – can exhibit a different equilibrium temperature at a given pressure for hydration and dehydration, respectively, which is known as hysteresis [21]. Since this influences the maximum temperature for the heat release, it was clear that it may affect the storage reactor's performance significantly, but so far it was not known at such high pressures of 9 bar. Concluding from the present experiments, it can be stated that even though the reaction system exhibits this significant hysteresis, the system is able to provide heat at a sufficiently high temperature to release the previously stored hydrogen.

4.1. Influence of MgO hydration pressure on the hydrogen release

The adiabatic storage reactor's main advantage is its combination of two independently controllable thermochemical gas–solid reactions. In comparison to similar concepts, such as the usage of a PCM [7], the advantage is that the temperature level at which heat is released or stored, can be adjusted with the gas pressure of the water vapor. Hence, gas pressure has an important influence on the reaction system. Fig. 7 shows the influence of the water vapor pressure on the MgO hydration, which is the exothermal release of the previously stored thermal energy required for the hydrogen release. The initial temperature spike, which is probably attributed to adsorption, does not increase the reacted fractions. Even though the water vapor pressure has only been raised by 300 mbar from 9.45 bar to 9.75 bar, an increase in the maximum temperature is obvious - compare Fig. 7(A). The maximum temperature reached in the MgO bed increases from 295 °C to 298 °C. This leads to a higher temperature in the magnesium hydride bed, where the H_2 release reaction can be sustained longer at the given rate, as it can be seen in Fig. 7(B). Additionally, this small increase in gas pressure accelerates

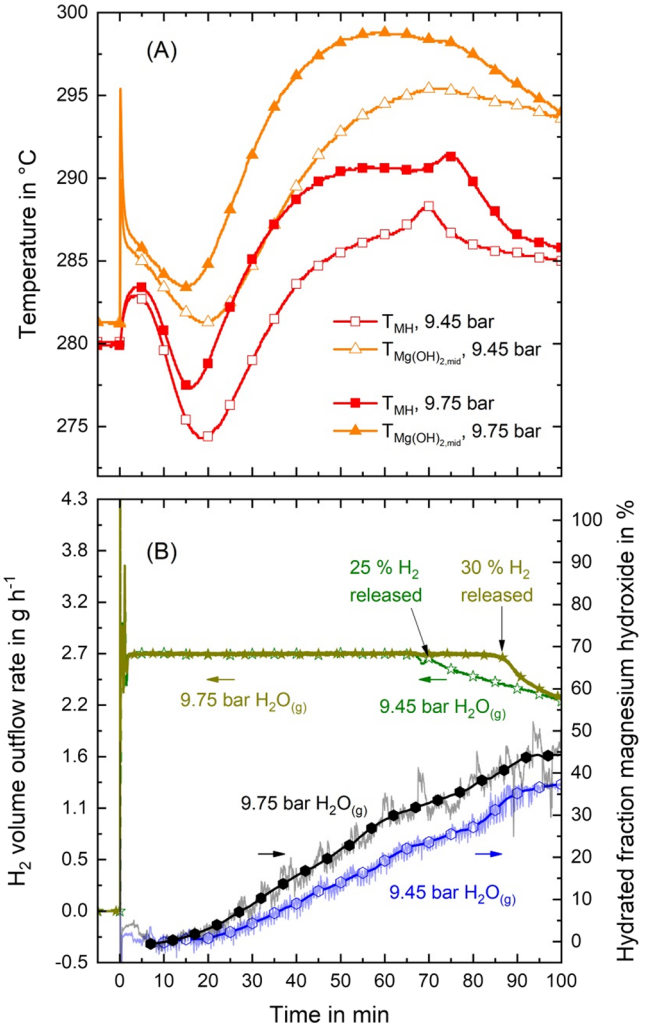

Fig. 7. Influence of MgO hydration pressure; Hydrogen outflow rate 2.7 g h^{-1}; Full markers: 9.75 bar; Open Markers: 9.45 bar.

the MgO hydration rate which can also be seen in Fig. 7(B).

Similar to the hydrogen storage process, thermal losses occur during the hydrogen release in the present system. As long as the temperature in the reactor is higher than the initial temperature, there is a temperature gradient to the ambient leading to thermal losses. This is the case for most of the time, as it can be seen in Fig. 7(A). Compared to the hydrogen storage process (Fig. 3), however, the temperature level of the exothermal reaction is 60 K lower. Therefore, the temperature gradient to the environment is lower and thermal losses are less pronounced. This can be seen in the values for the conversion in Fig. 7(B). For the 9.45 bar case, 25% of the stored hydrogen was released and 24% of the MgO hydrated at 70 min. Similarly, for the 9.75 bar case, 30% Hydrogen is released with 39% conversion in the MgO reaction at 85 min. Therefore, it can be concluded that the released heat during MgO hydration is being consumed by the MgH_2 dehydrogenation, rather than being lost to the environment. The experiment was stopped before 100% of the materials reacted since the hydrogen release rate started to decline rapidly, as it can be seen in Fig. 7(B).

4.2. Influence of operating mode on hydrogen release

Depending on the application, it may be a matter of interest to withdraw hydrogen from the reactor at a constant pressure or a constant mass flow rate. At a constant pressure, the reactor would operate at maximum power while it would be at constant power during the

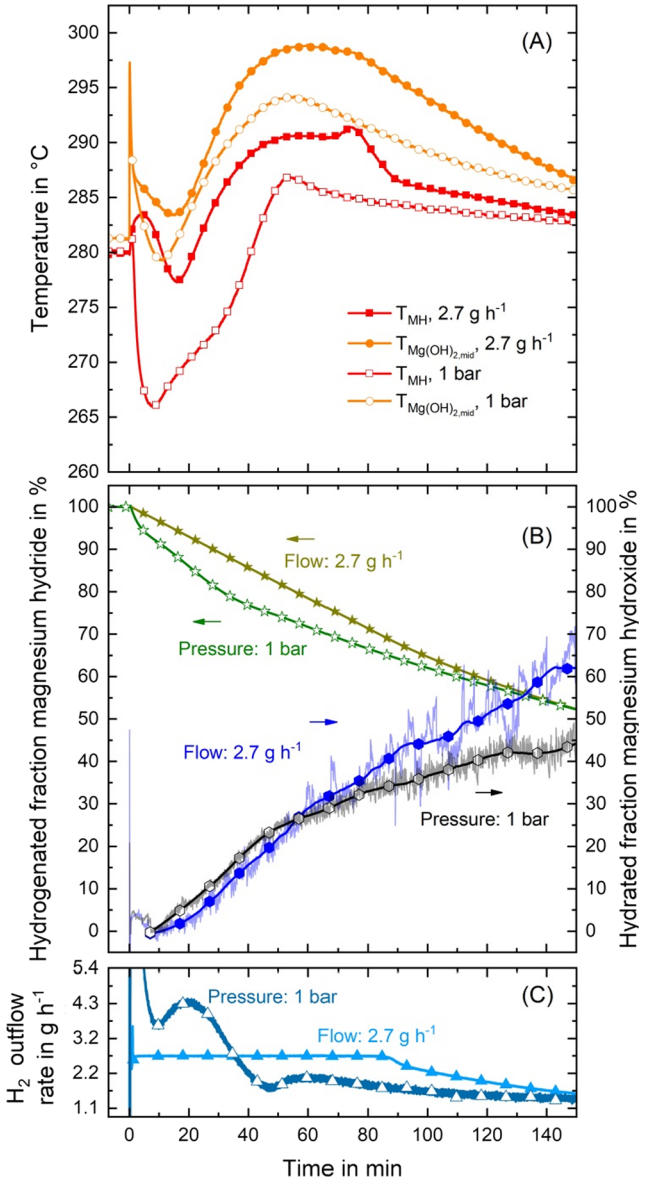

Fig. 8. Influence of operation mode maximum power or constant power; MgO hydration pressure: 9.75 bar; Full markers: Constant power at 2.7 g h^{-1} H_2 flow; Open markers: Maximum power at 1 bar H_2 pressure.

operating mode of constant mass flow rate. The comparison between the two modes at a pressure of 1 bar and 2.7 g h^{-1}, respectively, is shown in Fig. 8. The initial conditions are similar. It can be seen that the temperature in the maximum power case decreases rapidly since dehydrogenation is taking place consuming thermal energy from the materials. This initial temperature drop decreases the temperature level of the whole process, which is evident in Fig. 8(A). Subsequently, more hydrogen is released initially as it can be seen in Fig. 8(C). Therefore, the hydration of MgO happens at a lower temperature and results in slower reaction rate. This can be seen in Fig. 8(B) since the hydrated fraction is lower after 140 min.

Therefore it can be concluded here, that hydrogen can be withdrawn at maximum – or constant power. However, if the temperature in the reactor drops too low, the MgO hydration reaction is not able to deliver enough heat to maintain the maximum power because the bed cools down thereby reducing the reaction rate. Thus, if not operated carefully, the present adiabatic storage reactor is able to impede itself during hydrogen release since the reaction rates are sensitive to the temperature in the chosen conditions.

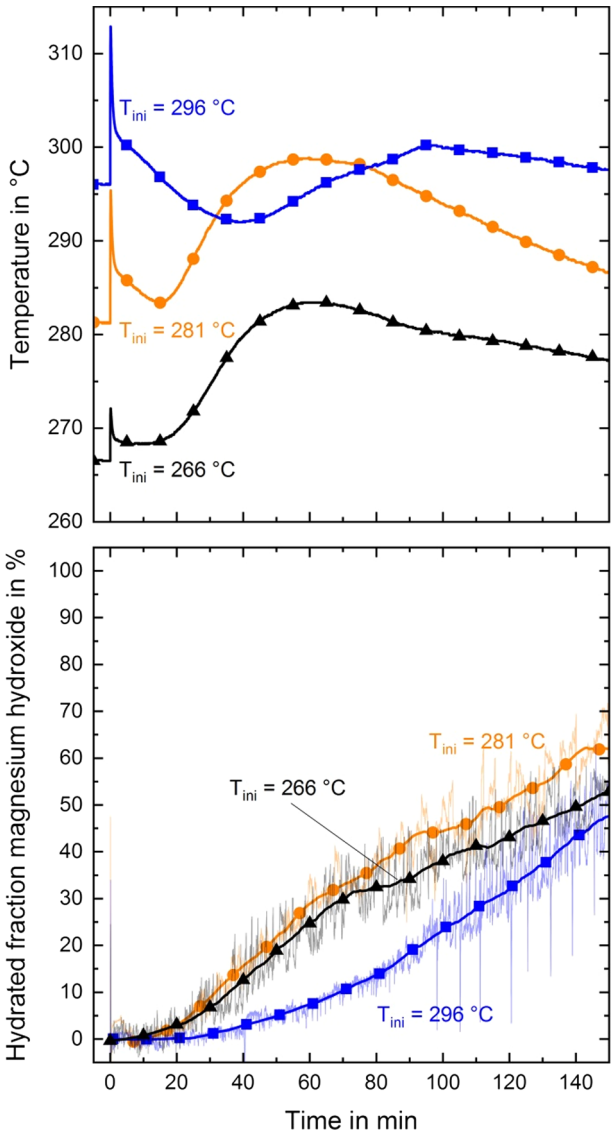

Fig. 9. Influence of initial temperature on MgO hydration; MgO hydration pressure: 9.75 bar; Hydrogen outflow rate: 2.7 g h^{-1}; Shown Thermocouple: $T_{Mg(OH)2,\ mid}$.

4.3. Influence of the temperature level on the MgO hydration

As it was discussed in the previous sections, the thermochemical heat storage reaction is the limiting factor in the present setup. During the hydrogen release process, rapid release of thermal energy would result in rapid hydrogen release. Little is known about the exothermal reaction of magnesium oxide with water vapor at such high pressures of more than 9 bar. Therefore, the initial temperature of the hydrogen release was varied for hydration at 9.75 bar and a hydrogen flow rate of 2.7 g h^{-1}. Fig. 9(A) and (B) show the temperature course in the MgO bed and the reacted fractions of the MgO, respectively. In all cases, the temperature drops in the beginning before it starts to increase again. The beginning of this increase occurs earlier for lower temperatures and later for higher temperatures. Apart from that, in the 281 °C and the 266 °C cases the temperature courses are almost identical, just shifted for 15 K. Additionally, for the 296 °C case, the temperature course is more flat.

The increase of temperature after the minimum indicates that the exothermal MgO hydration reaction starts to accelerate. This can be confirmed with Fig. 9(B), since the increase in temperature coincides with the increase in reacted fractions. According to Arrhenius's law, a reaction rate increases with increasing temperature, however, this behavior cannot be observed here. Instead, at higher temperatures the reaction starts to accelerate later and less pronounced. Therefore, it can be concluded that the chemical equilibrium is approached at the higher temperature which reduces the driving force, and thus, the reaction rate of the chemical reaction. Since the maximum temperature archived is different as well, it can be concluded that the reaction is hindered kinetically due to the proximity of the equilibrium. Otherwise, the maximum of the temperature achieved would be the same for all cases.

From the fact that the maximum temperature is approximately the same for the medium and high initial temperature, it can be concluded that the maximum possible temperature to be reached in this setup is around 300 °C.

5. Optimization approaches

The present prototype reactor was designed to proof the hydrogen storage and release capability of this adiabatic system and that the necessary temperature gradients can be established. The reactor design did not aim for high storage density, to minimize hydrogen storage/release times, to fully utilize the materials involved or to investigate the cycling behavior. The present non-optimized prototype exhibits a gravimetric and volumetric hydrogen density of approximately 0.40 g_{H2} kg^{-1} and 0.20 g_{H2} L^{-1}, respectively. These values include the prototype reactor's steel vessel, flanges, insulation and reactive materials assuming 100% hydrogenation of the metal hydride. Assuming 100% conversion for the magnesium hydride pellets and 80% conversion of the $Mg(OH)_2$ powder (Porosity 62%) and regarding only the volume of the two reactive materials, a volumetric density of 20.8 gH_2 L^{-1} can be achieved. The value of a real system in large scale will be a little lower, since the steel for the reactor and the insulation has to be taken into account. The amount of steel is depending on the overall reactor design and is not deducible from the prototype reactor. As the steel required for that purpose will add weight to the system but only little in volume and the insulation has to be applied on the reactor's exterior only, the comparison with other systems is justified. Operating below 10 bar, the volumetric storage density of the adiabatic storage reactor exceeds state of the art hydrogen storage in compressed tanks at 350 bar (16.1 g_{H2} L^{-1}) and is approximately equal to 700 bar compressed tanks (21–26 g_{H2} L^{-1}) [22]. Material modifications may increase the storage density of the adiabatic storage reactor to up to 25 g_{H2} L^{-1} which is at the upper end of the 700 bar pressure tank range. However, there is room for optimization, for example in the following suggestions.

First, the volumetric storage density of the storage reactor can be enhanced by compressing the thermochemical heat storage material to pellets with higher density and less porosity compared to a fine powder, similar to the magnesium hydride pellets. Second, the experimental results revealed a kinetic limitation of the $Mg(OH)_2$ / MgO reaction system which has been used as thermochemical heat storage material. Improving the reaction rates will lead to faster heat storage/release and subsequent faster hydrogen storage/release. Therefore, the material should be modified or doped, which already is a research topic [23,24].

Third, the prototype reactor designed in this work exhibits thermal losses, which means that released heat of the exothermal reaction is not being fully consumed by the other endothermal reaction. Instead, the heat is partially lost to the environment. Therefore, the reaction rate of the exothermal reaction is faster than the endothermal reaction rate, resulting in uneven conversions. For the adiabatic system to work reversibly, the heat of absorption has to be fully consumed by the thermochemical heat storage reaction. Otherwise the heat is not available for the hydrogen release. Since the prototype is only a single tube, thermal losses were expected. In a larger system thermal losses can be lower, since the surface-to-volume ratio can be reduced. Thermal losses in the present setup occurred mainly at the surface of the prototype reactor. Therefore, matching conversions can be expected in large scale

applications.

The cost of the proposed adiabatic storage reactor in large scale is difficult to determine, since it depends strongly on the design of the reactor and its surrounding infrastructure. The cost of the presented prototype exceeds any economic feasibility by far. However, the raw materials of the proposed system only require magnesium which can be obtained for 2–3 USD kg_{Mg}^{-1} [25]. Therefore, the lower threshold for the material cost is 52–78 USD kg_{H2}^{-1}. This is a prerequisite for large scale application.

6. Conclusion

In this work the experimental proof of concept of a novel hydrogen storage concept was demonstrated. It utilizes two thermochemical reactions for hydrogen storage and heat storage, respectively. Magnesium hydride (MgH_2) is used for hydrogen storage and the $Mg(OH)_2$/MgO system for heat storage. Hence, an exothermal reaction is coupled with an endothermal one compensating for each other. Due to the high hydrogen storage capacity of MgH_2, the storage concept exhibits high storage densities at low pressures below 10 bar. The materials used are non-toxic, cheap and abundantly available. Therefore, this storage technology may be a part of a hydrogen economy in the future. A lab scale reactor prototype was developed and characterized. Even though there is potential for optimization during upscaling, the working principle has been proofed. The thermochemical properties of the materials fit to each other for both hydrogen storage and release. Facing thermal losses and poor kinetics of the $Mg(OH)_2$/MgO system, 100% conversion was not achieved with simultaneous thermochemical cooling/heating during hydrogen storage/release, respectively. However, it has been demonstrated that hydrogen can be stored at a high volumetric capacity at a pressure below 10 bar, which makes the adiabatic storage reactor a promising option for stationary hydrogen storage. For hydrogen release, the previously stored heat has to be released. It has been shown that the hydration of MgO at a water vapor pressure of 10 bar results in a temperature level of 300 °C, which has never been experimentally investigated before. This temperature is sufficiently high to drive the MgH_2 dehydrogenation in the present system.

CRediT authorship contribution statement

Michael Lutz: Conceptualization, Methodology, Formal analysis, Investigation, Writing - original draft, Visualization. **Marc Linder:** Resources, Writing - review & editing, Supervision, Project administration, Funding acquisition. **Inga Bürger:** . **:** Conceptualization, Methodology, Writing - review & editing.

Declaration of Competing Interest

The authors declare that they have no known competing financial interests or personal relationships that could have appeared to influence the work reported in this paper.

Acknowledgments

The authors want to thank the Karl-Vossloh-Stiftung (Project No.: S047/10043/2017) for partially funding this work.

References

[1] Lewandowska-Bernat A, Desideri U. Opportunities of power-to-gas technology in different energy systems architectures. Appl Energy 2018;228:57–67.
[2] Maeda T, Nishida K, Tange M, Takahashi T, Nakano A, Ito H, et al. Numerical simulation of the hydrogen storage with reaction heat recovery using metal hydride in the totalized hydrogen energy utilization system. Int J Hydrogen Energy 2011;36(17):10845–54.
[3] The High Pressure Gas Safety Institute of Japan (KHK), https://www.khk.or.jp/english, [Online]. Available: https://www.khk.or.jp/Portals/0/resources/english/dl/hpgact_overview.pdf [accessed 12 09 2019].
[4] Sakintuna B, Lamari-Darkrim F, Hirscher M. Metal hydride materials for solid hydrogen storage: a review. Int J Hydrogen Energy 2007;32(9):1121–40.
[5] Yadav M, Xu Q. Liquid-phase chemical hydrogen storage materials. Energy Environ Sci 2012;5(12):9698–725.
[6] Niaz S, Manzoor T, Pandith AH. Hydrogen storage: Materials, methods and perspectives. Renew Sustain Energy Rev 2015;50:457–69.
[7] Garrier S, Delhomme B, De Rango P, Marty P, Fruchart D, Miraglia S. A new MgH2 tank concept using a phase-change material to store the heat of reaction. Int J Hydrogen Energy 2013;38(23):9766–71.
[8] Mellouli S, Ben Khedher N, Askri F, Jemni A, Ben Nasrallah S. Numerical analysis of metal hydride tank with phase change material. Appl Therm Eng 2015;90:674–82.
[9] Seo S-K, Yun D-Y, Lee C-J. Design and optimization of a hydrogen supply chain using a centralized storage model. Appl Energy 2020;262:114452.
[10] Alva G, Lin Y, Fang G. An overview of thermal energy storage systems. Energy 2018;144:341–78.
[11] Yartys V, Lototskyy M, Akiba E, Albert R, Antonov V, Ares J, et al. Magnesium based materials for hydrogen based energy storage: Past, present and future. Int J Hydrogen Energy 2019;44(15):7809–59.
[12] Sadhasivam T, Kim H-T, Jung S, Roh S-H, Park J-H, Jung H-Y. Dimensional effects of nanostructured Mg/MgH2 for hydrogen storage applications: a review. Renew Sustain Energy Rev 2017;72:523–34.
[13] Bhouri M, Bürger I, Linder M. Feasibility analysis of a novel solid-state H2 storage reactor concept based on thermochemical heat storage: MgH2 and Mg (OH) 2 as reference materials. Int J Hydrogen Energy 2016;41(45):20549–61.
[14] Bhouri M, Bürger I. Numerical investigation of H2 absorption in an adiabatic high-temperature metal hydride reactor based on thermochemical heat storage: MgH2 and Mg (OH) 2 as reference materials. Int J Hydrogen Energy 2017;42(26):16632–44.
[15] Lutz M, Bhouri M, Linder M, Bürger I. Adiabatic magnesium hydride system for hydrogen storage based on thermochemical heat storage: Numerical analysis of the dehydrogenation. Appl Energy 2019;236:1034–48.
[16] Multi, "Annual Work Plan 2014 - 2020 of the FCH JU," [Online]. Available: https://www.fch.europa.eu/sites/default/files/MAWP%20final%20version_endorsed%20GB%2015062018%20%28ID%203712421%29.pdf.
[17] Jensen JO, Vestbø AP, Li Q, Bjerrum N. The energy efficiency of onboard hydrogen storage. J Alloy Compd 2007;446–447:723–8.
[18] Schmidt M, Szczukowski C, Roßkopf C, Linder M, Wörner A. Experimental results of a 10 kW high temperature thermochemical storage reactor based on calcium hydroxide. Appl Therm Eng 2014;62(2):553–9.
[19] Pohlmann C, Röntzsch L, Kalinichenka S, Hutsch T, Weißgärber T, Kieback B. Hydrogen storage properties of compacts of melt-spun Mg90Ni10 flakes and expanded natural graphite. J Alloy Compd 2011;509:S625–8.
[20] Kato Y, Yamashita N, Kobayashi K, Yoshizawa Y. Kinetic study of the hydration of magnesium oxide for a chemical heat pump. Appl Therm Eng 1996;16(11):853–62.
[21] Kiyabu S, Lowe JS, Ahmed A, Siegel DJ. Computational screening of hydration reactions for thermal energy storage: new materials and design rules. Chem Mater 2018;30(6):2006–17.
[22] Hirscher M, Hirose K. Handbook of hydrogen storage: new materials for future energy storage. Weinheim: John Wiley & Sons; 2010. p. 13.
[23] Shkatulov AI, Aristov Y. Thermochemical energy storage using LiNO3-Doped Mg (OH) 2: a dehydration study. Energy Technol 2018;6(9):1844–51.
[24] Shkatulov A, Takasu H, Kato Y, Aristov Y. Thermochemical energy storage by LiNO3-doped Mg (OH) 2: Rehydration study. J Storage Mater 2019;22:302–10.
[25] Shao H, He L, Lin H, Li H-W. Progress and trends in magnesium-based materials for energy-storage research: a review. Energy Technol 2018;6(3):445–58.

Summary of individual contributions in Paper II:

- Formulation of the publication´s research goal:

  The goal was to experimentally proof the concept of the adiabatic hydrogen storage system. It was proofed that the specific pair of two thermally coupled thermochemical gas-solid reactions is suited for hydrogen storage. Both hydrogen storage and release were addressed.

- Development of the experimental setup:

  A test bench as well as a prototype reactor were designed, engineered, and investigated.

- Experimental design and execution of the experiments.
- Visualization and presentation of the data.

  Selection of relevant data and determining a comprehensible way of presenting it.

- Analysis and deductive reasoning:

  The influence temperatures, pressures, and operating modes on the hydrogen storage- and release process was investigated. The storage principle was proven experimentally. The limiting process was identified as the reaction kinetics of the Mg(OH)2 / MgO. The suitability of the used materials was assessed. Suggestions for an improved reactor design were given.

- Writing of the manuscript and publishing in Applied Energy.

On the error sources in the experimental work:

The aim of this publication is to proof the operating principle of the hydrogen storage system based on two thermochemical reactions. For that purpose, experimental data was gathered with thermocouples, mass flow controllers, pressure sensors and a level meter. The accuracy of the equipment is reported in the publication. Most of the presented data relies on the direct values of the equipment, such as temperature, pressure, or flow rates. The conclusions regarding the direct values were drawn on significantly larger differences than their respective errors. For example, the thermocouples exhibit an accuracy of ± 1.5 K. Conclusions using temperature changes were drawn with temperature differences significantly larger than ± 1.5 K. The most error-prone

device was the monitoring of the water-level in the evaporator/condenser. The raw signal was subject to comparatively large fluctuations. For that reason, the raw data was smoothed. These fluctuations are the main uncertainty during the measurement. With this data the conversion of the thermochemical heat storage material is calculated. However, to show the large fluctuations of the raw data, both the conversion rates based on the raw data as well as the conversion rates of the smoothed data is presented. Error bars were not added as the main purpose of the manuscript was the proof of concept and the identification of qualitative interrelations - not the quantitative reporting of precise conversion rates of the two thermochemical materials.

It was experimentally proven that the adiabatic hydrogen storage reactor is able to store and release hydrogen in the selected setup. The thermodynamics of the materials fit to each other and the thermochemical heat storage material is the limiting reaction. It could be concluded that unmodified material does not exhibit the desired features for the adiabatic hydrogen storage reactor. The material in general is feasible, but material modifications are necessary to enhance the reaction rate which is beyond the scope of this work. As a next step, the system was transferred to a closed thermally coupled system of two thermochemical reactions as introduced in Section 1.3.3. The focus in the third publication is on a system of a coupled metal hydride system which can be used for energy storage as well. Therefore, it is referred as a thermochemical battery. Instead of coupling the metal hydride with a thermochemical heat storage material, it is coupled with another metal hydride. Additionally, the two systems are not only coupled thermally, but also on the gaseous side. An energetic analysis and the features of the thermochemical battery are covered in the third journal publication.

Paper III

Electricity storage based on coupled thermochemical reactions: The thermochemical battery

Michael Lutz, Matthias Schmidt, Marc Linder, Inga Bürger

Journal of Energy Storage

Volume 33, January 2021, 102104

https://doi.org/10.1016/j.est.2020.102104

Journal of Energy Storage 33 (2021) 102104

Contents lists available at ScienceDirect

Journal of Energy Storage

journal homepage: www.elsevier.com/locate/est

Electricity storage based on coupled thermochemical reactions: The Thermochemical Battery

Michael Lutz [a,*], Matthias Schmidt [b], Inga Bürger [a], Marc Linder [a]

[a] Institute of Engineering Thermodynamics, German Aerospace Center (DLR), Pfaffenwaldring 38-40, D-70569 Stuttgart, Germany
[b] Institute of Engineering Thermodynamics, German Aerospace Center (DLR), Linder Höhe, D- 51147 Köln, Germany

ARTICLE INFO

Keywords:
Hydrogen storage
Thermochemical heat storage
Thermochemical battery
Metal hydride
Electricity storage

ABSTRACT

Thermochemical reactions are under investigation for a wide variety of applications. However, the system of two coupled gas-solid reactions exchanging both thermal energy and gas solely with each other has not been investigated yet. This approach allows realizing a compact thermochemical unit with two gas reservoirs at different pressure levels at approximately the same temperature. In this work, such a system is fundamentally analyzed and its technical potential as an energy storage component is investigated. While any two thermochemical gas-solid system can be used, this work exemplarily focusses on metal hydrides. Based on a thermodynamic analysis, it can be shown that the system is feasible, as the intrinsic difference in the reaction enthalpies of the metal hydrides can be compensated with heat integration of the compression unit. Following these findings, a thermochemical battery is investigated in more detail including an energetic analysis of efficiencies and potential storage densities. It is deduced that a higher pressure ratio between the hydrides yields in higher storage density but lower efficiency. Co-generation of cooling energy during discharging is feasible.

1. Introduction

With the change of the global energy system from fossil based to renewable, a need for energy conversion- and storage systems arises. Besides other technologies, thermochemical systems are under investigation for that purpose. In thermochemical systems, thermal energy drives the dissociation of a compound and combining the reactants again releases the thermal energy. The separation of the reactants should be easy, which is why gas-solid reactions are beneficial for that purpose.

Due to the nature of gas-solid reactions, during a cycle of absorption and desorption, the material can act as heat source and mass sink or heat sink and mass source, respectively. Subsequently, these system's thermal features can be used for heating or cooling. Especially hydrogen-metal systems are investigated to preheat fuel cell systems [1] or to utilize the potential energy of compressed hydrogen to drive an air conditioning unit in fuel cell vehicles [2]. Or, besides that, gas-solid reactions are also interesting for gas storage. Metal hydrides are in the discussion to serve as hydrogen storage compounds in a future hydrogen economy [3].

If the gaseous compound of a gas-solid reaction can be supplied to the material at varying pressures or temperatures, the range of applications extends even more. For this purpose, the system has to be coupled with a pressure dependent gas supply. For systems with a gaseous reactant easy to condense, such as water vapor, a temperature-dependent evaporator/condenser is beneficial. In case the gas is more difficult to condense, such as hydrogen, another thermochemical material can be used instead of an evaporator/condenser. In such a system, the gaseous side of two different thermochemical materials using the same gaseous reactant is coupled, while heat supply to the two beds is independent. In a setup like this, thermal energy can also be released at a higher temperature level than it has been stored before. This process is called heat transformation and has been investigated for both hydrogen- [4] and water vapor systems [5]. It is also possible to operate such a system as a heat pump [6].

Hence, single thermochemical systems can be used for thermal energy storage, gas storage, heating or cooling. Thermochemical systems coupled on the gaseous side while being independent on their thermal sides can additionally be applied for heat pumps and heat transformation. In this contribution we analytically investigate for the first time the potential applications and performance of a thermochemical system that is both coupled thermally and on the gaseous side. Hence, two different thermochemical materials working with the same gaseous

* Corresponding author.
E-mail address: michael.lutz@dlr.de (M. Lutz).

https://doi.org/10.1016/j.est.2020.102104
Received 27 June 2020; Received in revised form 11 November 2020; Accepted 13 November 2020
Available online 29 November 2020

Nomenclature

Symbol	*Description*	*Unit*
M	Molar mass	kg mol^{-1}
p	Pressure in reactor compartment 1	Pa
R	Universal gas constant	J mol^{-1} K^{-1}
T	Temperature	K
w	Work	J kg^{-1}
$\Delta_R H$	Reaction enthalpy	J mol^{-1}
$\Delta_R S$	Reaction entropy	J mol^{-1} K^{-1}
ΔT	Temperature difference for heat transfer between reactor compartments	K
η	Efficiency	-
κ	Specific heat ratio of the gas	-

Subscripts	*Description*
Ref	Reference
Isen	isentropic
Comp	Compression
Eq	Equilibrium

Acronyms	*Description*
CAS	Compressed air storage
M	Metal
MH	Metal hydride

reactant exchange both gas and thermal energy solely with each other. Such a setup offers two reservoirs for gas storage at different pressures that could be used e.g. for electricity storage. This paper outlines the newly developed storage concept. Taking basic systems properties into account, a first analysis on the concept's general potential efficiency and storage densities has been carried out. By stepwise including more aspects of a real technical system, like inefficiencies of the compression and expansion and thermodynamic losses due to heat transfer, the impact of these factors on the energy efficiency and storage density has been identified.

2. Process analysis - Basic concept

In this section, the basic principles of the thermochemical battery are presented. The system consists of two thermochemical gas-solid reactions coupled both thermally and on the gaseous side. While any two reactions involving the same gaseous reactant, such as water vapor or ammonia, could be used, this work focuses on metal-hydrogen systems. Metal hydrides have been studied intensively for most of the applications mentioned in the previous paragraph. Therefore, a wide variety of different metals with different thermodynamic properties are available. This variety of materials is a sufficient data basis for analyzing the properties of the thermochemical battery.

Metal hydrides are able to reversibly store and release hydrogen via a thermochemical reaction. Generalized, they can be described with the following reaction equation, with M representing a metal [3]:

$$M + \frac{x}{2}H_2 \rightleftharpoons MH_x \quad (1)$$

Due to the nature of gas-solid reactions, the reaction temperature of a metal hydride can be adjusted with the gas pressure and vice versa. This characteristic is different for every metal hydride. The relationship between the pressure and so called equilibrium temperature of such a system is commonly visualized in a van't Hoff plot. Figure 1 qualitatively illustrates the distinct coherence between the pressure of the gas and the temperature of the reaction for two different metal hydrides.

The proposed thermochemical battery utilizes the pressure difference between two different metal hydrides at a given temperature T_{ini}.

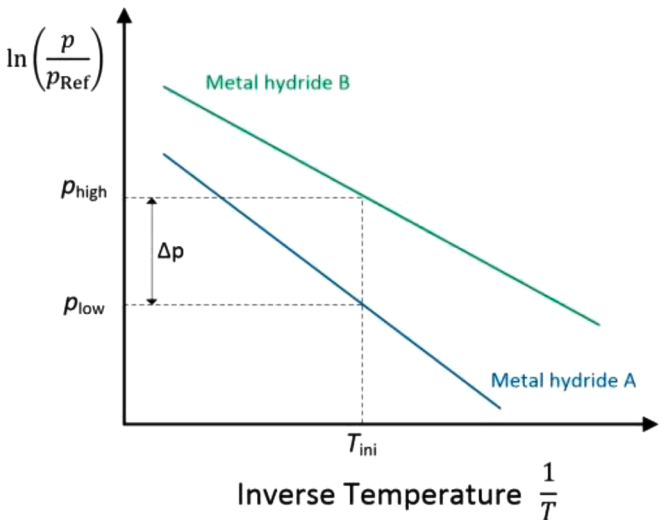

Figure 1. Two metal hydrides – van't Hoff plots.

The two hydrides are placed in separate compartments of the reactor operating as gas reservoir. They are in thermal contact to enable heat transfer between the materials. Additionally, they are coupled on the gaseous side.

A similar system also operating with a setup that is coupled both thermally and on the gaseous side was proposed by Honigmann in 1883 [7]. He used a steam engine which was heated by the interaction of the exhaust water vapor with sodium hydroxide. The heat released thereby was used to generate steam in a boiler which was thermally connected to the sodium hydroxide. The setup was in practical operation to power fireless locomotives. During the process, the sodium hydroxide became more and more diluted. To regenerate the system, the diluted sodium hydroxide solution was drained, boiled down and refilled. In recent days that operation principle was picked up by Jahnke in 2019 [8] to investigate the process for thermochemical energy storage. In contrast to sodium hydroxide, she used LiBr and proposed several strategies to release energy from the system and to regenerate it. For example, discharging with the extraction of mechanical work or cold production is feasible. For regeneration, the utilization of thermal energy or mechanical work is proposed.

Differences to the process proposed in this manuscript can be identified. First, the setup in this paper utilizes two thermochemical reactions for the two compartments. In contrast, the Honigmann process utilized one chemical reaction and the evaporation of water on the other side. In addition, the chemical reaction in the Honigmann process is of gas/liquid nature, while here two gas-solid reactions are involved. Second, the thermal characteristics of the water absorption in the Honigmann process and the present setup are different. As reported by Jahnke [8], the temperature level of the thermal energy release is not only dependent on the gas pressure, but also on the concentration of the solution. Therefore, the pressure has to rise during the water vapor absorption process, if the same temperature level shall be maintained. Subsequently, the pressure difference to extract work is reduced with the discharging time. That issue could be visualized with a distinct equilibrium line in Figure 1 for each concentration of the solution resulting in a series of curves. In the proposed setup in this work, it can be assumed that the temperature level of the exothermal reaction is independent of the loading of the metal hydride corresponding to a negligible plateau slope. Therefore, the same pressure difference can be maintained during the whole discharging process.

2.1. Reference Materials: Metal hydrides

For the thermochemical battery to be operable, two different metal

hydrides have to be used. For these materials, the equilibrium pressure $P_{eq,H2}$ at a given temperature T can be calculated using the standard enthalpy $\Delta_R H$ – and entropy $\Delta_R S$ of the hydride formation [9].

$$\frac{p_{Eq,H2}}{p_{Ref}} = \exp\left(\frac{-\Delta_R H}{R \cdot T} - \frac{-\Delta_R S}{R}\right) \quad (2)$$

with the reference pressure being $p_{Ref} = 1$ atm.

The thermochemical battery couples two metal hydrides both thermally and on the gaseous side. That means that the two materials exchange heat and gas solely with each other. Therefore, for full conversion of both materials, their total hydrogen capacity and total thermal capacity have to be equal. This seems to be a contradiction since the metal hydrides have to differ in terms of enthalpy of reaction offering two pressure levels. In other words, if the reaction enthalpies are different, the overall amount of thermal energy cannot add up, and only viewing material properties, there is an intrinsic imbalance in thermal energy. This imbalance has to be accounted for in the process design and will be addressed in this manuscript.

2.2. Reactor

The reactor for the thermochemical battery has to exhibit two different compartments for the two materials. They have to be in thermal contact to enable rapid heat transfer. Additionally, they should be designed in a way that the reactive gas can be supplied to the solid bed without mass transfer limitations. For this study, an idealized reactor without heat- or mass transfer limitations is assumed. The temperature and pressure inside the reactor compartments is always at the equilibrium conditions of the respective material. Additionally it was assumed that the reaction kinetics are not limiting.

3. The Thermochemical Battery

The thermochemical battery consists of three major parts – the reactor, the compression- and expansion unit - as it is illustrated in Figure 2. For the storage of electrical energy, a compressor is powered to desorb hydrogen from metal hydride A (MH-A). The compressor increases the hydrogen's pressure and it is absorbed by metal hydride B (MH-B). The heat released during hydrogen absorption in MH-B is transferred to MH-A driving the desorption. For heat transfer, a temperature gradient between the materials is necessary. For the first part of this analysis, it is assumed that heat transfer can take place anyways without a temperature difference. This assumption will be dropped in the course of the paper.

For the release of the stored electrical energy, the process is reversed. Hydrogen desorbs from MH-B at the same pressure as it has been stored previously. Afterwards its pressure is reduced to the equilibrium pressure of MH-A in an expander. Thereby, the hydrogen performs work, which can be converted to electrical energy in a generator. The hydrogen is absorbed in metal hydride A, where the heat of absorption is released and being transferred to metal hydride B to drive the desorption. The system is completely closed and can flexibly switch between charging and discharging operation. With the selection of a metal hydride pair, and the temperature level, a wide variety of pressure ratios is feasible.

3.1. Isothermal compression/expansion

An idealized description for compression of a gas is isothermal compression. For isothermal compression of an ideal gas, the work required to compress one kilogram of gas from pressure p_1 to a pressure p_2 at temperature T is calculated with R being the universal gas constant and M the molar mass of the gas:

$$w_{isothermal} = \frac{R \cdot T}{M} * \ln\left(\frac{p_2}{p_1}\right) \quad (3)$$

Isothermal compression is the minimum work that is required to compress an ideal gas [10]. Since it is an idealized process requiring that the thermal energy is dissipated to the environment instantly, technical realization is challenging. The equilibrium pressure of a thermochemical material at a certain temperature T can be calculated with Equation (2). Therefore, using the thermodynamic properties $\Delta_R H$ and $\Delta_R S$, the pressure ratio between the materials $\frac{p_2}{p_1}$ can be calculated with

$$\frac{p_2}{p_1} = \frac{\exp\left(\frac{-\Delta_R H_2}{R \cdot T} - \frac{-\Delta_R S_2}{R}\right)}{\exp\left(\frac{-\Delta_R H_1}{R \cdot T} - \frac{-\Delta_R S_1}{R}\right)} \quad (4)$$

The indices 1 and 2 refer to the compartments of the two metal hydrides. Assuming that the change of entropy ΔS_R is the same for every metal hydride [11], resulting in $\Delta_R S_2 = \Delta_R S_1$, Equation (4) simplifies to:

$$\frac{p_2}{p_1} = \exp\left[\frac{1}{R \cdot T}\left(\Delta_R H_1 - \Delta_R H_2\right)\right] \quad (5)$$

Combining Equations (3) and (5) gives:

$$w_{isothermal} \cdot M = \Delta_R H_1 - \Delta_R H_2 \quad (6)$$

Therefore, it can be concluded that the work required compressing

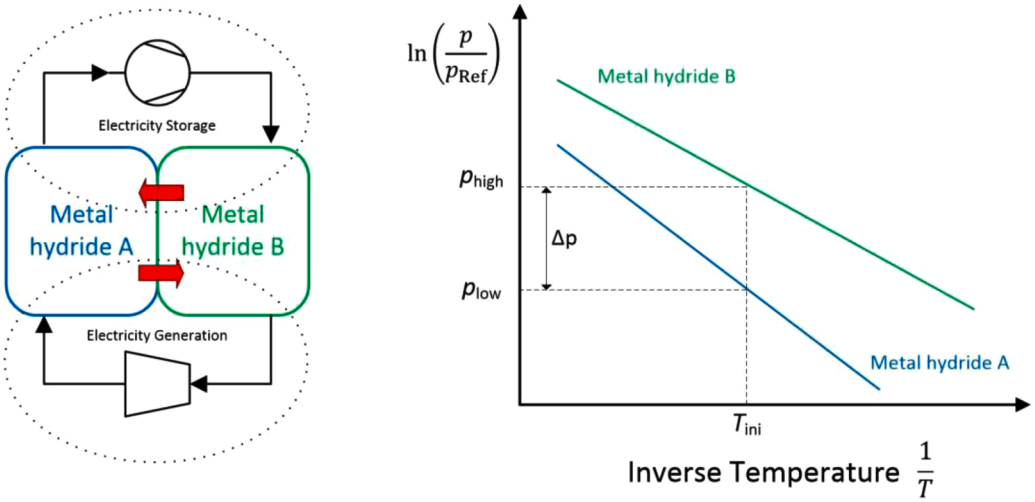

Figure 2. Basic principle of the thermochemical battery.

one mol hydrogen isothermally from p_1 to p_2 is equal to the difference in the reaction enthalpies of the two materials. It can be seen that the amount of energy required for that increases with the difference of the materials' reaction enthalpies. Therefore, more energy can be stored compressing the same amount of gas.

The temperature does not change during isothermal compression/expansion. Additionally, the pressure ratio is the same for compression and expansion. Therefore, in this idealized case, the efficiency η is calculated using Equation (3):

$$\eta_{\text{el, isothermal}} = \frac{\left|w_{\text{Expander,isothermal}}\right|}{\left|w_{\text{Compressor,isothermal}}\right|} = 100\% \tag{7}$$

It can be seen that for every pressure ratio and temperature, the efficiency of the thermochemical battery is 100% assuming isothermal compression.

3.2. Adiabatic compression/expansion

Temperature difference for heat transfer ΔT = 0°C

Another idealized process is the adiabatic compression, at which no heat is dissipated into the environment. In case the entropy of the gas does not change, it can be referred to as isentropic compression. The work to compress one kilogram of an ideal gas from pressure p_1 and temperature T_1 to a pressure p_2 is calculated with R being the universal gas constant and M the molar mass of the gas using the specific heat ratio $\kappa = \frac{c_p}{c_v}$ and assuming that κ is independent of the temperature [12]:

$$w_{\text{adiabatic, isentropic}} = \frac{R \cdot T_1}{M} \frac{\kappa}{\kappa - 1} \left[\left(\frac{p_2}{p_1} \right)^{\frac{\kappa-1}{\kappa}} - 1 \right] \tag{8}$$

The work for adiabatic compression is higher than for isothermal compression [10]. Both isothermal and adiabatic compressions are idealized processes. The real energy demand for gas compression is in between of those [10]. For the present analysis, the focus is on these idealized ways of compression since they serve as starting points to judge the potential of the thermochemical battery.

For the calculation of the efficiency in the adiabatic case, it was assumed that no temperature gradient is required for heat transfer between the two materials and the following roundtrip process takes place:

- Isentropic compression from T_1 and p_1 to $p_{2,\Delta T=0}$.
- Isobaric cool-down to the initial temperature T_1.
- Thermochemical hydrogen storage in metal hydride B at temperature T_1 and pressure $p_{2,\Delta T=0}$.
- Release of the hydrogen from metal hydride B at temperature T_1 and pressure $p_{2,\Delta T=0}$.
- Isentropic expansion from $p_{2,\Delta T=0}$ to p_1.
- Isobaric heat-up to the initial temperature T_1.

The electric efficiency of the process can be calculated using Equation (8).

$$\eta_{el,\ \text{isentropic},\ \Delta T=0°C} = \frac{\left|w_{\text{Expander,isentropic}}\right|}{\left|w_{\text{Compressor,isentropic}}\right|} = \frac{\left| \left(\frac{p_1}{p_{2,\Delta T=0}} \right)^{\frac{\kappa-1}{\kappa}} - 1 \right|}{\left| \left(\frac{p_{2,\Delta T=0}}{p_1} \right)^{\frac{\kappa-1}{\kappa}} - 1 \right|} \tag{9}$$

The indices 1 and 2 refer to the compartments of metal hydrides A and B in Figure 2, respectively. It can be seen that the efficiency is independent of the temperature since the temperature before the compressor and expander as well as the reactor is assumed to be identical.

Temperature difference for heat transfer ΔT ≠ 0°C

If the assumption of no temperature difference being necessary is dropped, the equations have to be adapted. Hydrogen is now being stored at a temperature T_3 which is ΔT higher than the initial temperature T_1.

$$T_3 = T_1 + \Delta T \tag{10}$$

Subsequently, the compartment B of the thermochemical battery now operates at T_3 with the corresponding equilibrium pressure $p_{2,\Delta T\neq 0} = p_3$, which is higher than in the case without a temperature gradient. Again it is assumed that the conditions at which hydrogen is stored and released are identical. The qualitative *T-S* diagram and the pressure/temperature levels are visualized in Figure 3.

The pressure after the expander is now denoted with p_4. Due to the temperature gradient, metal hydride A in Figure 2 has to operate at $2^*\Delta T$ higher during its absorption than during desorption. Since temperature and pressure of a metal hydride correlate via the van't Hoff relation, the pressure p_4 can be calculated based on the reaction enthalpy and the desorbing temperature T_1. Pressure p_4 is the pressure in the metal hydride if the temperature is raised by $2^*\Delta T$ from p_1 and T_1.

$$p_4 = p_1 {}^* e^{\frac{\Delta_R H_{1,*}}{R}\left(\frac{1}{T_1} - \frac{1}{T_1 + 2^*\Delta T}\right)} = p_6 \tag{11}$$

Therefore, the roundtrip for the case with a temperature difference can be described as follows:

- Isentropic compression from T_1 and p_1 to $p_{2,\Delta T\neq 0}$.
- Isobaric cool-down to the temperature T_3.
- Thermochemical hydrogen storage in metal hydride B at temperature T_3 and pressure $p_{2,\Delta T\neq 0}$.
- Release of the hydrogen from metal hydride B at temperature T_3 and pressure $p_{2,\Delta T\neq 0}$.
- Isentropic expansion from temperature T_3 and $p_{2,\Delta T\neq 0}$ to p_4.
- Isobaric heat-up to the temperature T_6.

The efficiency regarding a temperature difference for heat transfer calculates with:

$$\eta_{el,\ \text{isentropic},\ \Delta T\neq 0°C} = \frac{\left| T_3 \left[\left(\frac{p_4}{p_{2,\Delta T\neq 0}} \right)^{\frac{\kappa-1}{\kappa}} - 1 \right] \right|}{\left| T_1 \left[\left(\frac{p_{2,\Delta T\neq 0}}{p_1} \right)^{\frac{\kappa-1}{\kappa}} - 1 \right] \right|} \tag{12}$$

The dependencies of the roundtrip efficiency on the pressure ratio for all three previously discussed cases are shown in Figure 4. The roundtrip efficiency for the isothermal process is 100% for every pressure ratio. For single stage adiabatic, isentropic compression/expansion the threshold value for the efficiency at a given pressure ratio is determined by setting the temperature gradient for heat transfer to zero which is independent of the material pair. It can be seen that the electric efficiency drops with increasing pressure ratio (black curve, square markers). This is due to the temperature increase of the hydrogen during isentropic compression. That heat-up is more pronounced at high pressure ratios. Therefore, at high pressure ratios, more thermal energy has to be dissipated to the environment since it cannot be utilized otherwise, which reduces the electric efficiency. The calculations for cases with $\Delta T \neq 0°C$ are dependent on material A in Figure 2 as Equation (11) reveals. The sharp initial rise in these cases is attributed to the fact that a certain pressure ratio is necessary to establish the desired temperature gradient. Below that pressure ratio, the process is impossible. That rise increases to a maximum after which it starts to decline again. Therefore, in terms of efficiency, an optimal system design can be identified. Note that the lines for isothermal the isothermal case (grey, Equation (7)) and the isentropic case without temperature difference (black, Equation (9)) are valid for every material pair, while the other curves were calculated for $LaNi_{4.8}Sn_{0.2}$ with the properties listed in Table 1.

If a temperature gradient is introduced, the efficiency decreases with larger temperature difference. This is due to the temperature difference that translates into a reduced pressure difference for expansion. The

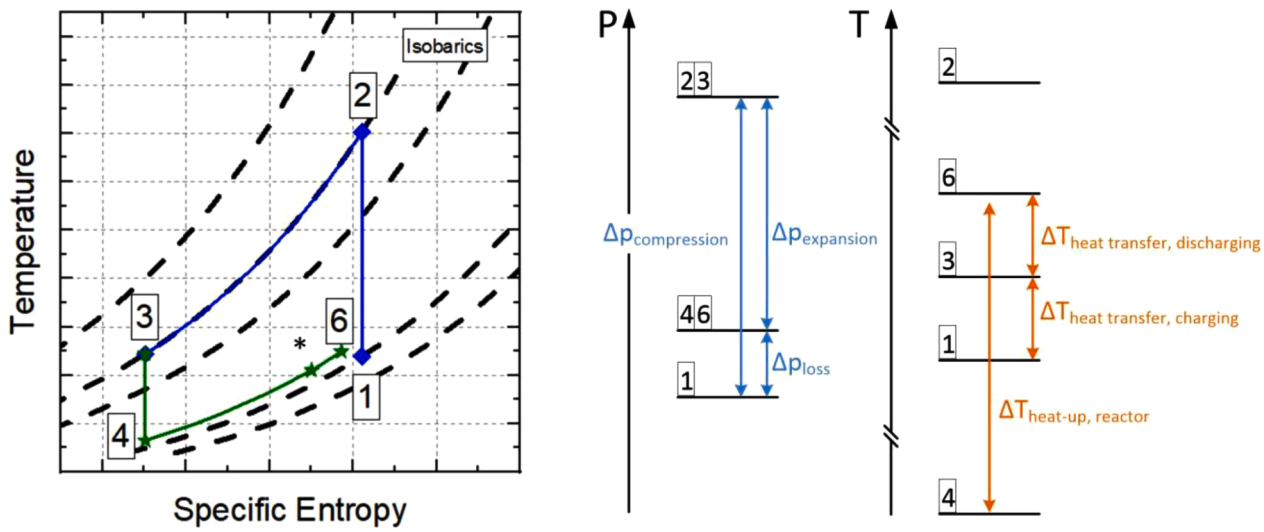

Figure 3. Temperature and pressure levels during adiabatic compression/expansion; * Point 5 will be introduced later.

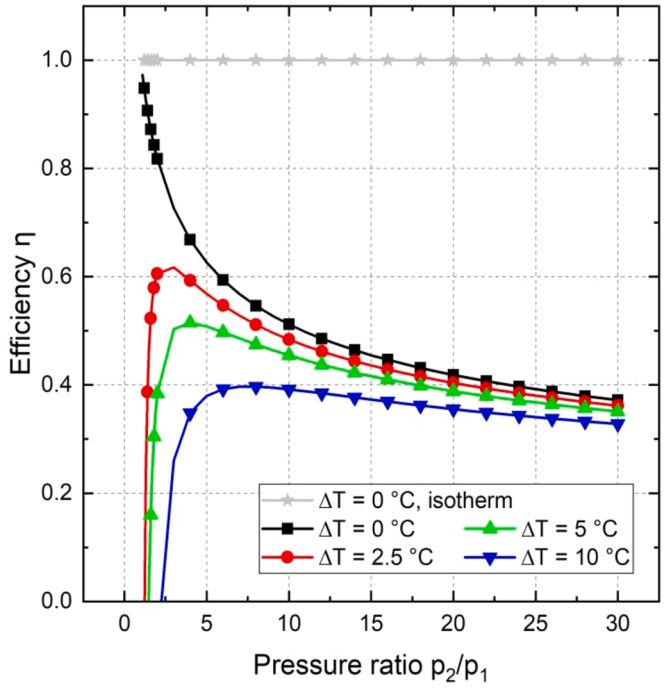

Figure 4. Pressure ratio and efficiencies at different temperature differences for heat transfer; grey line: Isothermal compression/expansion; other lines: adiabatic, isentropic, single stage compression/expansion; Cases with ΔT: $LaNi_{4.8}Sn_{0.2}$ as Material A with appropriate partner.

difference between pressures p_1 and p_4 increases which is not available for expansion which is visualized with Δp_{loss} in Figure 3.

With an increased temperature difference in the same reactor design, the power increases, as heat transfer proceeds faster. Therefore, increasing the power of the thermochemical battery coincides with a reduced efficiency and vice versa. The pressure ratio translates directly in the amount of energy that can be stored with one unit of hydrogen. A high pressure ratio requires a high amount of energy for compression and results in a high amount of energy withdrawal during expansion. Hence, increasing the pressure difference results in higher storage densities, but reduced efficiency. Therefore, a correlation between efficiency, storage density and pressure ratio can be observed.

Table 1
Parameters for the machinery and materials. Material data from [9].

Parameters	Value
Motor electrical efficiency	0.95
Motor mechanical efficiency	0.998
Pump isentropic efficiency	0.85
Pump mechanical efficiency	0.99
Turbine isentropic efficiency	0.9
Turbine mechanical efficiency	0.99
Generator efficiency	0.9857
$LaNi_{4.8}Sn_{0.2}$ $-\Delta_R H$	32.80 kJ mol_{H2}^{-1}
$LaNi_{4.8}Sn_{0.2}$ $-\Delta_R S$	105.0 J $mol_{H2}^{-1}K^{-1}$
$MmNi_{4.15}Fe_{0.85}$ $-\Delta_R H$	25.00 kJ mol_{H2}^{-1}
$MmNi_{4.15}Fe_{0.85}$ $-\Delta_R S$	105.4 J $mol_{H2}^{-1}K^{-1}$

3.3. Thermal integration of the compression unit

So far, it was assumed that the charging and discharging processes are feasible even though the demand and supply of thermal energy for the involved thermochemical reactions are different. During charging, more thermal energy is required to desorb hydrogen from metal hydride A than released by the absorption in metal hydride B. This imbalance has to be accounted for.

There is a surplus of thermal energy in the hydrogen after the compressor, since the hydrogen is heated up during non-isothermal compression. It would be beneficial for the process efficiency to store the thermal energy of this compressed hydrogen. The stored thermal energy could then be used to heat the hydrogen before the expander during discharge. The proposed system is able to partially store this thermal energy in the reactor itself without requiring an additional device. Storing thermal energy is even a necessity to drive the process. As introduced before, the reaction enthalpy per mole of hydrogen in MH-A (desorbing) in Figure 2 has to be higher than the one of MH-B (absorbing). Thermal energy of the compressed hydrogen can now be used to compensate for that difference. For the reverse reaction, MH-A releases more thermal energy than required by MH-B. This excess thermal energy can be used for intermediate heating of the hydrogen between several stages of expansion and to heat up hydrogen after the final stage to the reactor temperature of MH-A, which will be analyzed later. The amount of stored thermal energy is only dependent on the selected materials. It is independent of the compression ratio or the temperature level the process occurs.

Isothermal compression is the minimum of work required for

compression. It was found that the energy required to compress hydrogen isothermally from the lower to the higher pressure reservoir is exactly the same as the difference in the reaction enthalpies regarding the mentioned assumptions. Adiabatic compression requires more energy than isothermal compression. That energy remains in the gas increasing its temperature. Therefore, it can be concluded that there is enough thermal energy in the hot gas after the compression to compensate for the difference in the reaction enthalpies. Even after compensating that, there is still a surplus of thermal energy in the hot gas. If that thermal energy cannot be utilized, it has to be dissipated to the environment, which lowers the electrical storage efficiency.

3.4. Optimization and operational strategies

So far, mostly qualitative data was presented. In this section selected cases for a material pairing are evaluated quantitatively, involving temperatures, pressures, storage densities and efficiencies. First, a case is shown with single stage adiabatic compression. Thereby, the influence of the isentropic and mechanical efficiencies of the machineries on the thermochemical battery will be evaluated. Afterwards, a case with three-stage compression and expansion will be presented, to reduce the fraction of unused thermal energy. Thereby, the compression work and the electricity output can be reduced and increased, respectively.

3.4.1. Stages of compression and expansion

For the calculation of the hydrogen's properties and the machinery, the EBSILON®Professional software was used. The following assumptions and considerations have been taken into account:

- Hydrogen is assumed to behave as an ideal gas.
- Pressure- and heat losses in the heat exchangers and piping are disregarded.
- The reactors are not limited by heat or mass transport. They are always operating at their respective equilibrium conditions.
- Efficiencies of the compression and expansion units are regarded as listed in Table 1.
- Material properties are listed in Table 1.
- The temperature difference for heat transfer between the metal hydrides was set to 5 K.
- The temperature difference for inter-stage cooling/heating between the hot/cold hydrogen and the reactor was set to 10 K.
- Steady state and energetic analysis only.
- Ambient temperature is 20°C.

Single stage process

In this subsection, the performance of the thermochemical battery is analyzed for a specific case. The previously taken assumption that the efficiency of the machinery is 100% is eliminated now. Hence, the efficiency losses is the machinery are also accounted for. In that specific case, the metal hydride pairing $LaNi_{4.8}Sn_{0.2}$ and $MmNi_{4.15}Fe_{0.85}$ are used. They were chosen, since they are both operable around ambient temperature and their reported specific changes of entropy are almost identical. It can be seen that their reaction enthalpies differ for 7.8 kJ mol_{H2}^{-1} or 3900 kJ kg_{H2}^{-1}. Hence, for full conversion during the charging process of the thermochemical battery, 3900 kJ kg_{H2}^{-1} additional thermal energy is required which is approximately 24% of the thermal energy required for desorption. Subsequently, a surplus of, 3900 kJ kg_{H2}^{-1} thermal energy is available during discharge.

The roundtrip process for charging and discharging can be described as follows. The corresponding *T-S*-Diagram is shown in Figure 5.

Charging

1: Hydrogen desorption from $LaNi_{4.8}Sn_{0.2}$ at 39°C. The majority of the thermal energy required for that process is provided by the hydrogen absorption in $MmNi_{4.15}Fe_{0.85}$.
1 -> 2: Adiabatic hydrogen compression to the absorption pressure of $MmNi_{4.15}Fe_{0.85}$ of 24.6 bar. This is the equilibrium pressure of the $MmNi_{4.15}Fe_{0.85}$ at a temperature of 44°C. The gas temperature increases.
2 -> 3: Isobaric hydrogen cool-down to the hydrogen absorption temperature of $MmNi_{4.15}Fe_{0.85}$ of 44°C. The thermal energy can partially be used to account for the difference in reactions enthalpies between the two materials (3900 kJ kg_{H2}^{-1}). Additional surplus thermal energy is dissipated into the environment.

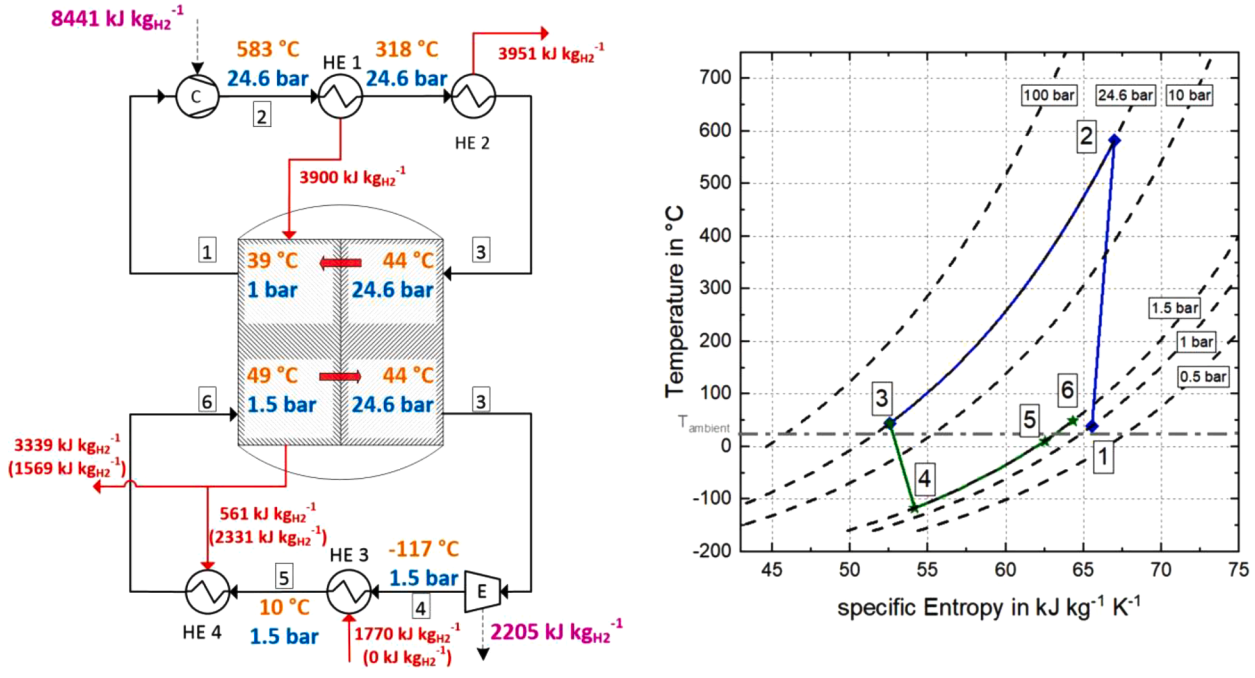

Figure 5. Case 1, singe stage adiabatic compression/expansion, $LaNi_{4.8}Sn_{0.2}$ and $MmNi_{4.15}Fe_{0.85}$.

3: Hydrogen absorption in $MmNi_{4.15}Fe_{0.85}$ at 44°C. For heat transfer between the materials, the temperature level of hydrogen absorption in $MmNi_{4.15}Fe_{0.85}$ has to be $\Delta T = 5$ K higher than the temperature level of hydrogen desorption in $LaNi_{4.8}Sn_{0.2}$.

Discharging

3: Hydrogen desorption from $MmNi_{4.15}Fe_{0.85}$ at 44°C and 24.6 bar. The thermal energy for that process is fully provided by the hydrogen absorption in $LaNi_{4.8}Sn_{0.}2$. Excess thermal energy is available.
3 -> 4: Adiabatic hydrogen expansion to the absorption pressure of $LaNi_{4.8}Sn_{0.2}$ of 1.5 bar. The gas temperature drops subzero to -117°C. Hydrogen remains gaseous at these conditions and does not liquefy or freeze which might damage the machinery
4 -> 5: Isobaric hydrogen heat-up close to the ambient temperature. Thermal energy of 1770 kJ kg_{H2}^{-1} is withdrawn from the environment.
5 -> 6: Further isobaric hydrogen heat-up to the reactor temperature of $LaNi_{4.8}Sn_{0.2}$ of 49°C partially using the previously stored thermal energy. The temperature level of the ambient is not high enough. Therefore, the reactor itself has to heat up the hydrogen. This is possible, since the absorption of the hydrogen releases more thermal energy than is required for full desorption. For that purpose, 3900 kJ kg_{H2}^{-1} are available, but due to preheating via the environment only 561 kJ kg_{H2}^{-1} are required.
Alternatively: 4 -> 6: Instead of using energy from the ambient, the hydrogen can also be heated up directly with the excess thermal energy that is available during hydrogen absorption. This is illustrated with the numbers in brackets in Figure 5.
6: Hydrogen absorption in $LaNi_{4.8}Sn_{0.2}$ at 49°C. For heat transfer between the materials, the temperature level of hydrogen absorption in $LaNi_{4.8}Sn_{0.2}$ has to be $\Delta T = 5$ K higher than the temperature level of hydrogen desorption in $MmNi_{4.15}Fe_{0.85}$ at 44°C. Compared to the electricity charging, the temperature gradient between the beds is reversed.

It can be seen that in this single stage process, the thermal energy in the hydrogen after the compressor is being stored thermochemically in the $LaNi_{4.8}Sn_{0.2}$ to about 50%. The other half has to be dissipated to the environment, which negatively affects the efficiency. Additionally, the stored thermal energy cannot be converted into electricity, since the temperature level is not high enough to preheat the hydrogen before the expander. A fraction of it can be used for reheating after the expander. The other fraction cannot be used which is detrimental with respect to efficiency. Additionally, it has to be noted that a hot gas temperature of 583°C after the compressor poses significant engineering effort. The efficiencies and storage densities are reported in Table 2. The values for the energies in Figure 5 are shown with respect to the working fluid hydrogen. The actual storage density of the thermochemical battery is dependent on the weight and volume of the two materials storing that hydrogen. With the material properties of the $LaNi_{4.8}Sn_{0.2}$ ($\rho_{solid} = 8400$ kg m^{-3} [13], 1.4 wt% [13]) and $MmNi_{4.15}Fe_{0.85}$ ($\rho_{solid} = 8100$ kg m^{-3} [13], 1.14 wt% [13]), and assuming 30% porosity, the storage density with respect to the materials can be calculated as it is listed in Table 2.

Three stage process

Due to the high temperature increase in the single stage compressor, and subsequent loss of thermal energy, a three stage compression/expansion with intermediate cooling/heating is analyzed. Apart from that, the system's parameters and materials are identical. The pressure ratio for each stage is approximately the same for all compressors (2.9) and expanders (2.5). The expander's pressure ratio is lower since the overall pressure drop is lower due to the temperature gradient as it has been discussed before. The flow chart and *T-S* diagram for that case are shown in Figure 6. In contrast to the single stage case, the compression ratio for each compressor is lower. Therefore, the outlet temperature of the compressor is lower (approximately 170°C). The hot gas after each compression stage is cooled down to 49°C, and the thermal energy is transferred to the reactor. Since the desorbing metal hydride operates at 39°C, 10 K are available for heat transfer. Once the difference in reaction enthalpies has been balanced, the additional thermal energy has to be dissipated to the environment. After the last compression stage, the gas is still too hot to enter the reactor. Therefore, this surplus energy of 1825 kJ kg_{H2}^{-1} has to be dissipated to the environment. Note that this value is lower than the dissipation of 3951 kJ kg_{H2}^{-1} in the single stage case. Due to the multiple stages with intermediate cooling, the overall energy to compress the hydrogen from 1 bar to 24.6 bar is lower than in the single stage process. However, the amount of stored thermal energy to account for the difference in the reaction enthalpies of 3900 kJ kg_{H2}^{-1} is the same.

For the discharging of the battery, the previously stored thermal energy is available again. Its temperature level is too low to preheat the hydrogen before the first expander. However, it can be used to reheat the hydrogen between the stages up to 39°C, assuming 10 K for heat transfer. Therefore, the previously stored thermal energy can be partially converted to electricity. Again, after the last stage, the environment can be cooled via heating the hydrogen to 10°C. Since the temperature drop in the expander stages is much lower compared to the single stage process, the cooling power is reduced. An overview of the results of the three-stage process can be found in Table 3. It is evident that for the efficiency of electricity to electricity, the three stage process is beneficial, since less energy is needed for compression and the thermochemically stored thermal energy can partially be converted to electricity. This is an intrinsic feature of the thermochemical battery, and since the thermal energy is stored thermochemically, long-term loss free storage is possible.

The energy losses directly affecting the efficiency of the three setups are shown in Figure 7. It is evident that the majority of the losses occur in terms of thermal losses after the compressor and non-utilization of the excess heat of absorption during the discharging process. In comparison, losses in the machinery contribute only a fraction. The overall energy demand for compression decreases and the recoverable electric energy increases with increasing stages with isothermal compression as threshold. Since there is a lot of thermal energy that has to be dissipated to the environment in the presented cases, it would be beneficial to use it in another process.

3.4.2. *Utilization of heating- & cooling energy*

As it has been derived before, adiabatic compression/expansion coincides with a temperature increase/drop of the hydrogen, respectively. Therefore, thermal energy at a high temperature level is available during the charging process while thermal energy can be withdrawn from the ambient during discharge. Viewing Figures 5 and 6, the cool-down of the hydrogen after the compressor takes place between points 2 und 3. That thermal energy has to be used to make up the difference in the reaction enthalpies. The additional surplus can be used for additional heating purposes. The amount- and temperature level of that surplus thermal energy is strongly dependent on the specific case. Obviously, more thermal energy is available for heating if fewer stages for compression are used.

After the expander the hydrogen temperature is below the temperature level of the reactor. In contrast to other energy storage systems working with the expansion of a gas, even subzero temperatures are

Table 2
Efficiencies and energy densities of the thermochemical battery for single stage adiabatic compression/expansion.

Roundtrip efficiency electric electric	26%
Additional cooling power	1770 kJ kg_{H2}^{-1}
Storage Density w.r.t. hydrogen	2205 kJ kg_{H2}^{-1}
Storage Density w.r.t. material volumes	22.2 Wh L_{Mat}^{-1}

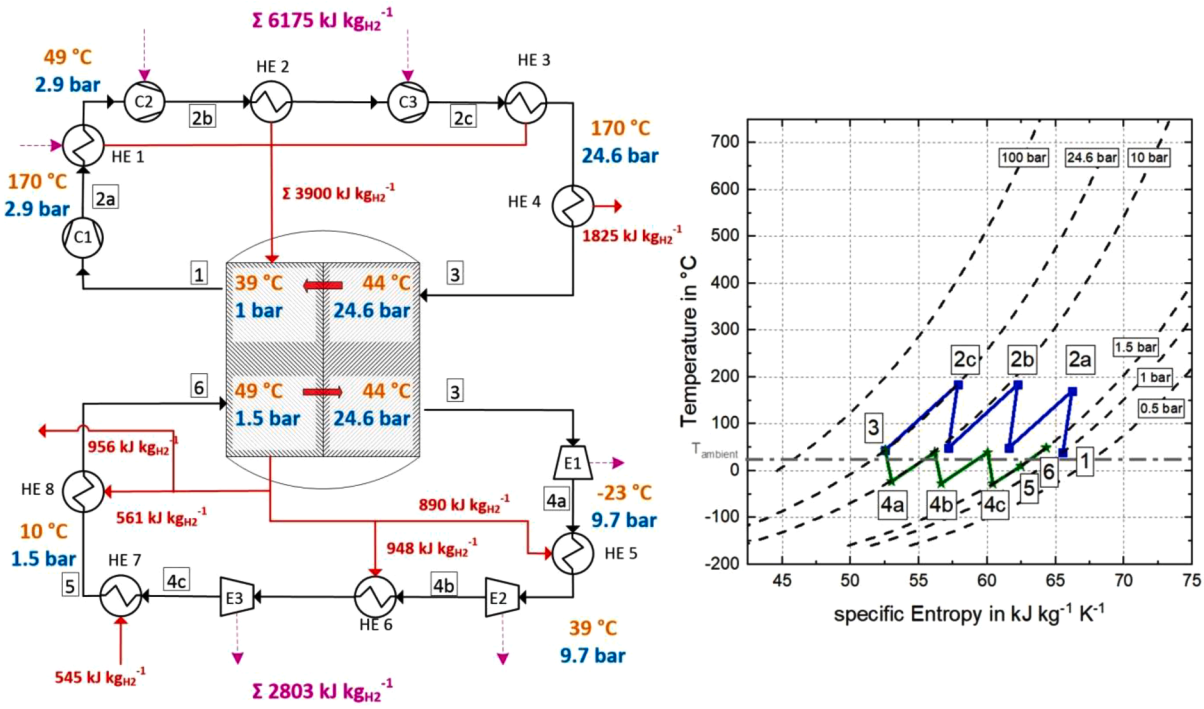

Figure 6. Case 2, three stage adiabatic compression/expansion with intermediate cooling/heating, $LaNi_{4.8}Sn_{0.2}$ and $MmNi_{4.15}Fe_{0.85}$.

Table 3
Efficiencies and energy densities of the thermochemical battery for three stage and one stage adiabatic compression/expansion.

	Three stage process	One stage process
Efficiency electricity to electricity	45%	26%
Storage Density w.r.t. hydrogen	2803 kJ kg_{H2}^{-1}	2205 kJ kg_{H2}^{-1}
Storage Density w.r.t. material volumes	28.2 Wh L_{Mat}^{-1}	22.2 Wh L_{Mat}^{-1}

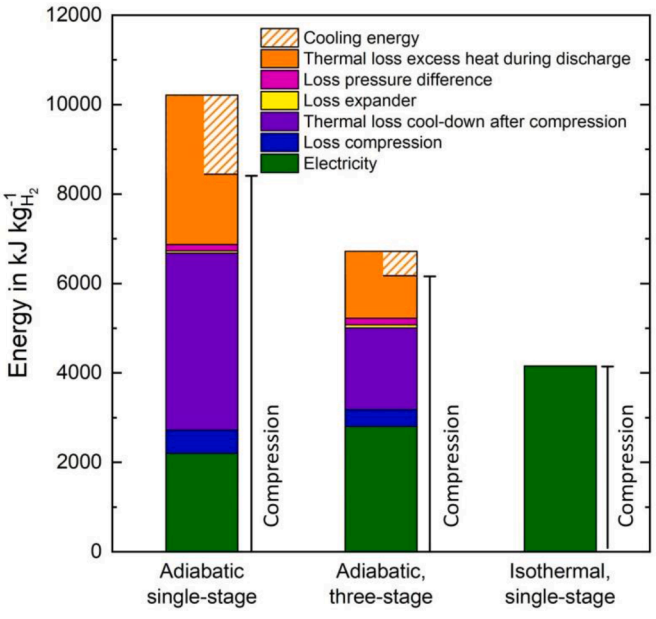

Figure 7. Losses during a cycle of charging and discharging.

possible and feasible with the thermochemical battery, since hydrogen's critical temperature is 33.2 K [14]. Therefore, the cold hydrogen can be used to withdraw thermal energy from the ambient. Heating the hydrogen with thermal energy from the ambient is shown in Figures 5 and 6 between points 4 and 5. It is 1770 kJ kg_{H2}^{-1} and 545 kJ kg_{H2}^{-1} for the single stage and three stage expansion, respectively. Referring these values to the electric energy for compression, an additional cooling efficiency of 21% and 9% can be calculated which is a benefit on top of the electric efficiency. For the three stage expansion, the values are lower since the temperature drop of the hydrogen is less pronounced. The temperature until which the hydrogen can be heated up depends on the ambient temperature. In addition, the temperature of the hydrogen after the expander is strongly dependent on the specific process design, especially on the number of expansion stages. It can be concluded here, that the thermochemical battery can be designed in a way to co-generate high temperature heat during charging and cooling energy during discharge.

3.4.3. *Thermal energy storage*

As it has been demonstrated in the previous sections, a characteristic of the thermochemical battery is its ability to partially store the thermal energy of the hot gas after the non-isothermal compressor. This feature is based on the differences in the reaction enthalpies of the two materials. With a larger difference in enthalpy, more thermal energy has to be stored during the charging process of the thermochemical battery. It would be beneficial for the efficiency if that thermal energy can be converted to electricity during the discharging process. For the reference material combination that fraction is shown in Figure 8. For that analysis it was assumed that all expansion stages are operating at the same pressure ratio. Furthermore, it was assumed that the hydrogen is reheated to the reactor temperature after each compressor using the thermochemically stored thermal energy from the reactor. The thermochemically stored thermal energy is 3900 kJ kg_{H2}^{-1} which corresponds to 100%.

It can be seen that with only one expansion stage, utilization of the stored thermal energy is not possible because it can only be used to reheat the gas after the expander. Increasing the theoretical number of expansion stages reveals that there is a threshold value for the fraction of the stored thermal energy that can be converted to electricity that way. Without regarding the efficiencies of the machinery, the threshold value

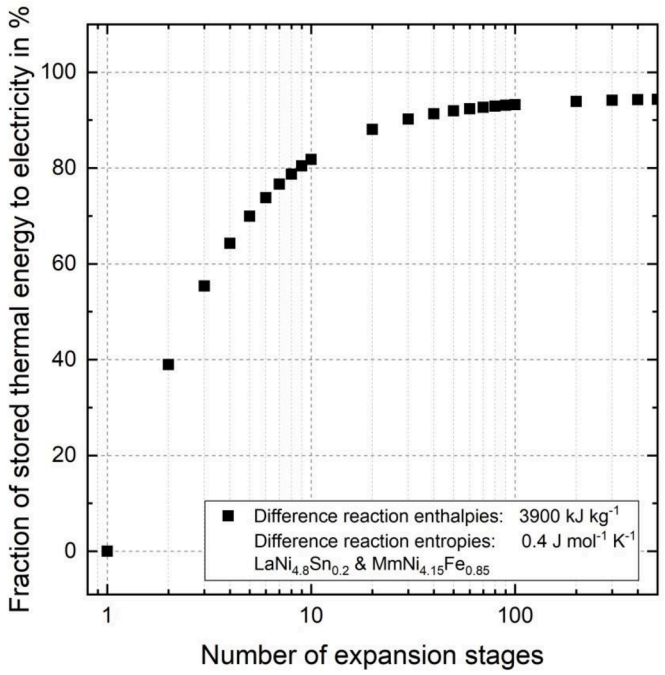

Figure 8. Fraction of thermochemically stored thermal energy converted to electric energy depending on the number of expansion stages for the reference material pair – Without regarding machinery losses.

is 94% for the selected case. The missing fraction to 100% is attributed to the temperature difference which is required for heat transfer and subsequent reduction of the available pressure difference during expansion which is denoted with Δp_{loss} in Figure 3.

4. Discussion and technological classification

After the presented thermochemical battery has been discussed, the technology will be classified in comparison with existing technologies for energy storage.

The proposed thermochemical battery exhibits several features making it a technology worthy of investigation. The three main components of the system, which are the compression unit, the reactor and the expansion unit, can be dimensioned independently. A separation of power and capacity is possible. For example, the capacity of the reactors can be increased without affecting the machinery. Subsequently, the energy storage capacity can be increased while keeping the power constant. Additionally, the power uptake and release are independent since the compression unit can be dimensioned independently of the expansion unit. Therefore, it is possible to consume energy from the grid with high power and supplying it at a lower power to a consumer when there is demand. Since the storage is based on thermochemical reactions, loss-free long time storage is possible. Hence, the thermochemical battery is suited for both short term and seasonal energy storage.

An intrinsic feature of the thermochemical battery is the co-generation of high-temperature heat during charging and the co-supply of cooling energy during discharging. Depending on the desired application and surrounding, it is possible to adapt the thermochemical battery to specific requirements. With the proper selection of materials, pressure ratio and operating temperature, it can be dimensioned with focus on efficiency, storage density or cooling/heating power. An overview of potential focusses is shown in Table 4 where two additional scenarios for three-stage adiabatic compression are presented. The presented values can be understood as the threshold values that can be achieved at most. For example, a comparatively high storage density but lower efficiency can be achieved if a metal hydride pair with a high pressure ratio is chosen. The higher pressure ratio yields in more thermal energy that has to be dissipated to the environment after the compression unit. Another option is to increase the overall working temperature of the thermochemical battery. Table 4 shows another material pair with the same pressure difference as in the reference case, but operating at a higher temperature. Even though the densities of the materials are similar, higher storage densities can be achieved, because the temperature before the expansion stage is higher. In comparison with the previously analyzed reference case, no cooling power is provided with respect to 20°C ambient temperature, but the storage density increases with approximately the same electric efficiency.

As it has been mentioned before, probable limitations of the overall process like heat- or mass transfer or kinetic limitations have not been addressed in this manuscript. Considering any of the mentioned limitations would affect the speed of the overall process, which translates into the power density. The scope of this work is an energetic analysis only, without drawing conclusion on the power of the energy storage or release process. For an evaluation of the power density, the limiting process has to be known. Using a reactor which does not exhibit heat- or mass transfer limitations, the reaction kinetics of the metal hydrides are the limiting factor. Therefore, the kinetics of the metal hydrides should be considered for the material selection [3]. The reaction kinetics are sensitive on the operating conditions as it was exemplarily shown by Perejón *et al.* [15] for magnesium hydride.

As it has been demonstrated previously, the storage density of the thermochemical battery is in the range of 22-62 Wh L_{mat}^{-1} and 5-11 Wh kg_{mat}^{-1} with respect to electrical output. These values involve the materials only. For a final value, the data of the compression- and expansion units have to be taken into account as well. Since their dimensioning is strongly dependent on the overall storage capacity and desired power, reliable values for those are not educible. The volumetric storage density of the thermochemical battery is in the rage of NiCd batteries [16]. The advantage of metal hydrides in general is their large volumetric hydrogen storage density while their gravimetric hydrogen storage density is a few percent at most. Therefore, the gravimetric storage density of the thermochemical battery cannot compete with other

Table 4
Selection of several scenarios of the thermochemical battery; Values calculated only regarding materials; Three stage, adiabatic compression/expansion, each with approx. identical pressure ratio for each stage; Efficiencies reported in Table 1. Material properties used (TD: Thermodynamic properties, 30% porosity assumed): * TD [9], $\rho_{solid} = 8400\ kg\ m^{-3}$ [13], 1.4 wt% [13]; + TD [9], $\rho_{solid} = 8100\ kg\ m^{-3}$ [13], 1.14 wt% [13]; # TD [9], $\rho_{solid} = 8000\ kg\ m^{-3}$ [Assumption], 1.33 wt% [18]; ~ TD [9], $\rho_{solid} = 8000\ kg\ m^{-3}$ [Assumption], 1.7 wt% [19].

Metal hydride A	Metal hydride B	MH-A (des) Pressure Temp.	MH-B Pressure Temp.	Pressure Ratio Compression	Efficiency electricity to electricity	Storage density w.r.t. energy output
*$LaNi_{4.8}Sn_{0.2}$ *Reference*	+$MmNi_{4.15}Fe_{0.85}$	1.0 bar 39°C	24.6 bar 44°C	24.6	45%	28.2 Wh L_{mat}^{-1} 4.9 Wh kg_{mat}^{-1}
#$MmNi_{4.8}Al_{0.2}$ *High pressure ratio*	~$ZrFe_{1.8}Ni_{0.2}$	0.1 bar 12°C	241 bar 17°C	2410	31%	62.6 Wh L_{mat}^{-1} 11.2 Wh kg_{mat}^{-1}
#$MmNi_{4.8}Al_{0.2}$ *High operating temperature*	+$MmNi_{4.15}Fe_{0.85}$	5.8 bar 112°C	143 bar 117°C	24.6	47%	34.2 Wh L_{mat}^{-1} 6.1 Wh kg_{mat}^{-1}

energy storage systems and is at the lower end of flywheel energy storage range [16]. Another aspect that has to be considered judging energy storage system is the cycling stability. Depending on the metal hydride cycling stability can vary a lot [3] and should be considered during material selection.

When it comes to energy storage via compression and expansion of a gas in the thermochemical battery, compressed air storage (CAS) has a similar working principle. For energy storage, air is compressed to a higher pressure, cooled down and stored in a cavity. The thermal energy of the hot air is either dissipated to the environment or it is stored in a thermal energy storage device [17]. To avoid liquefaction or freezing, the air has to be preheated before the expander either with additional combustion of a fuel or using the previously stored thermal energy. The similarities to the working principle of the thermochemical battery are evident. Both technologies work with the compression and expansion of a gas. While the volumetric storage density of the thermochemical battery potentially exceeds the CAS's one, the volume has to be filled with metal hydride increasing the cost and weight. In contrast, an empty cavern can be utilized for gas storage in CAS systems. Hence, the gravimetric energy density of CAS systems is higher than in the thermochemical battery. Since water-free hydrogen is the working fluid in the thermochemical battery, subzero temperatures are feasible. Unlike in CAS, an additional characteristic of the thermochemical battery is the incorporated thermochemical heat storage feature due to the difference in the reaction enthalpies of the materials. During multi-stage expansion the thermal energy can be used to reheat the fluid after the expansion stages. Therefore, the stored thermal energy can be partially converted into electricity without the necessity of an additional thermal energy storage device as in CAS. On the one hand, in comparison to CAS, the combustion of fuel or an additional thermal energy storage device can be avoided. On the other hand, CAS systems are able to reach higher temperatures of the air before the expansion unit. Therefore, higher efficiencies can be archived. Additionally, the feasibility of CAS systems has already been demonstrated in large scale [17].

The thermochemical battery was analyzed with respect to metal hydrides and hydrogen as working fluid. However, the system can also be designed utilizing other gas-solid reactions. It is important that two different materials reacting with the same gas are used. Therefore, material pairs using other gases such as ammonia, carbon dioxide or water vapor are theoretically feasible as well.

5. Conclusions

In this work, a system based on two thermochemical reactions coupled both thermally and on the gaseous side has been presented. The two reactions exchange heat and gas solely with each other. Due to the different characteristic pressure at a certain temperature, a pressure difference between the materials arises. Compression of gas from the lower pressure to the upper one consumes electrical energy while its expansion recovers it. Therefore, such a system can act as a thermochemical battery when it is combined with a compression and expansion device. It was analyzed in general and an energetic potential analysis with respect to two metal hydrides as thermochemical materials was carried out. Configurations with comparatively high storage densities yield in competitively low electrical efficiencies and vice versa. With a three-stage compression/expansion unit and two metal hydrides as thermochemical materials, electric efficiencies of up to 47% can be reached. The maximum storage density of the investigated cases was 62.6 Wh L_{mat}^{-1} based on the two reactive materials only, without the compression/expansion unit. Additionally, the thermochemical battery acts as a thermochemical energy storage device. The stored thermal energy can be utilized during multistage expansion for intermediate reheating of the gas. During electricity charging and discharging, high-temperature heat and cold is co-generated, respectively. The amount of heat and cold generated is strongly dependent on the material chosen, the design of the compression and expansion unit as well as the temperature level of the process. Depending on one's preferences, the system can be designed with focus on electrical efficiency, storage density or cold/heat production. The qualitative behavior of the thermochemical battery is transferable to material combinations reaction with different gasses than hydrogen.

CRediT authorship contribution statement

Michael Lutz: Conceptualization, Methodology, Formal analysis, Investigation, Writing - original draft, Visualization. **Matthias Schmidt:** Conceptualization, Methodology, Writing - review & editing, Project administration, Funding acquisition. **Inga Bürger:** Conceptualization, Methodology, Writing - review & editing, Supervision, Project administration, Funding acquisition. **Marc Linder:** Conceptualization, Methodology, Resources, Writing - review & editing.

Declaration of Competing Interest

The authors declare that they have no known competing financial interests or personal relationships that could have appeared to influence the work reported in this paper.

References

[1] M. Kölbig, I. Bürger, M. Linder, Characterization of metal hydrides for thermal applications in vehicles below 0°C, International Journal of Hydrogen Energy 44 (10) (2019) 4878–4888.
[2] C. Weckerle, M. Nasir, R. Hegner, I. Bürger, M. Linder, A metal hydride air-conditioning system for fuel cell vehicles-Functional demonstration, Applied Energy 259 (2020), 114187.
[3] B. Sakintuna, F. Lamari-Darkrim, M. Hirscher, Metal hydride materials for solid hydrogen storage: a review, International journal of hydrogen energy 32 (9) (2007) 1121–1140.
[4] B.H. Kang, A. Yabe, Performance analysis of a metal-hydride heat transformer for waste heat recovery, Applied thermal engineering 16 (8-9) (1996) 677–690.
[5] J. Stengler, M. Linder, Thermal energy storage combined with a temperature boost: An underestimated feature of thermochemical systems, Applied Energy 262 (2020), 114530.
[6] K. Altinişik, T.N. Veziroğlu, Metal hydride heat pumps, International Journal of Energy Research 15 (7) (1991) 549–560.
[7] M. Honigmann, "Verfahren zur Entwicklung gespannten Dampfes durch Absorption des abgehenden Maschinendampfes in Aetznatron oder Aetzkali". Kaiserliches Patentamt Patent 24993, 8 Mai 1883.
[8] A. Jahnke, Untersuchung des Honigmann-Prozesses zur thermochemischen Energiespeicherung, Doctoral Thesis, Technische Universität, Berlin, 2019.
[9] M. Lototskyy, V. Yartys, B. Pollet, R. Bowman Jr, Metal hydride hydrogen compressors: a review, International journal of hydrogen energy 39 (11) (2014) 5818–5851.
[10] J.O. Jensen, A.P. Vestbø, Q. Li, N. Bjerrum, The energy efficiency of onboard hydrogen storage, Journal of Alloys and Compounds 446-447 (2007) 723–728.
[11] K. Buschow, P. Bouten, A. Miedema, Hydrides formed from intermetallic compounds of two transition metals: a special class of ternary alloys, Reports on progress in physics 45 (9) (1982) 937.
[12] E. Tzimas, C. Filiou, S. Peteves and J. Veyret, "Hydrogen storage: state-of-the-art and future perspective," EU Commission, JRC Petten, EUR 20995EN, Petten, 2003.
[13] G. Sandrock, A panoramic overview of hydrogen storage alloys from a gas reaction point of view, Journal of alloys and compounds 293 (1999) 877–888.
[14] M. Hirscher, K. Hirose, Handbook of Hydrogen Storage: New Materials for Future Energy Storage, John Wiley & Sons, Weinheim, 2010, p. 9.
[15] A. Perejón, P.E. Sánchez-Jiménez, J.M. Criado, L.A. Pérez-Maqueda, Magnesium hydride for energy storage applications: The kinetics of dehydrogenation under different working conditions, Journal of Alloys and Compounds 681 (2016) 571–579.
[16] X. Luo, J. Wang, M. Dooner, J. Clarke, Overview of current development in electrical energy storage technologies and the application potential in power system operation, Applied energy 137 (2015) 511–536.
[17] M. Budt, D. Wolf, R. Span, J. Yan, A review on compressed air energy storage: Basic principles, past milestones and recent developments, Applied Energy 170 (2016) 250–268.
[18] M. Mendelsohn, D. Gruen, A. Dwight, The effect of aluminum additions on the structural and hydrogen absorption properties of AB5 alloys with particular reference to the LaNi5- xAlx ternary alloy system, Journal of the Less Common Metals 63 (2) (1979) 193–207.
[19] T. Zotov, R. Sivov, E. Movlaev, S. Mitrokhin, V. Verbetsky, IMC hydrides with high hydrogen dissociation pressure, Journal of alloys and compounds 509 (2011) S839–S843.

Summary of individual contributions in Paper III:

- Formulation of the publication´s research goal:

  The goal was to extend the concept of utilizing the temperature difference between two thermochemical materials reported in Paper I and II. A similar concept was investigated to utilize the pressure difference as well.

- Description, calculation, and analysis of the process:

  The concept of the newly presented "thermochemical battery" utilizing the pressure difference between two thermochemical materials was described. It was started with a simplified description. Step by step assumptions were dropped leading to the detailed energetic roundtrip calculation of an exemplary use case.

- Visualization and presentation of the data.

  Selection of relevant data and determining a comprehensible way of presenting it.

- Analysis and deductive reasoning:

  A new concept for the storage of electrical energy was presented – the thermochemical battery. From the very basic formulation of the operational principle, two metal hydrides have been exemplarily used as thermochemical materials. Starting from isothermal compression and idealized heat transfer, the importance of thermal integration was demonstrated. The thermochemical battery has been analytically analyzed regarding important parameters, such as pressure ratios or temperature gradients, and classified in comparison with other systems for the storage of electric energy.

- Writing of the manuscript and publishing in the *Journal of Energy Storage*.

3 Discussion of the results in the overall scientific context

The three previous publications demonstrate that coupled thermochemical reactions are feasible for energy storage in various forms. As illustrated before, one material pair was investigated numerically and experimentally for hydrogen storage. A similar configuration of coupled thermochemical reactions was presented for electricity storage which can be referred as a thermochemical battery.

From the numerical analysis (Paper I) it was found that a water vapor pressure of 10 bar is sufficient to release the stored thermal energy at a temperature level high enough to drive the MgH_2 dehydrogenation which is illustrated in Figure 8. The temperature level to evaporate water vapor at 10 bar is approximately 180 °C. Therefore, instead of the supplying heat at 300 °C or more to the MgH_2, a heat source of 180 °C is sufficient, which is easier to provide. As a result of Paper I the system integration with a high temperature PEM fuel cell as a heat source at 180 °C is

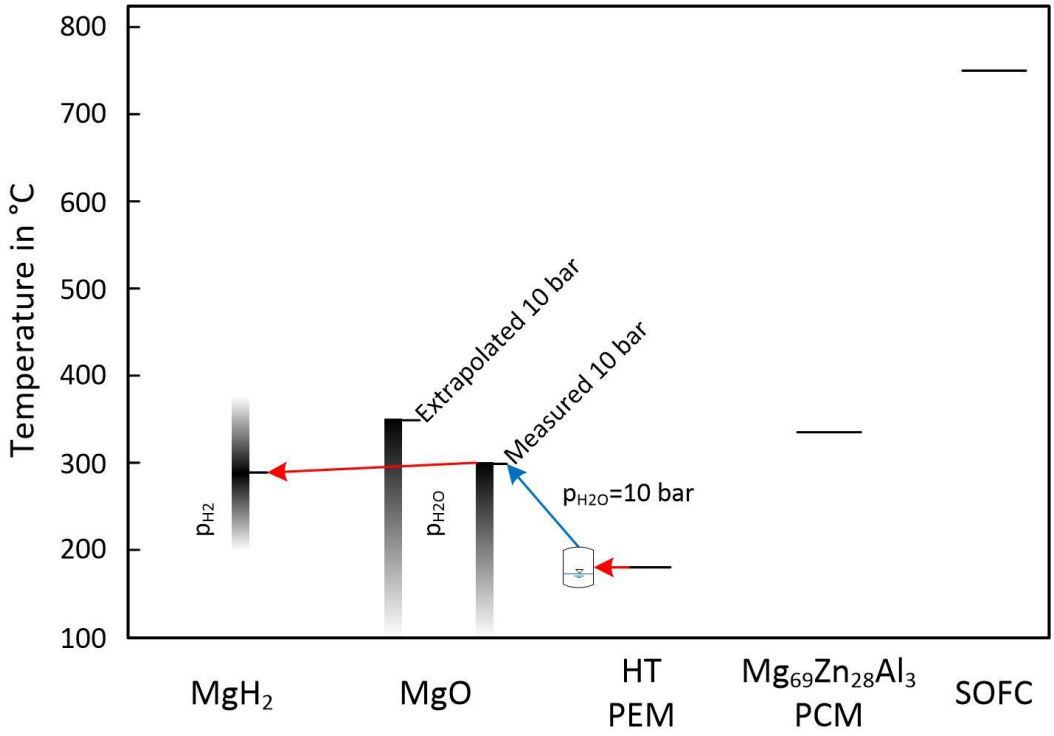

Figure 8 - Illustration of temperature levels during hydrogen release from the adiabatic hydrogen storage reactor; Red arrows: Heat flux; Blue arrow: Gas flow; Shaded areas: Pressure dependence of the temperature level.

feasible. Thus, in conjunction with the fuel cell, the adiabatic hydrogen storage system can be operated as a standalone system. Compared to the approach of thermally integrating the magnesium hydride tank with a solid oxide fuel cell operating above 750 °C, the system can be

held at a lower temperature. Depending on the hydrogen pressures a maximum of 420 °C and 310 °C have been measured during hydrogen storage and release, respectively. This is significantly lower as in the SOFC system. Figure 8 also illustrates that the temperature levels of both the magnesium hydride and the magnesium hydroxide are not fixed since they depend on the corresponding gas pressure. In contrast, the temperature level of the PCM is fixed. Therefore, during hydrogen absorption, the pressure in the MgH_2 has to be increased in order to reach a temperature level that is above the PCM. Using the MgO system, the water vapor pressure can be lowered during hydrogen absorption. Therefore, the temperature gradient can be established without increasing the hydrogen absorption pressure. Subsequently, the system exhibits an additional degree of freedom.

Compared to the approach of storing thermal energy in a phase change material, the present system exhibits higher gravimetric and volumetric storage densities, as it is shown in Figure 9. For comparison, state of the art pressure tanks are included as well. The values for the pressure tanks are calculated based on the whole system, including the high pressure vessel while the top end of the bars of the MgH_2 storage systems are calculated based on the storage materials only. The demand of steel for the vessels and insulation at the exterior of the tank strongly depends on the overall reactor design – and capacity. Therefore, it cannot be quantified at this point. However, the striped sections for the MgH_2 systems illustrate the reduced densities if a steel demand of 50 $g_{Steel}\ g_{H2}^{-1}$ is assumed. It can be seen that the steel reduces the gravimetric density significantly, while it has a comparatively low effect on the volumetric storage density. For the adiabatic hydrogen storage reactor it is still in the same range as the 350 bar pressure tank. However, instead of 350 bar, only 10 bar are required to store the hydrogen. Therefore, the energy to compress the hydrogen to 350 bar can be avoided and less extensive safety measurements have to be installed. Viewing the gravimetric storage densities, it can be seen that the pressure tanks exhibit two or three times higher values. Therefore pressure tanks are feasible for hydrogen storage for mobile applications while the adiabatic hydrogen storage reactor is preferably used for stationary applications. For stationary applications the weight of the system is almost irrelevant compared to mobile applications while a comparatively low volume and low pressure may be desired.

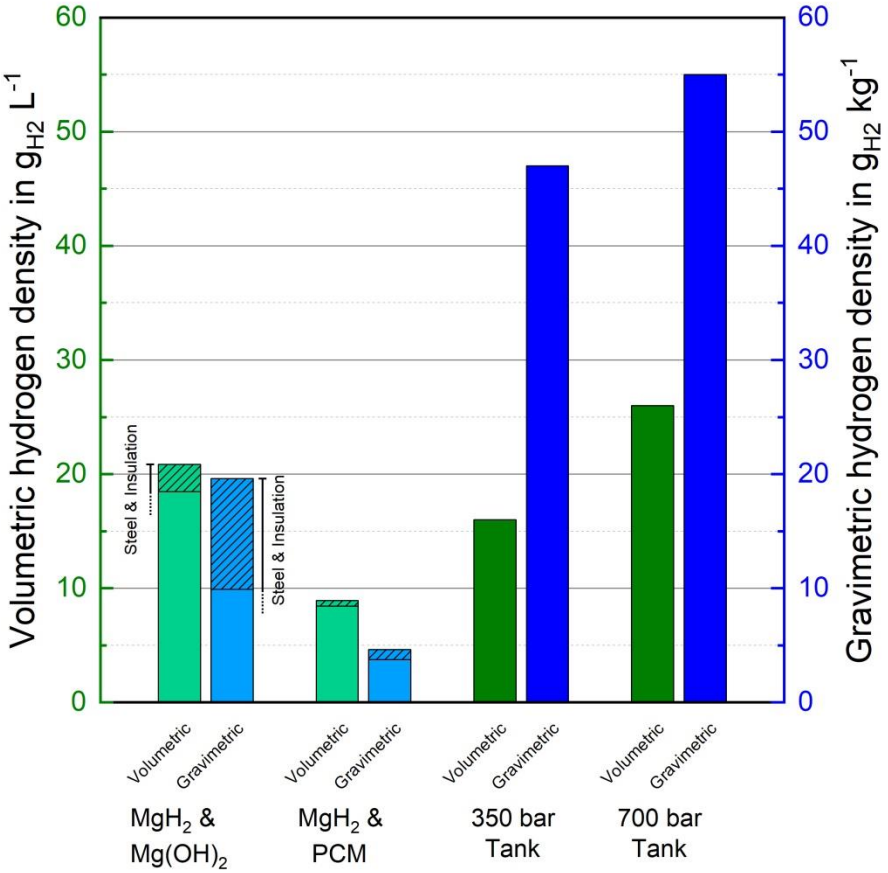

Figure 9 – Comparison of hydrogen storage densities; MgH_2 systems: Materials only; Pressure tanks: System values; Striped area at MgH_2 systems: Assumed reduction due to reaction vessel and insulation.

Compared to existing technologies for hydrogen storage, the adiabatic hydrogen storage reactor is more complex. While it is sufficient to open a valve to release hydrogen from a pressure tank, two thermochemical reactions have to be handled for the adiabatic hydrogen storage reactor. In addition, heat and mass transfer has to be accounted for. To enhance the hydrogen release, it is necessary to identify the bottleneck of the coupled system. Assuming thermodynamic feasibility, the bottleneck may be the reaction kinetics, heat- or mass transfer to one of the two materials. Due to the lack of experimental data for the hydration of MgO at approximately 10 bar, data obtained at lower pressures was extrapolated for the chemical equilibrium and a reaction rate was assumed. In the first publication with the numerical analysis of the hydrogen release, heat transfer was identified to be the limiting process. The assumed reaction rate did not influence the hydrogen release in the range of ± one order of magnitude. Additionally it was found that the

chemical equilibrium of the MgO hydration strongly influences the hydrogen release since it correlates with the maximum temperature level that can be achieved. The experimental data presented in Paper II revealed that for a temperature of 300 °C in the MgO compartment a pressure of approximately 10 bar is required while the extrapolation in paper I indicated that a pressure of 3 bar is sufficient. That discrepancy is also illustrated in Figure 8. Additionally it was experimentally found that the reaction kinetics seem to be the bottleneck for the hydrogen release.

The experimental results from paper II proofed that the reaction system Mg/MgH_2 and $Mg(OH)_2/MgO$ is suited for adiabatic hydrogen storage while some of the assumptions taken for the MgO hydration in the numerical analysis are not accurate to describe the present system. However, the numerical study can be seen as an optimal case that can be achieved with modifications of the $Mg(OH)_2/MgO$ system as soon as the kinetics or thermodynamics are not limiting any more. One possible way to improve the properties of the Mg(OH)2 / MgO system for the use in the adiabatic hydrogen storage reactor could be doping with lithium nitrate. Shkatulov and Aristov found that this way the dehydration temperature can be reduced by 76 °C [71] while the rehydration is slower comparted to the undoped material in the chosen pressure range [72].

A promising alternative material paring for future analysis is the combination of $LiBH_4$-MgH_2 [16] and $Ca(OH)_2$ / CaO as hydrogen storage material and thermochemical energy storage material, respectively. The operating temperature of that pair is approximately 100 K higher than the MgH_2 / $Mg(OH)_2$ system. However, a water vapor pressure of only 1 bar is expected to be necessary to reach the desired temperature level during the CaO hydration. The findings of this thesis are transferrable to that system. The test bench and reactor concept developed in this work can be used to investigate that material pair as well.

The adiabatic hydrogen storage reactor is composed of two thermally coupled gas-solid reactions. Additional coupling of the gaseous side results in the system which is illustrated in Figure 6 and Figure 7 in Section 1.3.3. Such a system of coupled gas-solid reactions can be operated adiabatically and can be used to directly store electric energy which is investigated in Paper III. While any two thermochemical reactions can be selected for that process, the focus in the publication is on metal hydrides exchanging hydrogen and thermal energy.

With the utilization of a compression- and expansion device the system is able to operate as an energy storage device. Therefore, it can be referred to as thermochemical battery with a volumetric energy density in the range of 22-62 Wh L_{mat}^{-1} based on the two materials only. This value is in the range of NiCd batteries [73].

Similarities to compressed air storage (CAS) [74] are evident at which air instead of hydrogen is compressed, stored and expanded. Differences compared to CAS can be identified as well since the thermochemical battery incorporates a thermochemical energy storage feature and depending on the setup, cold can be co-generated.

In addition, similarities to the Honigmann process can be identified. That process, developed by Moritz Honigmann, was initially applied to power locomotives. For the release of energy from the storage system and to power the locomotive, water was evaporated in a boiler and expanded with the extraction of work. The water is then led into a tank of sodium hydroxide where it dissolved and gradually diluted the sodium hydroxide solution. That exothermal process releases enough heat to generate more steam. The operating principle of the Honigmann process has been picked up by Jahnke [75] who investigated the process for thermochemical energy storage using LiBr instead of sodium hydroxide. The Honigmann process is a process that is both coupled thermally and on the gaseous side, which is similar to the thermochemical battery. The difference is that water is evaporated directly, while for the thermochemical battery, another thermochemical system replaces the water boiler. As described by Jahnke [75], in the Honigmann process, the gas pressure has to increase with time to maintain a constant temperature level in the absorbing/heat releasing LiBr since it becomes more and more diluted. In contrast to that, the pressure level in the thermochemical battery in the absorbing material can be kept constant, since the temperature level of hydrogen absorption in the metal hydride is – in the idealized case – not dependent on the reaction progress. Subsequently, the pressure difference to extract work becomes smaller with ongoing discharge at the Honigmann process while it remains constant at the thermochemical battery.

The thermochemical battery shows promising results to store electrical energy. Due to the additional supply of high temperature heat during charging and cold during discharging, system integration to utilize those is important. Depending on the selection of materials and operating

conditions, the amount of co-generated heat and cold changes. Future work may be targeted to identify use cases and designing the thermochemical battery to the specific requirements.

4 Summary of Contributions

In this thesis, systems utilizing thermochemical gas-solid reactions have been investigated for their applications in energy storage. Two different setups both being thermally coupled were investigated. Therefore, in an idealized view, these systems can be operated with minimal external heat management.

The first of the investigated systems is able to store hydrogen. Therefore, magnesium hydride $Mg_{90}Ni_{10}$ is used since it has the potential to store hydrogen with a high volumetric storage density at low pressures. However, the material requires the supply of thermal energy preferably above 300 °C to dehydrogenate. To overcome that disadvantage, the thermal energy during the hydrogen absorption is stored via another thermochemical reaction. Therefore, a thermally coupled system of gas-solid reactions is formed. In preceding studies, the system $Mg(OH)_2$ / MgO was identified to be promising for that purpose. In this thesis, the hydrogen release from the adiabatic hydrogen storage reactor was investigated numerically and it was found that the thermodynamic properties of the two materials regarding temperature- and pressure levels fit to each other. However, the numerical study was accompanied with several uncertainties because the hydration reaction of MgO to $Mg(OH)_2$ has not yet been investigated at a water vapor pressure of up to 10 bar. The assumed reaction kinetics equation for that reaction was found not to be limiting in the range of ± one order of magnitude. Additionally it was found that the maximum temperature that can be reached during the MgO hydration has a strong influence on the hydrogen release rate. However, that temperature had to be extrapolated from data gathered at lower hydration pressures.

To proof that the proposed system is able to store and release hydrogen, an experimental study was conducted. Therefore, a test bench has been extended to provide two independent gas infrastructures supplying both hydrogen and water vapor at a pressure of up to 10 bar to a prototype reactor. A prototype reactor was designed, constructed and tested. The reactor consists of a double walled tube with magnesium hydride in the inner tube and the magnesium hydroxide in the outer tube. For the MgH_2, a melt spun alloy of 90% magnesium and 10% nickel which has been mixed with expanded natural graphite and compressed to pellets was purchased. For the magnesium hydroxide, unmodified power was used. It was experimentally proofed that the thermally coupled system is able to store and release hydrogen. Hydrogen absorption and

desorption were enhanced due to the thermochemical cooling and heating, respectively. However, it was found that the reaction properties of the hydration of MgO to $Mg(OH)_2$ were different compared to the assumptions in the numerical study. In the experimental system, a water vapor of approximately 10 bar was necessary to obtain the same temperature in the MgO bed at 3 bar in the numerical analysis. A temperature of 300 °C was reached during the hydration which has never been investigated before. It was also found that the reaction hydration kinetic is probably the limiting step in the prototype reactor. Therefore, it was concluded that the adiabatic hydrogen storage reactor is feasible, but it is recommended to enhance the reaction rates of $Mg(OH)_2$ / MgO reaction system via material modifications or doping.

The second of the investigated systems is a thermochemical battery. Therefore, the two gas-solid reactions are not only coupled thermally, but also on the gaseous side. That way, they exchange both heat and gas solely with each other. With the incorporation of a compression- and expansion unit, gas can be compressed, stored and expanded. Hence, electrical energy is taken up to power the compressor and is released via the expansion in an expander connected to a generator. This system was analytically investigated by means of two metal hydrides. It was found that the storage of electrical energy is feasible. However, due to different reaction enthalpies of the materials and since the thermochemical battery is cut off from external heat supply, thermal integration of thermal energy produced and consumed by the compressor and expander, respectively, is of utmost importance. A necessity to drive the system is the internal thermochemical storage of thermal energy to compensate the difference of the materials' reaction enthalpies. Depending on the selected material pair, different storage densities and efficiencies can be achieved. Among the investigated pairs, a storage density of 62.6 Wh L_{mat}^{-1} based on the two materials only has been identified. Using a three stage expansion/compression unit with intermediate heating/cooling a maximum electric efficiency of 47% was obtained. Since hydrogen is the working gas, which does not condense or freeze at the conditions investigated, subzero temperatures are feasible after the expander. Therefore, the environment can be cooled if thermal energy from the ambient is used to reheat the hydrogen after the expander.

Summing it up, this thesis composed of three journal publications contributes to a deeper understanding of coupled thermochemical reactions for energy storage. Focusing on hydrogen storage and metal hydride systems, new insights for the development of the "[…] coal of the future" [1] have been obtained.

Bibliography

[1] J. VERNE, L'Île mystérieuse, PARIS: BIBLIOTHÈQUE D'ÉDUCATION ET DE RÉCRÉATION J. HETZEL ET Cie, 18, RUE JACOB, 1874.

[2] C. Zou, Q. Zhao, G. Zhang and B. Xiong, "Energy revolution: From a fossil energy era to a new energy era," *Natural Gas Industry B,* vol. 3, no. 1, pp. 1-11, 2016.

[3] S. Niaz, T. Manzoor and A. H. Pandith, "Hydrogen storage: Materials, methods and perspectives," *Renewable and Sustainable Energy Reviews,* vol. 50, pp. 457-469, 2015.

[4] M. Jehan and D. Fruchart, "McPhy-Energy's proposal for solid state hydrogen storage materials and systems," *Journal of alloys and compounds,* vol. 580, pp. S343-S348, 2013.

[5] T. Setoyama, T. Takewaki, K. Domen and T. Tatsumi, "The challenges of solar hydrogen in chemical industry: how to provide, and how to apply?," *Faraday discussions,* vol. 198, pp. 509-527, 2017.

[6] L. Schlapbach and A. Züttel, "Hydrogen-storage materials for mobile applications," *Materials for sustainable energy: a collection of peer-reviewed research and review articles from nature publishing group,* pp. 265-270, 2011.

[7] B. Sakintuna, F. Lamari-Darkrim and M. Hirscher, "Metal hydride materials for solid hydrogen storage: a review," *International journal of hydrogen energy,* vol. 32, no. 9, pp. 1121-1140, 2007.

[8] I. Sreedhar, K. M. Kamani, B. M. Kamani, B. M. Reddy and A. Venugopal, "A Bird's Eye view on process and engineering aspects of hydrogen storage," *Renewable and Sustainable Energy Reviews,* vol. 91, pp. 838-860, 2018.

[9] M. Hirscher and K. Hirose, Handbook of Hydrogen Storage: New Materials for Future Energy Storage, Weinheim: John Wiley & Sons, 2010, p. 9.

[10] U. Eberle, M. Felderhoff and F. Schueth, "Chemical and physical solutions for hydrogen storage," *Angewandte Chemie International Edition,* vol. 48, no. 36, pp. 6608-6630, 2009.

[11] M. Hirscher and K. Hirose, Handbook of hydrogen storage: new materials for future energy storage, Weinheim: John Wiley & Sons, 2010, p. 13.

[12] J. O. Jensen, A. P. Vestbø, Q. Li and N. Bjerrum, "The energy efficiency of onboard hydrogen storage," *Journal of Alloys and Compounds,* Vols. 446-447, pp. 723-728, 2007.

[13] V. R. Bakuru, M. E. DMello and S. B. Kalidindi, "Metal-Organic Frameworks for Hydrogen Energy Applications: Advances and Challenges," *ChemPhysChem,* vol. 20, no. 10, pp. 1177-1215, 2019.

[14] R. Lan, J. T. Irvine and S. Tao, "Ammonia and related chemicals as potential indirect hydrogen storage materials," *International Journal of Hydrogen Energy,* vol. 37, no. 2, pp. 1482-1494, 2012.

[15] D. Teichmann, W. Arlt, P. Wasserscheid and R. Freymann, "A future energy supply based on Liquid Organic Hydrogen Carriers (LOHC)," *Energy & Environmental Science,* vol. 4, no. 8, pp. 2767-2773, 2011.

[16] J. Jepsen, C. Milanese, A. Girella, G. A. Lozano, C. Pistidda, J. M. B. von Colbe, A. Marini, T. Klassen and M. Dornheim, "Compaction pressure influence on material properties and sorption behaviour of LiBH4--MgH2 composite," *International journal of hydrogen energy,* vol. 38, no. 20, pp. 8357-8366, 2013.

[17] H. E. Friedrich and B. L. Mordike, Magnesium Technology - Metallurgy, Design Data, Applications, Berlin Heidelberg: Springer, 2006, p. 32.

[18] V. Yartys, M. Lototskyy, E. Akiba, R. Albert, V. Antonov, J. Ares, M. Baricco, N. Bourgeois, C. Buckley, J. B. von Colbe, J.-C. Crivello, F. Cuevas, R. Denys, M. Dornheim, M. Felderhoff, D. Grant, B. Hauback, T. Humphries, I. Jacob, T. Jensen, P. de Jongh, J.-M. Joubert, M. Kuzovnikov, M. Latroche, M. Paskevicius, L. Pasquini, L. Popilevsky, V. Skripnyuk, E. Rabkin, M. Sofianos, A. Stuart, G. Walker, H. Wang, C. Webb and M. Zhu, "Magnesium based materials for hydrogen based energy storage: Past, present and future," *International Journal of Hydrogen Energy,* vol. 44, no. 15, pp. 7809-7859, 2019.

[19] Y. Wang and Y. Wang, "Recent advances in additive-enhanced magnesium hydride for hydrogen storage," *Progress in Natural Science: Materials International,* vol. 27, no. 1, pp. 41-49, 2017.

[20] P. Pardo, A. Deydier, Z. Anxionnaz-Minvielle, S. Rougé, M. Cabassud and P. Cognet, "A review on high temperature thermochemical heat energy storage," *Renewable and Sustainable Energy Reviews,* vol. 32, pp. 591-610, 2014.

[21] F. Manchester and D. Khatamian, "Mechanisms for activation of intermetallic hydrogen absorbers," *Materials Science Forum,* vol. 31, pp. 261-296, 1988.

[22] A. K. Singh, A. K. Singh and O. Srivastava, "On the synthesis of the Mg2Ni alloy by mechanical alloying," *Journal of alloys and compounds,* vol. 227, no. 1, pp. 63-68, 1995.

[23] S. Kalinichenka, L. Röntzsch, T. Riedl, T. Gemming, T. Weißgärber and B. Kieback, "Microstructure and hydrogen storage properties of melt-spun Mg-Cu-Ni-Y alloys," *International journal of hydrogen energy,* vol. 36, no. 2, pp. 1592-1600, 2011.

[24] H. Zhong and J. Xu, "Tuning the de/hydriding thermodynamics and kinetics of Mg by mechanical alloying with Sn and Zn," *International Journal of Hydrogen Energy,* vol. 44, no. 5, pp. 2926-2933, 2019.

[25] S. Kalinichenka, L. Röntzsch, C. Baehtz and B. Kieback, "Hydrogen desorption kinetics of melt-spun and hydrogenated Mg90Ni10 and Mg80Ni10Y10 using in situ synchrotron, X-ray diffraction and thermogravimetry," *Journal of alloys and compounds,* vol. 496, no. 1-2, pp. 608-613, 2010.

[26] C. Pohlmann, L. Röntzsch, S. Kalinichenka, T. Hutsch, T. Weißgärber and B. Kieback, "Hydrogen storage properties of compacts of melt-spun Mg90Ni10 flakes and expanded natural graphite," *Journal of Alloys and Compounds,* vol. 509, pp. S625-S628, 2011.

[27] C. Pohlmann, B. Kieback and L. Röntzsch, "Composite materials of melt-spun Mg90Ni10 and graphite: Microstructural changes during cyclic hydrogenation and the impact on gas and heat transport characteristics," *International journal of hydrogen energy,* vol. 39, no. 16, pp. 8331-8339, 2014.

[28] C. Pohlmann, L. Röntzsch, T. Weißgärber and B. Kieback, "Heat and gas transport properties in pelletized hydride-graphite-composites for hydrogen storage applications," *International journal of hydrogen energy,* vol. 38, no. 3, pp. 1685-1691, 2013.

[29] S. Kumar, Y. Kojima and V. Kain, "Nano-engineered Mg-MgH2 system for solar thermal energy storage," *Solar Energy,* vol. 150, pp. 532-537, 2017.

[30] M. Paskevicius, D. Sheppard, K. Williamson and C. Buckley, "Metal hydride thermal heat storage prototype for concentrating solar thermal power," *Energy,* vol. 88, pp. 469-477, 2015.

[31] S. Garrier, A. Chaise, P. de Rango, P. Marty, B. Delhomme, D. Fruchart and S. Miraglia, "MgH2 intermediate scale tank tests under various experimental conditions," *International Journal of Hydrogen Energy,* vol. 36, no. 16, pp. 9719-9726, 2011.

[32] B. Delhomme, A. Lanzini, G. A. Ortigoza-Villalba, S. Nachev, P. De Rango, M. Santarelli, P. Marty and P. Leone, "Coupling and thermal integration of a solid oxide fuel cell with a magnesium hydride tank," *International Journal of Hydrogen Energy,* vol. 38, no. 11, pp. 4740-4747, 2013.

[33] B. Delhomme, P. De Rango, P. Marty, M. Bacia, B. Zawilski, C. Raufast, S. Miraglia and D. Fruchart, "Large scale magnesium hydride tank coupled with an external heat source," *International journal of hydrogen energy,* vol. 37, no. 11, pp. 9103-9111, 2012.

[34] V.-T. Giap, Y. D. Lee, Y. S. Kim and K. Y. Ahn, "A novel electrical energy storage system based on a reversible solid oxide fuel cell coupled with metal hydrides and waste steam," *Applied Energy,* vol. 262, p. 114522, 2020.

[35] A. A. R. Darzi, H. H. Afrouzi, A. Moshfegh and M. Farhadi, "Absorption and desorption of hydrogen in long metal hydride tank equipped with phase change material jacket," *International Journal of Hydrogen Energy,* vol. 41, no. 22, pp. 9595-9610, 2016.

[36] S. Garrier, B. Delhomme, P. De Rango, P. Marty, D. Fruchart and S. Miraglia, "A new MgH2 tank concept using a phase-change material to store the heat of reaction," *International Journal of Hydrogen Energy,* vol. 38, no. 23, pp. 9766-9771, 2013.

[37] S. Mellouli, N. Ben Khedher, F. Askri, A. Jemni and S. Ben Nasrallah, "Numerical analysis of metal hydride tank with phase change material," *Applied Thermal Engineering,* vol. 90, pp. 674-682, 2015.

[38] S. Mellouli, E. Abhilash, F. Askri and S. B. Nasrallah, "Integration of thermal energy storage unit in a metal hydride hydrogen storage tank," *Applied Thermal Engineering,* vol. 102, pp. 1185-1196, 2016.

[39] H. El Mghari, J. Huot and J. Xiao, "Analysis of hydrogen storage performance of metal hydride reactor with phase change materials," *International Journal of Hydrogen Energy,* vol. 44, no. 54, pp. 28893-28908, 2019.

[40] M. Bhouri, I. Bürger and M. Linder, "Feasibility analysis of a novel solid-state H2 storage reactor concept based on thermochemical heat storage: MgH2 and Mg (OH) 2 as reference materials," *International Journal of Hydrogen Energy,* vol. 41, no. 45, pp. 20549-20561, 2016.

[41] Y. Kato, J. Nakahata and Y. Yoshizawa, "Durability characteristics of the hydration of magnesium oxide under repetitive reaction," *Journal of materials science,* vol. 34, no. 3, pp. 475-480, 1999.

[42] M. Bhouri and I. Bürger, "Numerical investigation of H2 absorption in an adiabatic high-temperature metal hydride reactor based on thermochemical heat storage: MgH2 and Mg (OH) 2 as reference materials," *International Journal of Hydrogen Energy,* vol. 42, no. 26, pp. 16632-16644, 2017.

[43] S. Gregg and R. Razouk, "S 8. The kinetics of the thermal decomposition of magnesium hydroxide," *Journal of the Chemical Society (Resumed),* pp. S36-S44, 1949.

[44] E. Piperopoulos, E. Mastronardo, M. Fazio, M. Lanza, S. Galvagno and C. Milone, "Synthetic strategies for the enhancement of Mg (OH) 2 thermochemical performances as heat storage material," *Energy Procedia,* vol. 155, pp. 269-279, 2018.

[45] J. Yan, C. Zhao and Z. Pan, "The effect of CO2 on Ca (OH) 2 and Mg (OH) 2 thermochemical heat storage systems," *Energy,* vol. 124, pp. 114-123, 2017.

[46] C. Knoll, D. Müller, W. Artner, J. M. Welch, E. Eitenberger, G. Friedbacher, A. Werner, P. Weinberger and M. Harasek, "Magnesium oxide from natural magnesite samples as thermochemical energy storage material," *Energy Procedia,* vol. 158, pp. 4861-4869, 2019.

[47] E. Mastronardo, L. Bonaccorsi, Y. Kato, E. Piperopoulos and C. Milone, "Efficiency improvement of heat storage materials for MgO/H2O/Mg (OH) 2 chemical heat pumps," *Applied Energy,* vol. 162, pp. 31-39, 2016.

[48] M. Zamengo, J. Ryu and Y. Kato, "Composite block of magnesium hydroxide-expanded graphite for chemical heat storage and heat pump," *Applied thermal engineering,* vol. 69, no. 1-2, pp. 29-38, 2014.

[49] G. K. LAYDEN and G. Brindley, "Kinetics of vapor-phase hydration of magnesium oxide," *Journal of the American Ceramic Society,* vol. 46, no. 11, pp. 518-522, 1963.

[50] Y. Kato, N. Yamashita , K. Kobayashi and Y. Yoshizawa, "Kinetic study of the hydration of magnesium oxide for a chemical heat pump," *Applied Thermal Engineering,* vol. 16, no. 11, pp. 853-862, 1996.

[51] R. J. Bratton and G. W. Brindley, "Kinetics of vapour phase hydration of magnesium oxide. Part 2.-Dependence on temperature and water vapour pressure," *Transactions of the Faraday Society,* vol. 61, pp. 1017-1025, 1965.

[52] K. Saitou, R. Kurosawa and J. Ryu, "Dehydration and Hydration Reactivity of Citrate-Added Mg(OH)2 for Thermo-chemical Energy Storage," in *Grand Renewable Energy proceedings Japan council for Renewable Energy*, 2018.

[53] E. Mastronardo, L. Bonaccorsi, Y. Kato, E. Piperopoulos, M. Lanza and C. Milone, "Thermochemical performance of carbon nanotubes based hybrid materials for MgO/H2O/Mg (OH) 2 chemical heat pumps," *Applied Energy,* vol. 181, pp. 232-243, 2016.

[54] A. A. Pilarska, Ł. Klapiszewski and T. Jesionowski, "Recent development in the synthesis, modification and application of Mg (OH) 2 and MgO: A review," *Powder Technology,* vol. 319, pp. 373-407, 2017.

[55] M. Baerns, H. Hofmann and A. Renken, Chemische Reaktionstechnik - Band 1 von Lehrbuch der technischen Chemie, Stuttgart, New York: Thieme, 1987, p. 24ff.

[56] P. Stephan, K. Schaber, K. Stephan and F. Mayinger, Thermodynamik - Grundlagen und technische Anwendungen - Band 2: Mehrstoffsysteme und chemische Reaktionen, Berlin Heidelberg: Springer-Verlag Berlin Heidelberg, 2010, p. 359.

[57] S. Vyazovkin, A. K. Burnham, J. M. Criado, L. Pérez-Maqueda, C. Popescu and N. Sbirrazzuoli, "ICTAC Kinetics Committee recommendations for performing kinetic computations on thermal analysis data," *Thermochimica acta,* vol. 520, no. 1-2, pp. 1-19, 2011.

[58] Y. Pang and Q. Li, "A review on kinetic models and corresponding analysis methods for hydrogen storage materials," *International journal of hydrogen energy,* vol. 41, no. 40, pp. 18072-18087, 2016.

[59] X. Chen, Z. Zhang, C. Qi, X. Ling and H. Peng, "State of the art on the high-temperature thermochemical energy storage systems," *Energy conversion and management,* vol. 177, pp. 792-815, 2018.

[60] C. Weckerle, M. Nasir, R. Hegner, I. Bürger and M. Linder, "A metal hydride air-conditioning system for fuel cell vehicles-Functional demonstration," *Applied Energy,* vol. 259, p. 114187, 2020.

[61] M. Kölbig, I. Bürger and M. Linder, "Characterization of metal hydrides for thermal applications in vehicles below 0° C," *International Journal of Hydrogen Energy,* vol. 44, no. 10, pp. 4878-4888, 2019.

[62] M. Lototskyy, V. Yartys, B. Pollet and R. Bowman Jr, "Metal hydride hydrogen compressors: a review," *International journal of hydrogen energy,* vol. 39, no. 11, pp. 5818-5851, 2014.

[63] I. Jain, C. Lal and A. Jain, "Hydrogen storage in Mg: a most promising material," *International Journal of Hydrogen Energy,* vol. 35, no. 10, pp. 5133-5144, 2010.

[64] M. Fichtner, "Conversion materials for hydrogen storage and electrochemical applications - Concepts and similarities," *Journal of alloys and compounds,* vol. 509, pp. S529-S534, 2011.

[65] B. H. Kang and A. Yabe, "Performance analysis of a metal-hydride heat transformer for waste heat recovery," *Applied thermal engineering,* vol. 16, no. 8-9, pp. 677-690, 1996.

[66] D. Hebecker, "Wärmetransformation," in *Abfallenergienutzung : technische, wirtschaftliche und soziale Aspekte (Forschungsberichte / Interdisziplinäre Arbeitsgruppen, Berlin-Brandenburgische Akademie der Wissenschaften ; 2)*, Berlin, 2016, pp. 61-81.

[67] A. Chaise, P. De Rango, P. Marty, D. Fruchart, S. Miraglia, R. Olivès and S. Garrier, "Enhancement of hydrogen sorption in magnesium hydride using expanded natural graphite," *International Journal of Hydrogen Energy,* vol. 34, no. 20, pp. 8589-8596, 2009.

[68] Y. Kato, M. Zamengo and K. Fujioka, "Effect of thermal conductivity enhancement of thermochemical energy storage material on unused heat utilization system," in *Proceedings of The 15th International Heat Transfer Conference (IHTC-15)*, Kyoto, 2014.

[69] M. Linder, R. Mertz and E. Laurien, "Experimental results of a compact thermally driven cooling system based on metal hydrides," *International Journal of Hydrogen Energy,* vol. 35, no. 14, pp. 7623-7632, 2010.

[70] F. Yang, X. Meng, J. Deng, Y. Wang and Z. Zhang, "Identifying heat and mass transfer characteristics of metal hydride reactor during adsorption: improved formulation about parameter analysis," *International Journal of Hydrogen Energy,* vol. 34, no. 4, pp. 1852-1861, 2009.

[71] A. I. Shkatulov and Y. Aristov, "Thermochemical Energy Storage using LiNO3-Doped Mg (OH) 2: A Dehydration Study," *Energy Technology,* vol. 6, no. 9, pp. 1844-1851, 2018.

[72] A. Shkatulov, H. Takasu, Y. Kato and Y. Aristov, "Thermochemical energy storage by LiNO3-doped Mg (OH) 2: Rehydration study," *Journal of Energy Storage,* vol. 22, pp. 302-310, 2019.

[73] X. Luo, J. Wang, M. Dooner and J. Clarke, "Overview of current development in electrical energy storage technologies and the application potential in power system operation," *Applied energy,* vol. 137, pp. 511-536, 2015.

[74] M. Budt, D. Wolf, R. Span and J. Yan, "A review on compressed air energy storage: Basic principles, past milestones and recent developments," *Applied Energy,* vol. 170, pp. 250-268, 2016.

[75] A. Jahnke, *Untersuchung des Honigmann-Prozesses zur thermochemischen Energiespeicherung,* Technische Universität Berlin: Doctoral Thesis, 2019.